High blood pressure and cyclic stretch alter cerebral amyloid deposition and endothelial function

Sumudu VS Gangoda (Bachelor of Biotechnology, Honours)
MQ student ID: 43533019

A thesis of The Australian School of Advanced Medicine, Faculty of Human Sciences, Macquarie University, submitted in fulfilment of the requirements for the degree of Masters of Research.

Principal supervisor:
Professor Alberto P Avolio

Associate supervisor:
Dr Mark Butlin

Co-supervisor:
Dr Vivek Gupta

Australian School of Advanced Medicine, Macquarie University, Sydney, Australia.

October 2014

MACQUARIE UNIVERSITY

THE AUSTRALIAN SCHOOL OF ADVANCED MEDICINE

Declaration of originality

I hereby declare that the work presented in this thesis has not been submitted for a higher degree to any other university or institution. To the best of my knowledge this submission contains no material previously published or written by another person, except where due reference is stated otherwise. Any contribution made to the research by others is explicitly acknowledged.

Sumudu V. S. Gangoda

Australian School of Advanced Medicine
Faculty of Human Science
Macquarie University

Date of submission: 10th October 2014

Word count: 16 267
Character count of the abstract: 1703 with spaces (250 words)
No of figures: 19

Declaration of contributions

Rat brains for analysis of amyloid beta were provided from separate rat experiments conducted by Dr. Mark Butlin and Parisa Kouchaki and the brain slices were prepared by Dr. Vivek Gupta.

Acknowledgements

I convey my deepest gratitude to a number of people who supported and guided me during my MRes year. First I would like to acknowledge my primary supervisor, Professor Alberto Avolio for giving me this opportunity to broaden my research and communication skills, and for providing me insights into the broader concepts specific to the current project as well as in broadening my understanding and knowledge and expanding my horizons when it comes to the field of research. This work would not have been possible without his invaluable advice, direction and inspiration provided to me throughout this project.

I am also grateful to my associate-supervisor, Dr. Mark Butlin. His kind and positive attitude and enthusiasm enabled me to pursue this project in an open and friendly working environment. His patient approach has taught me valuable skills in data interpretation and critical evaluation of the findings allowing me to accomplish the outcomes of this project.

I would also like to acknowledge my co-supervisor, Dr. Vivek Gupta for his kind assistance and guidance in western blotting and for providing the tissue samples for the animal studies. Thank you for always being available and providing me with much needed guidance in troubleshooting in cell and tissue work.

Furthermore, I would like to thank Dr. Lisa Sedger for her guidance that helped me understand molecular biology concepts and troubleshooting in cell work. My special thanks to Professor Roger Chung for kindly providing the amyloid antibody for the amyloid studies and to the following PhD students; Bhargava Avadhanam, Nurul Jufri, Marina Santiago, Phill Bokiniec, Isabella Tan, Mi-ok Kim, Parisa Kouchaki and Kayla Viegas for all their support, guidance and making it an enjoyable journey for me.

I acknowledge the Australian School of Advanced Medicine and Macquarie University for provision of my postgraduate scholarship and research funding.

Lastly, I extend my gratitude to my parents; Chandra and Shanthi Gangoda, my siblings; Sanuja, Sandamali, Ayesha, Dasun, and Dinuja and my uncle, Jayantha Gangoda whose love, care, guidance and support I have been blessed with for which I am forever thankful. Special thank you to my grandmother, Sirimangala Basnayake for her love, care and enriching my student life with her religious perspective.

Conflict of Interest

The research was conducted in the absence of any commercial or financial relationships that could be constructed as potential conflict of interest.

Publications

Honours thesis

Gangoda, S. V. S. Effects of HYPER on oxidative stress and inflammation in human coronary artery endothelial cells. University of Technology Sydney, November 2012.

Conference presentations

Gangoda, S. V. S., Jang, S. A., Jufri, N. F., Koo, H. J., Butlin, M., Avolio, A. P. and Sohn, E. H. Ethanol impaired estrogen receptors and increased ICAM-1 and Galectin-3 in HUVECs and HBMECs. The Annual Scientific Meeting of The High Blood Pressure Research Council of Australia, Melbourne, Australia, November 2013.

Gangoda, S. V. S., Jang, S. A., Jufri, N. F., Koo, H. J., Butlin, M., Avolio, A. P. and Sohn, E. H. Ethanol impairs expression of estrogen receptors and increases ICAM-1 and Galectin-3 in human umbilical vein and cerebral microvascular endothelial cells. The MQ BioFocus Research Centre Annual Interdisciplinary Research Conference, Sydney, Australia, December 2013.

Gangoda, S. V. S., Butlin, M., Gupta, V. and Avolio, A. P. High blood pressure and cyclic stretch alter cerebral amyloid deposition and endothelial function. The Annual Scientific Meeting of The High Blood Pressure Research Council of Australia, Adelaide, Australia, November 2014.

Abstract

Background: Amyloid β (Aβ) deposition is a hallmark of Alzheimer's disease (AD). Increased pulsatility, endothelial dysfunction (ED) and inflammation, indicators of vascular stiffness, are associated with AD. Additionally, vascular stiffness is linked to hypertension, a risk factor for AD.

Aim: This study aimed to determine effects of high blood pressure (BP) on cerebral Aβ deposition in rodent models, spontaneously hypertensive (SHR) and normotensive Wistar Kyoto rats (WKY) and investigate effects of cyclic stretch (CS) on expression of amyloid precursor protein (APP), endothelial nitric oxide synthase (eNOS) and intercellular cell adhesion molecule-1 (ICAM-1) in human cerebral microvascular endothelial cells (hCMEC).

Methods: Hippocampal (HC) and frontal cortex (FC) regions of SHR and WKY rats were analysed using western blotting to determine effect of BP on cerebral Aβ deposition. hCMEC were subjected to 5%, 10% or 20 % CS compared to control (0% CS) to evaluate pulsatility, ED and inflammation using western blotting and/or RTqPCR.

Results: Aβ oligomerisation increased in SHR compared to WKY in HC ($P<0.01$) and FC ($P<0.001$). APP mRNA expression increased at 5%, decreased at 20% CS; eNOS decreased at both ($P<0.0001$). APP and ICAM-1 protein expression dose-dependently increased at 5% and 10% CS ($P<0.01$) and decreased at 20% CS. eNOS protein levels decreased at all CS ($P<0.0001$).

Conclusions: Results suggest that high BP and CS respectively alter the processing and expression of cerebral APP. Prolonged CS may induce ED by increasing ICAM-1, thereby mitigating eNOS expression. Findings mechanistically support the association of elevated pulsatility and arterial stiffness with AD.

Key words: Cyclic stretch; Alzheimer's disease; hypertension; SHR; eNOS; ICAM-1; APP

Table of Contents

List of Figures

List of Abbreviations

ABC	Adenosine triphosphate-binding cassette
AD	Alzheimer's disease
ADAM	A disintegrin and metalloproteinase
AF	Annulus fibrosus
AICD	Amyloid precursor protein intracellular domain
Akt	Serine/threonine-specific protein kinase
APH 1	Anterior pharynx-defective 1
APP	Amyloid precursor protein
Aβ	Amyloid-beta
BACE1	Beta-site APP cleaving enzyme 1
BAEC	Bovine aortic endothelial cells
BBB	Blood brain barrier
BCEC	Primary bovine capillary ECs
BP	Blood pressure
C-terminus	Carboxy terminus
cDNA	Complementary deoxyribonucleic acid
cGMP	Cyclic guanosine monophosphate
CS	Cyclic stretch
DIV-BBB	Dynamic *in vitro* BBB model
EC	Endothelial cell
ECM	Extracellular matrix protein
ED	Endothelial dysfunction
EDTA	Ethylene diamine tetraacetic acid
eNOS	Endothelial nitric oxide synthase
ET-1	Endothelin-1
FC	Frontal cortex
GAPDH	Glyceraldehyde 3-phosphate dehydrogenase
HC	Hippocampus
HCEC	Human capillary and microvascular endothelial cells
HCMEC-SV40	Human cerebral microvascular cells-Simian virus
HRP	Horse radish peroxidase
HUVEC	Human umbilical vein endothelial cells
ICAM-1	Intercellular cell adhesion molecule-1
L-NAME	N (G)-Nitro-L-Arginine Methyl Ester

LRP-1	Lipoprotein receptor-related protein 1
mRNA	Messenger ribonucleic acid
NFκB	Nuclear factor kappa B
NO	Nitric oxide
NOS	Nitric oxide synthase
PBS	Phosphate buffered saline
PEN-2	Presenilin enhancer-2
PI3K	Phosphatidylinositol 3 OH-kinase
PKA	Protein kinase A
PrI	Propidium iodide
PVDF	Polyvinylidene difluoride
RAGE	Receptor for advanced glycation end products
RIPA	Radioimmunoprecipitation assay
RNA	Ribonucleic acid
ROS	Reactive oxygen species
RT-qPCR	Reverse transcription quantitative polymerase chain reaction
SBP	Systolic blood pressure
SD	Standard deviation
SDS	Sodium dodecyl sulfate
SDS-PAGE	Sodium dodecyl sulfate polyacrylamide gel electrophoresis
SHR	Spontaneously hypertensive rat
SHR-SP	Spontaneously hypertensive stroke-prone rats
SHR-SR	Spontaneously hypertensive rat-stroke resistant
SOD	Superoxide dismutase
SPA	Asynchronous mechanical force patterns
SS	Shear stress
TBS-T	Tris buffered saline-Tween
Tg	Transgenic
tMCAO	Transient middle cerebral artery occlusion
TNF-α	Tumour necrosis factor-alpha
TRP	Transient receptor potential
TRPV4	TRP-Vanilloid-4
VEGF	Vascular endothelial growth factor
WKY	Wistar Kyoto rat
β2m	Beta-2 microglobulin

1 Introduction

Alzheimer's Disease (AD) is considered the most prevalent cause of dementia accounting for 60% of all dementias (Dias et al., 2006). Dementia is a syndrome that results in cognitive impairment, which, in a Delphi consensus study in 2005, was estimated to increase by 4·6 million cases every year globally (Ferri et al., 2005; Dias et al., 2006). The numbers are increasing considerably as a consequence of the aging population, a lack of effective treatments and not having adequate diagnostic techniques (Dias et al., 2006; Ferri et al., 2005). Due to the significant disease burden and the impact on disability of dementia, AD, the foremost cause of dementia, has attracted considerable attention in research and is yet to be addressed adequately (Ferri et al., 2005; Dias et al., 2006).

Amyloid plaques and neurofibrillary tangles in the brain are well known characteristics of AD (Ferri et al., 2005). These were first described by Dr. Alois Alzheimer, 'as miliary foci scatted throughout the cerebral cortex due to the deposition of a peculiar substance', after examining the postmortem brain tissue of his patient Auguste D who suffered from AD and died in 1908 (Ferri et al., 2005; Masters and Selkoe, 2012). Later on, during the mid to late 1980's, it was discovered that the plaques are mainly composed of the small amyloid peptide called amyloid-beta (Aβ), which is 39-42 amino acid long, while the intraneuronal neurofibrillary tangles comprise aggregates of abnormally hyperphosphorylated tau protein (Grundke-Iqbal et al., 1989; LaFerla et al., 2007). The present study focused only on the former, Aβ.

The main contributor to Aβ plaques, 'Aβ peptides' are derived from the amyloid precursor protein (APP), which is a transmembrane protein expressed in a number of cell types including endothelial cells (ECs; Selkoe, 2001). The cleavage and processing of APP occur in two distinct pathways, namely, non-amyloidogenic and amyloidogenic pathways (Selkoe, 2001). As implied by the names, the former does not result in Aβ secretion while the latter does (Selkoe, 2001).

Briefly, the non-amyloidogenic pathway is the common pathway of APP cleavage, in which, α-secretases produce a large amino (N)-terminal ectodomain (sAPPα), 83 amino acids away from the carboxy (C) terminus, which is then secreted into the extracellular medium. This 83-amino-acid-long C terminal fragment known as C83 is retained in the membrane to be cleaved off by γ-secretases to produce the short fragment p3 at a subsequent stage. Notably, the initial cleavage of APP by α-secretases occurs within the Aβ domain, thus formation of Aβ is prevented. In contrast, the amyloidogenic pathway importantly is an alternative APP cleavage pathway, which leads to Aβ generation. In this pathway, the proteolysis is initiated by β-secretases rather than α-secretases, 99 amino acids away from the C terminus. This cleavage releases sAPPβ into the extracellular space, subsequently, leaving the 99-amino-acid C-terminal stub known as C99, anchored to the membrane. The C99 fragments, which have N termini corresponding to the first amino acid of Aβ, are then cleaved off by γ-secretases between 38 and 43 residues liberating intact Aβ peptides, which could be in soluble or fibrillar forms (Figure 1; Scheuermann et al., 2001; Maltese et al., 2001).

In the normal brain, the accumulation of Aβ is prevented through adequate regulation of APP processing and clearance (Castellano et al., 2011). However, in the AD brain, these processes are thought to be disrupted leading to consequent Aβ-plaque formation (Castellano et al., 2011). This is considered to occur via several mechanisms (Castellano et al., 2011; Pflanzner et al., 2011; Deane et al., 2004). These include enhanced cleavage of

APP to Aβ, over-expression of APP, and reduced clearance of Aβ from the central nervous system as evidenced by mutational studies of familial AD (Rajadas et al., 2013). The APP-derived Aβ peptides via the amyloidogenic pathway are removed from the brain through two major mechanisms such as efflux and proteolytic degradation (Lee and Landreth, 2013). Intact soluble Aβ are cleared through either of these mechanisms while fibrillar Aβ being cleared through proteolytic degradation (Lee and Landreth, 2013). The efflux of soluble Aβ involves crossing the blood brain barrier (BBB) either to enter the circulation or into the lymphatic system (Lee and Landreth, 2013). The former is mediated by low-density lipoprotein receptor-related protein 1 (LRP1) in concert with the P-glycoprotein efflux pump while the latter is through bulk flow of interstitial fluid/ cerebrospinal fluid (Owen et al., 2010; Pflanzner et al., 2011). These efflux mechanisms are considered to be either facilitated or inhibited through binding of chaperone proteins, such as ApoE, ApoJ, α2-macroglobulin, transthyretin and albumin (Gupta et al., 2011; Song et al., 2012; Stanyon and Viles, 2012; Faxén-Irving et al., 2013). However, it should be noted that the cleared-Aβ into the bloodstream could also be transported back into the brain via receptor for advanced glycation end products (RAGE)-mediated Aβ influx (Wang et al., 2006a).

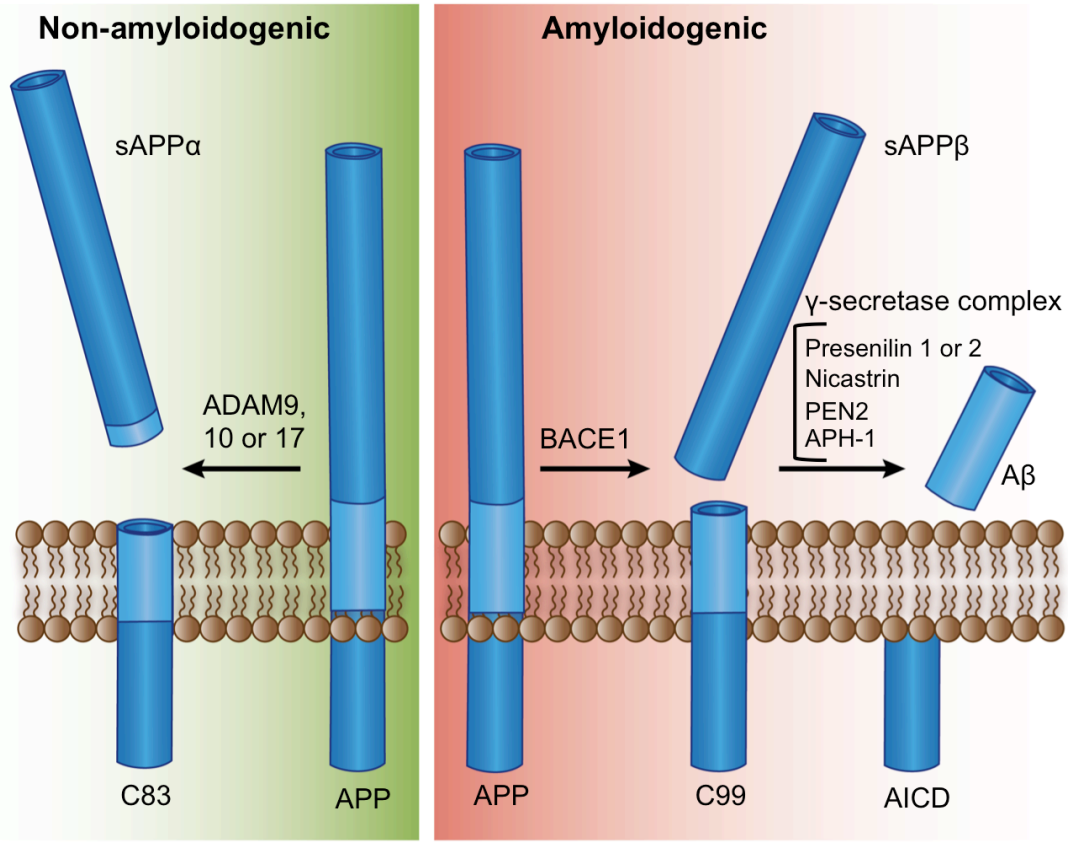

Figure 1. Non-amyloidogenic and amyloidogenic processing of APP. APP is cleaved into sAPPα and C83 residue by ADAM9, ADAM10 or ADAM17 in the non-amyloidogenic pathway (left). In contrast, in the amyloidogenic pathway (right), APP is first cleaved into sAPPβ and C99 residue by BACE1. The C99 fragment is then further cleaved off by the γ-secretase complex including presenilin 1 or 2, nicastrin, PEN2 and APH-1 and AICD, into intact Aβ peptides (Modified from LaFerla et al., 2007). Abbreviations: ADAM, a-disintegrin-and-metalloproteinase; Aβ, Amyloid beta; AICD, amyloid precursor protein intracellular domain; APH-1, anterior pharynx-defective 1; APP, amyloid precursor protein; BACE1, beta-site APP cleaving enzyme 1; PEN-2, presenilin enhancer-2.

As blood flow is involved in the clearance of Aβ and due to the possible vascular involvement in the pathogenesis of AD, perivascular plaque recently has gained much consideration, highlighting a possible role of blood vessel integrity in AD (Park et al., 2014; Ghiso et al., 2014). Perivascular Aβ plaque formation refers to the accumulation of Aβ surrounding cerebral blood vessels including arteries, arterioles, and capillaries (Park et al., 2014; Ghiso et al., 2014). As implied by the term 'perivascular', vascular factors are involved in this aspect.

Of the numerous vascular factors associated with AD, high pulsatility, endothelial dysfunction (ED) and vascular inflammation, are less well studied (Toda and Okamura, 2012). However, there is evidence in the literature indicating that these factors are concomitantly overlapped in AD (Akiyama et al., 2000; d'Uscio et al., 2012; Tan et al., 2014; Mitchell et al., 2011). For example, studies have shown that higher pulsatility index and pulse pressure were associated with AD, lower memory scores and cerebral microvascular damage (Mitchell et al., 2011; Stefani et al., 2009; Nation et al., 2013). These two factors are independent markers of 'vascular stiffness', which refers to the lack of vessel compliance (Tan et al., 2012). Vascular stiffness is also related to ED, which is consequent of impaired endothelium-dependent vasodilation (Wallace et al., 2007). In the vascular endothelium, nitric oxide (NO) is one of the major vasodilators that mediate vasodilation (Huang et al., 1994; Trochu et al., 2000). The enzyme, endothelial nitric oxide synthase (eNOS) is of much importance in mediating this vasodilatory response, as it is one of the main sources of NO in the vasculature (Trochu et al., 2000). Inhibition or deficiency of eNOS was associated with higher APP protein expression and secretion of Aβ (Austin et al., 2013b, 2010, 2013a). Additionally, vascular stiffness could lead to inflammation in the vasculature (Wu et al., 2014; Tan et al., 2014). Elevated expression and localisation of inflammatory markers such as intercellular cell adhesion molecule-1 (ICAM-1) surrounding AD-plaques have been demonstrated (Apelt et al., 2002; Verbeek et al., 1996; Rozemuller et al., 1989). Together these data corroborated that high pulsatility, ED and vascular inflammation were independently associated with AD (Stefani et al., 2009; Nation et al., 2013; Austin et al., 2013b; Apelt et al., 2002). Moreover, these factors are also present in the milieu of hypertension, which is a major risk factor for AD (Barnes and Yaffe, 2011; Sabayan et al., 2012; Panes et al., 1996; Csiszar et al., 2013). Collectively, these associations highlighted the involvement of pulsatile mechanical stretch in AD and hypertension.

In light of this existing evidence, the present study aimed to study whether:

(i) APP processing and/or Aβ aggregation were altered in an animal model of hypertension.

(ii) variations in pulsatility in terms of 5%, 10% and/or 20% of cyclic stretch (CS) had any effect on the messenger ribonucleic acid (mRNA) expression and protein expression of APP in human cerebral microvascular EC-Simian virus (HCMEC-SV40) cell line.

(iii) variations in pulsatility in terms of 5%, 10% and/or 20% of CS had any effect on the mRNA expression and protein expression of eNOS in HCMEC-SV40 cell line.

(iv) variations in pulsatility in terms of 5%, 10% and/or 20% of CS had any effect on the protein expression of ICAM-1 in HCMEC-SV40 cell line.

To achieve these aims, the present study employed the well-established animal model for

hypertension, spontaneously hypertensive rat (SHR) along with the normotensive Wistar Kyoto (WKY) rat control. This model of hypertension has been extensively used in previous studies, showing the reliability as an *in vivo* representation of hypertensive and normotensive scenarios. For the *in vitro* studies, the Shellpa mechanical stretch system was used as it provided convenient analysis of the effect of CS alone that was exerted on the ECs in a well-controlled setting.

It was hypothesised that hypertension may impose changes in Aβ burden and/or APP processing of the SHR hypertensive model and that CS may mediate alterations in endothelial cell functions in terms of APP expression, eNOS expression and inflammation in the *in vitro* model of the EC line representative of the ECs in the BBB.

2 Materials and methods

2.1 Animals

Male WKY (n=3) and SHR (n=3) models were obtained from the Animal Research Centre, Perth, Western Australia. All experimental procedures were approved by the Macquarie University Animal Ethics Committee and were carried out in accordance with the guidelines of the National Health and Medical Research Council of Australia.

Animals were sacrificed (urethane anaesthesia, 1.3 g/kg i.p. followed by intravenous injection of 1 ml of 3 M potassium chloride) and the brains were harvested and stored fresh at -80^0C. The hippocampus (HC) and frontal cortex (FC) regions of the brains were surgically excised from the brain. The HC is located between the thalamus and mid brain between the stereotaxic coordinates bregma: -1.9 mm to -5.2 mm and interaural +7.1 mm to +3.8 mm in the coronal sections (Figure 2; Paxinos and Watson, 2007). FC is located between the stereotaxic coordinates bregma: 4.68mm to 2.76 mm and interaural 13.68 mm to 11.76mm (Figure 3; Paxinos and Watson, 2007). The brain tissue samples were processed to be analysed using western blotting as described in section 2.2.4.

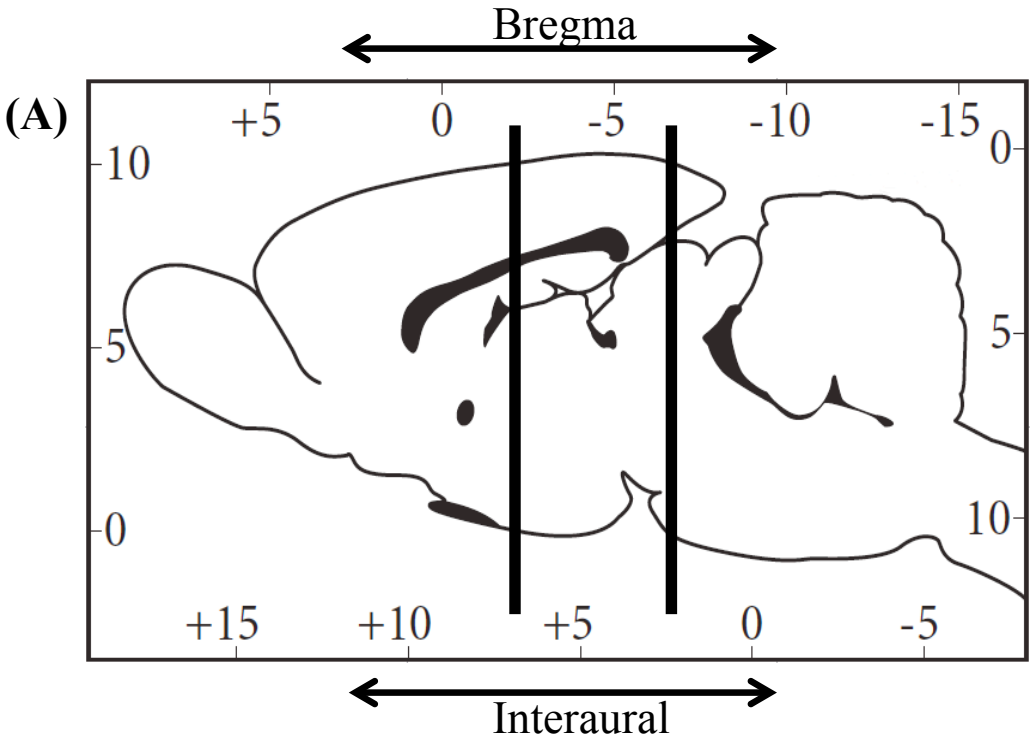

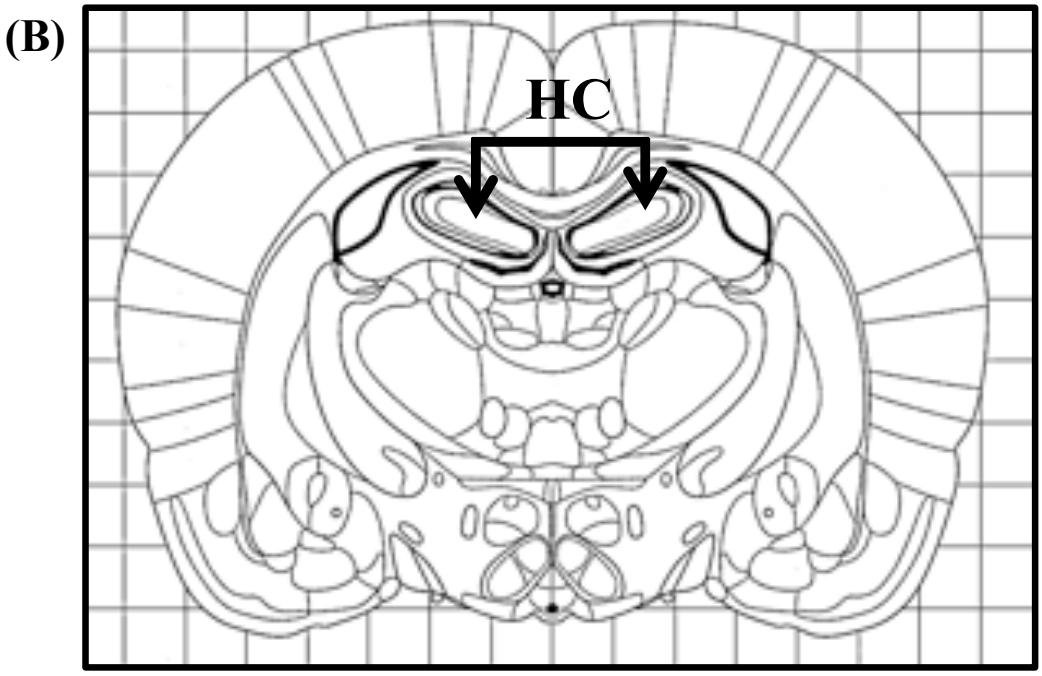

Figure 2. Diagrammatical representation of HC region of the rat brain in a representative coronal section. (A) The two vertical lines indicate approximate stereotaxic coordinates of the HC; bregma: -1.9 mm to -5.2 mm and interaural +7.1 mm to +3.8 mm. **(B)** represents a coronal section including the HC with the arrowheads pointing to the HC region (Modified from Paxinos and Watson, 2007). Abbreviations: HC, hippocampus.

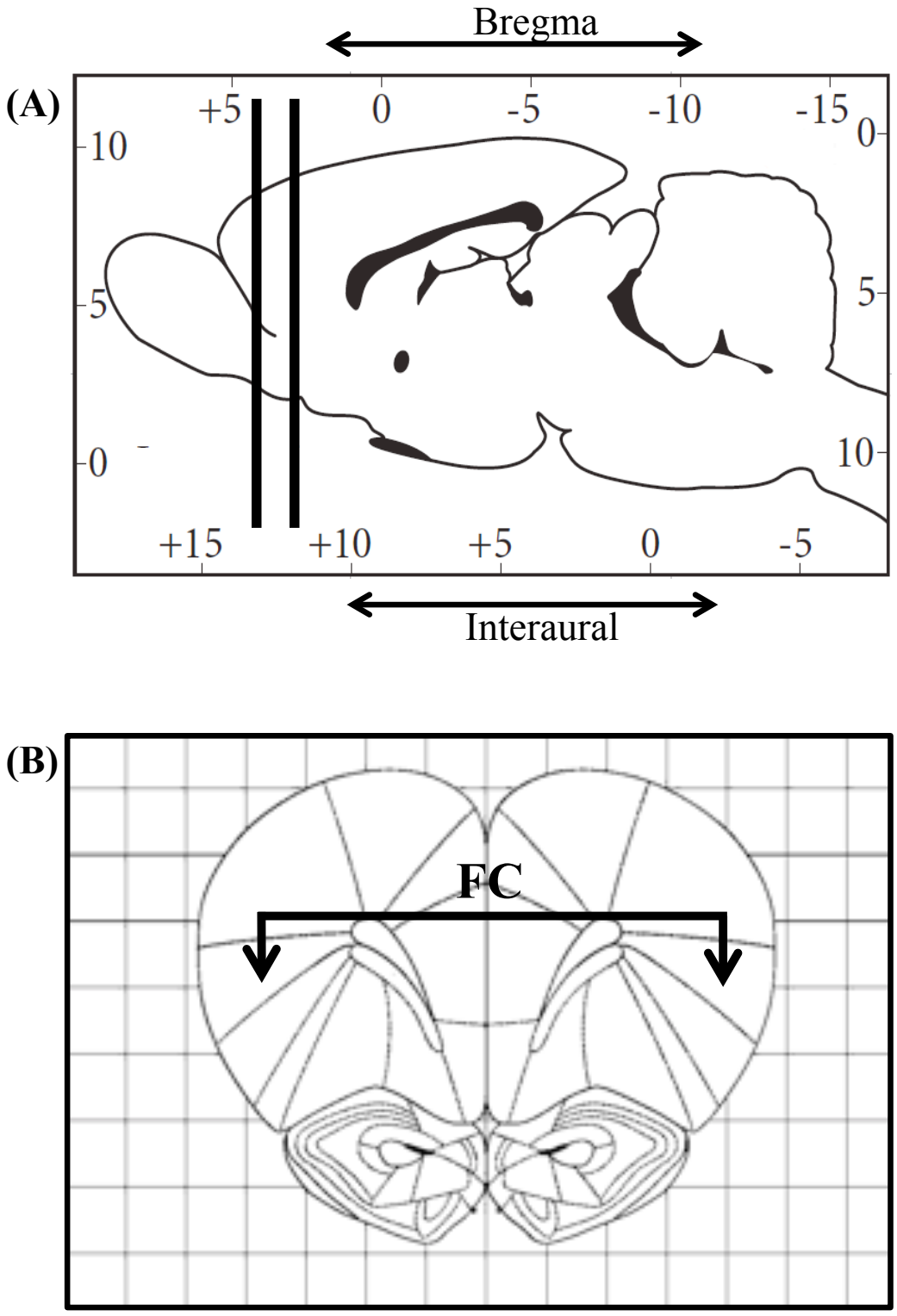

Figure 3. Diagrammatical representation of FC region of the rat brain in a representative coronal section. (A) The two vertical lines indicate approximate stereotaxic coordinates of the FC; bregma: 4.68mm to 2.76 mm and interaural 13.68 mm to 11.76mm. **(B)** represents a coronal section including the FC with the arrowheads pointing to the FC region (Modified from Paxinos and Watson, 2007). Abbreviations: FC, frontal cortex.

2.2 CS in HCMEC-SV40

2.2.1 Cell culture conditions and cell maintenance

Immortalized HCMEC-SV40 purchased from Applied Biological Materials Inc. were maintained in M199 media (Sigma-Aldrich) supplemented with 10% fetal bovine serum and 1% penicillin/streptomycin at 37^0C with an atmospheric humidity of 5% CO_2.

Upon achieving a cellular confluency of 80-90%, the cells were passaged into new flasks or seeded on fibronectin-coated (375 μg/mL) silicon chambers 24 hours prior to stretching at a seeding density of $8x10^5$ cells/mL. In passaging, the cells were briefly washed with warm phosphate buffered saline (PBS; Life Technologies) followed by trypsinisation with 0.05% trypsin-ethylene diamine tetraacetic acid (EDTA; Invitrogen). After adding M199 to inactivate the trypsin-EDTA, cells were stained with trypan-blue and counted using the Countess automated cell counter (Life Technologies) according to the manufacturer's protocol prior to seeding. Cell viability data were also obtained from the automated cell counter. Photographs of the cells were taken before and after 18 hours of stretching using phase contrast microscopy (Nikon Ecplise TS100). Passages 14-19 were used for all experiments.

2.2.2 Stretching apparatus and conditions

Cells were subjected to uni-axial CS as previously described (Naruse et al., 1998b), using the ShellPa stretch System (Menicon Life Science, B-Bridge International) mounted in an incubator at 37^0C with an atmospheric humidity of 5% CO_2. The silicon chambers were autoclaved and sterilised by soaking in 12.5% bleach for 2.5 hours, in 70% ethanol for 30 minutes followed by 1 hour of ultraviolet exposure in a tissue culture hood. The silicon chambers have 200 μm thick transparent bottoms with sidewall thickness of 400 μm to prevent contracting at their bottom center (Suzuki et al., 1997). The chambers were mounted in the ShellPa stretching apparatus where one end of the chamber is fixed and the other connected to an actuator operated by compressed air (Figure 4). The actuated arm was set to apply a stretch ratio of 5%, 10% or 20% at a frequency of 60 cycles/min (1 Hz) for 18 hours in all experiments (Figure 4, Figure 5 & Figure 6).

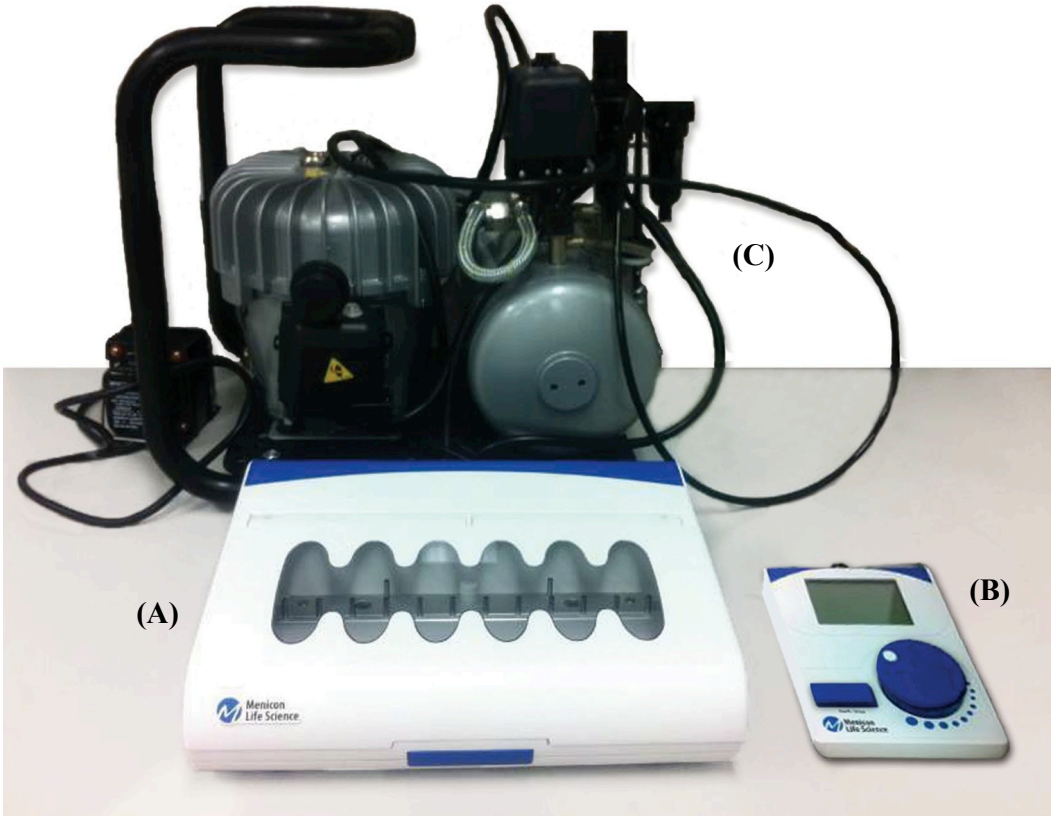

Figure 4. The ShellPa cell stretching system. The ShellPa system comprises three main parts, **(A)** main unit **(B)** controller and **(C)** air compressor. Cell-seeded silicon chambers are placed within the main unit, which is placed in an incubator with desired culture conditions. The stretch frequency can be adjusted using the controller unit.

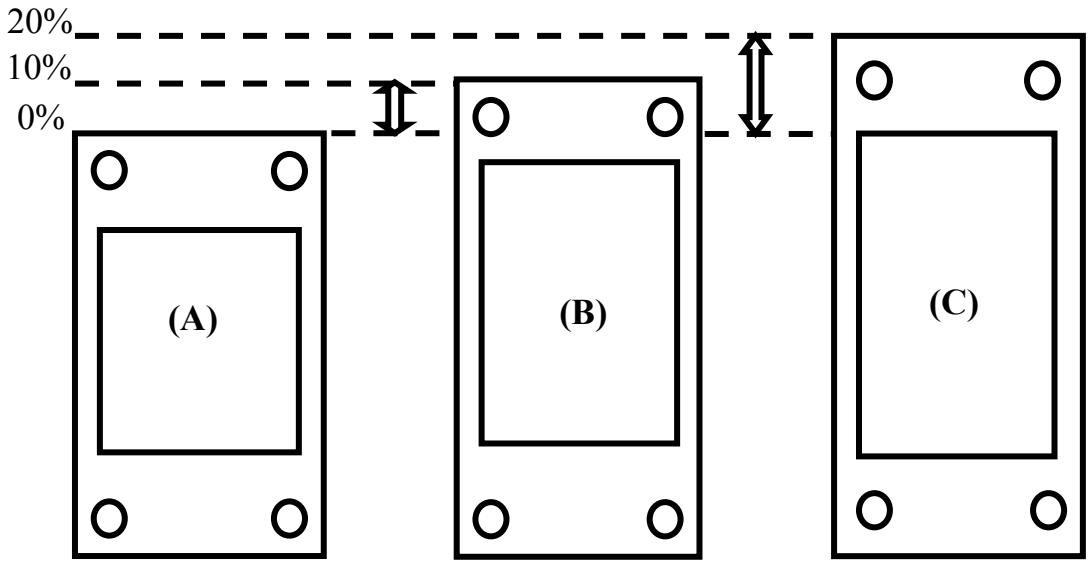

Figure 5. Diagrammatic representation of stretch of the silicon chambers. The degree of stretch (%) is noted as relative elongation of the chamber. **(A)**, **(B)** and **(C)** represent 0%, 10% and 20% stretch respectively. Adapted from (Menicon Life Science, ShellPa Mechanical stretch system product brochure, http://menicon-lifescience.com).

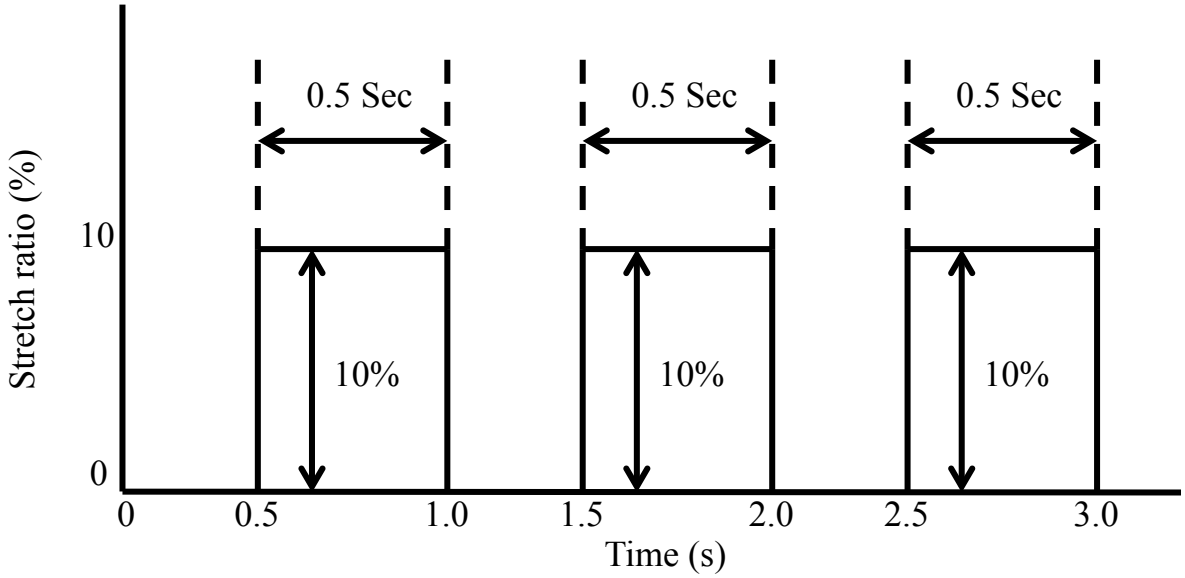

Figure 6. A representative wave pattern produced by the ShellPa mechanical stretching system. The illustrated wave pattern shows a wave pattern with a stretch ratio of 10% and a stretch frequency of 1 Hz.

2.2.3 Real-time quantitative reverse transcription polymerase chain reaction (RT-qPCR)

Total RNA was extracted using TRIZOL (Invitrogen) according to the manufacturer's instructions after stretching and was normalized to 100 ng/μL using the Nano-Drop spectrophotometer. A 260/280 ratio of approximately 1.8-1.9 was used to ensure the RNA quality. Total RNA of 0.4 μg was then reverse transcribed using the SuperScript VILO complementary deoxyribonucleic acid (cDNA) synthesis kit (Life Technologies) according to the manufacturers protocol. Negative control samples (RT-) were prepared by substituting the reverse transcriptase with dH_2O as a control for genomic contamination. This was followed by real-time qPCR using TaqMan® gene expression assays and TaqMan® gene expression master mix (Applied Biosystems) according to the manufacturers protocol. The qPCR program comprised 120 s at 50^0C (incubation for optimal activity of uracil-DNA glycosylase), 600 s at 95^0C (optimal AmpliTaq Gold, Ultra Pure enzyme activity), 15 s at 95^0C (denaturation) followed by 60 s at 60^0C (annealing and extension) repeated for 40 cycles.

The following pre-designed primer-probe TaqMan® assays by Life Technologies that have been validated were used: APP (Hs00169098_m1), eNOS (Hs01574659_m1), Glyceraldehyde 3-phosphate dehydrogenase (GAPDH) (Hs99999905_m1), beta-2 microglobulin (β2m) (Hs00984230_m1). Relative changes in mRNA levels were determined by the comparative ΔΔCT method using human β2m and GAPDH levels as the reference genes (Schmittgen and Livak, 2008).

2.2.4 Western blotting

After 18 hours of stretching, the media was aspirated and the cells were briefly washed twice with cold PBS followed by addition of radioimmunoprecipitation assay (RIPA) lysis buffer (50 mM Tris-hydrochloride, pH 7.4, 150 mM sodium chloride, 5 mM EDTA, 10mM sodium fluoride, 10 mM sodium pyrophosphate, 1% IGEPAL CA-630, 0.5% sodium deoxycholate, 0.1% sodium dodecyl sulfate (SDS) with protease inhibitor (10

μL/mL) added immediately prior to lysis. Cells were then harvested by scraping and the lysates were centrifuged at 14 000 x g for 15 minutes at 4^0C after sonication (twice for 15 seconds). The protein content was quantified using bicinchoninic acid assay (Pierce) according to manufacturers protocol prior to electrophoresis of both the cell as well as tissue lysates.

In the case of the rat brain tissue, samples were lysed and the protein bands were transferred to polyvinylidene difluoride-plus (PVDF) membranes (Life Technologies) after resolution on the SDS- polyacrylamide gel electrophoresis (PAGE) electrophoresis as previously described (Gupta et al., 2012; Wan et al., 2012). Equal amounts of cell lysates (20-50 μg) were mixed with 4x NuPAGE sample buffer (Life Technologies) and were heated at 44^0C (for APP) or 80^0C (for eNOS) for 10 minutes before loading on 10% or 4-12% NuPAGE® Novex® Bis-Tris gels. The PVDF membranes were blocked in 5% skim milk buffer in tris buffered saline-Tween (TBST; 20 mM tris-HCl, pH 7.4, 0.5 M NaCl, 0.1% Tween 20) to be probed with anti-APP (1: 1000; Covance), anti-eNOS (1: 1000; Cell Signaling Technologies), anti-ICAM-1 (1: 1000; R & D), anti-GAPDH (1: 1000) or anti-actin (1: 1000; R & D) antibodies followed by incubating with secondary antibodies (1:2000; R & D) as previously described (Wan et al., 2012). The western blot membranes were cut to exclude higher molecular weight bands in order to enhance the contrast and improve the detection of low molecular weight amyloid β peptide bands (usually weak bands)- since the main focus of this project was on the quantification of amyloid β deposition in the rat brains. The blots were developed using Clarity™ Western ECL Substrate Kit (Bio-Rad) according to the manufacturers protocol. The protein bands were quantified using the Image Lab 5.1 software within the linear range of detection as % change in density or relative % control (Bio-Rad Labs. Inc).

2.3 Statistical data analysis

2.3.1 Animal work

The graphs represent mean ± standard deviation (SD) from n=3 for both WKY and SHR. Two-way ANOVA was performed with PRISM version 6.0e with post-hoc Bonferroni-corrected multiple comparison tests.

2.3.2 CS in HCMEC-SV40

The graphs represent mean ± standard deviation (SD) from n=1 with 6 replicates for 10 %, and n=3 with 2 replicates for 0 %, 5 % and 20 %. One-way ANOVA was performed with PRISM version 6.0e post-hoc Bonferroni-corrected multiple comparison tests.

3 Results

3.1 APP processing in a rodent model of hypertension

The APP processing in different regions of the brains of SHR and WKY rats were investigated. As shown on the representative western blot, the Aβ oligomer that was resolved approximately at 25 kDa was increased in SHR HC and FC regions (Figure 7). Densitometric analysis revealed that the Aβ oligomer formation was significantly higher ($P<0.01$ for HC, $P<0.001$ for FC; $n = 3$) in SHR compared to WKY normotensive rats for both HC and FC regions (Figure 7).

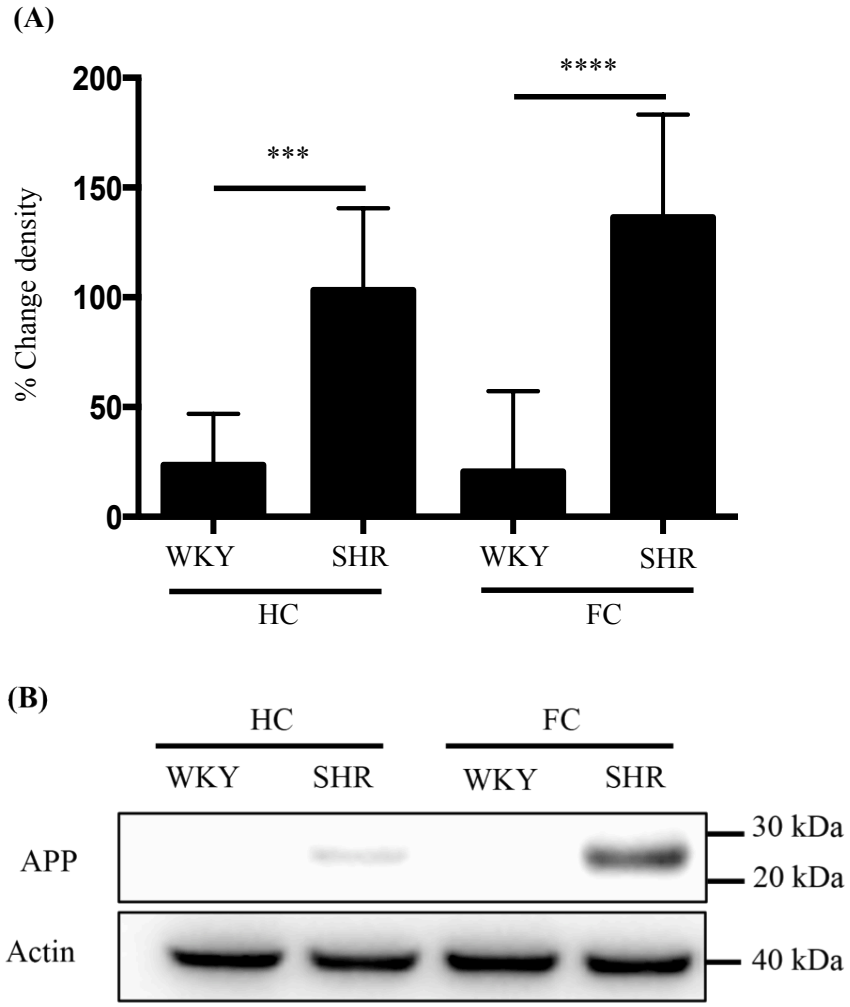

Figure 7. APP processing in SHR and WKY HC and FC regions. (A) Densitometric analysis of % change of the band intensity in SHR relative to WKY. Data shown represents mean ± SD for SHR (n=3); ***P<0.001, P****<0.0001 compared to WKY (n=3) by two-way ANOVA with post-hoc Bonferroni-corrected multiple comparison tests. **(B)** Representative western blots demonstrating altered APP processing (upper panels) in hippocampal and frontal cortical regions of WKY and SHR. The lower portion of the membrane was probed with Actin (lower panels) for normalization. Protein standards for 40, 30 and 20 kDa are shown. Abbreviations: APP, Amyloid precursor protein; FC, frontal cortex; HC, hippocampus; SHR, spontaneously hypertensive rat; WKY, Wistar-Kyoto rat.

3.2 Effect of CS on endothelial function in HCMEC-SV40

3.2.1 CS differentially regulates APP mRNA expression at different magnitudes of stretch

The results of the study of the SHR and WKY rat models indicated that APP processing is altered significantly in hypertensive rats, suggesting that the pulsatile nature of the vasculature may play a role in AD pathology. To explore this in terms of CS in an *in vitro* setting, the mRNA expression of APP was first investigated.

No genomic DNA contamination was detected in the RT- controls. The mRNA expression of APP was measured after exposing the HCMEC-SV40 to 5% and 20% of CS (1 Hz over 18 hours) and compared to no stretch (0%). The mRNA expression of APP at 5% CS was significantly up-regulated compared to both the static control and the 20% CS condition ($P<0.0001$; Figure 8). In contrast, the 20% CS resulted in a significant down-regulation of APP mRNA expression compared to the static control and the 5% CS condition ($P<0.0001$; Figure 8).

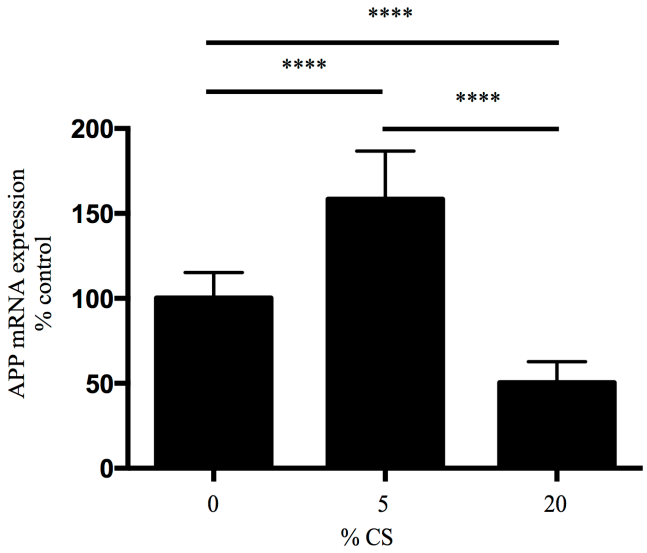

Figure 8. Effect of CS on APP mRNA expression in HCMEC-SV40. Real-time RTqPCR results of APP mRNA expression in HCMEC-SV40 after 18 h 0%, 5% or 20% CS at 1 Hz. Data shown represents mean ± SD % control (n=6 from a single passage); ****P<0.0001 by one-way ANOVA with post-hoc Bonferroni-corrected multiple comparison tests. Abbreviations: APP, Amyloid precursor protein; CS, cyclic stretch; HCMEC-SV40, human cerebral microvascular endothelial cells- Simian virus 40; mRNA, messenger ribonucleic acid; RTqPCR, quantitative reverse transcription polymerase chain reaction.

3.2.2 CS differentially regulates APP protein expression at different levels of CS

A differential expression pattern of APP at the transcriptional level was observed at 5% and 20% CS for 18 hours. To explore whether the mRNA expression coincided at the translational level, the protein expression of APP was quantified. Since the mRNA fluctuated at both 5% and 20% of CS, an additional intermediate stretching length of 10% was performed to observe whether there was a threshold effect.

The densitometric analysis of protein expression of APP showed that APP expression was significantly higher at 10% of CS compared to the static control ($P<0.01$; Figure 9). The APP protein expression was slightly, but not significantly higher than the static control at 5% and 20% CS (Figure 9). The increasing APP levels at corresponding CS conditions were also indicated by the representative western blot (Figure 9).

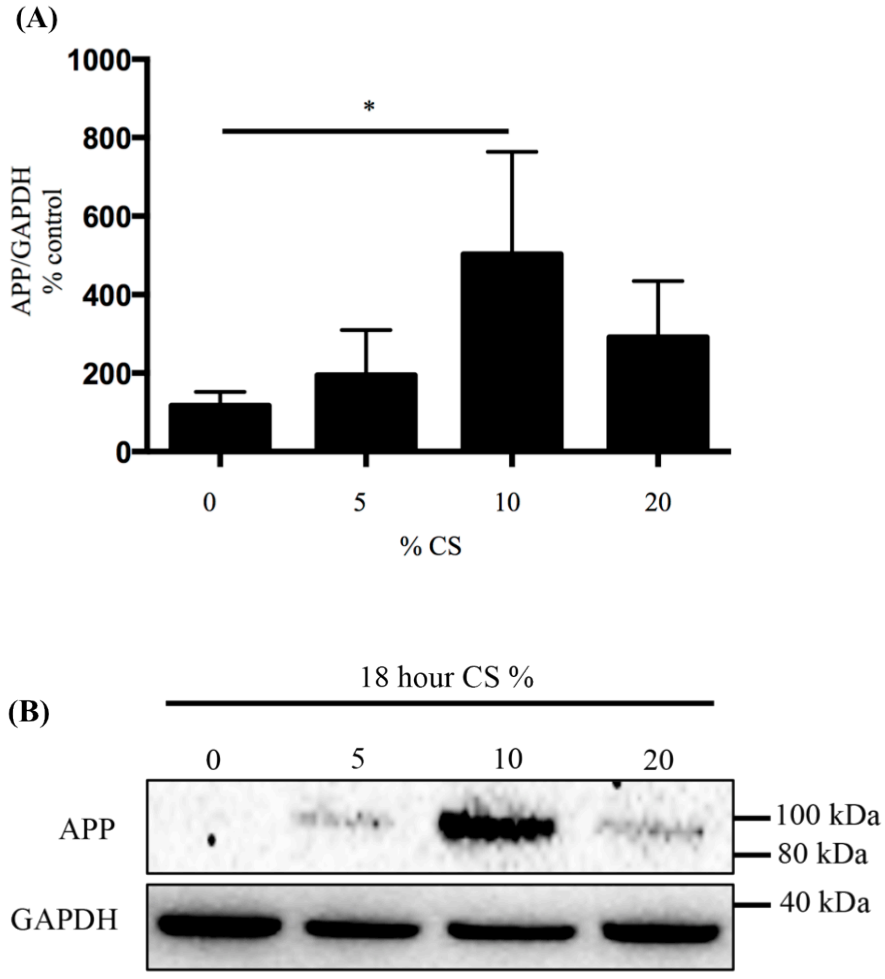

Figure 9. Effect of CS on APP protein expression in HCMEC-SV40. (A) Densitometric analysis of % control of the band intensity in HCMEC-SV40 after 18 hours of 0%, 5%, 10% or 20% CS at 1 Hz. Data shown represents mean ± SD, (n=1 with 6 replicates for 10 %, n=3 with 2 replicates for 0%, 5% and 20%); *P<0.01 by one-way ANOVA with post-hoc Bonferroni-corrected multiple comparison tests. **(B)** Representative western blots demonstrating altered APP expression (upper panels) in HCMEC-SV40 after 18 h of 0%, 5%, 10% or 20% CS at 1 Hz. The lower portion of the membrane was probed with GAPDH (lower panels) for normalization. Protein standards for 100, 80 and 40 kDa are shown. Abbreviations: APP, Amyloid precursor protein; CS, cyclic stretch; GAPDH, Glyceraldehyde 3-phosphate dehydrogenase; HCMEC-SV40, human cerebral microvascular endothelial cells- Simian virus 40.

3.2.3 CS suppresses eNOS mRNA expression

The enzyme eNOS, which is expressed constitutively in ECs and produces the vasodilator NO in the endothelium is known to modulate the expression of APP (Austin et al., 2010). To explore the effects of CS on eNOS in the HCMEC-SV40 cell line, first at transcriptional level, the mRNA expression of eNOS was measured at two different CS conditions, 5% and 20%. Cells were subjected to 18 hours of 5% or 20% CS and compared to static conditions.

No genomic DNA contamination was detected in the RT- controls. The mRNA expression at both 5% and 20% of CS in HCMEC-SV40 was suppressed significantly compared to the static control (P<0.0001; Figure 10).

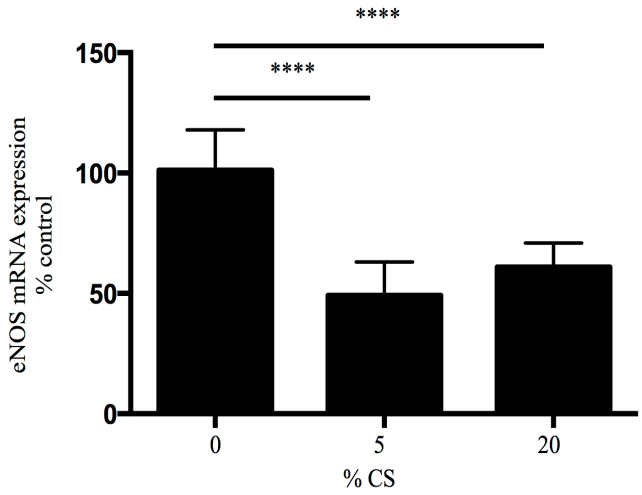

Figure 10. Effect of CS on eNOS mRNA expression in HCMEC-SV40. Real-time RTqPCR results of eNOS mRNA expression in HCMEC-SV40 after 18 h 0%, 5% or 20% CS at 1 Hz. Data shown represents mean ± SD % control (n=6 from a single passage); ****P<0.0001 by one-way ANOVA with post-hoc Bonferroni-corrected multiple comparison tests. Abbreviations: CS, cyclic stretch; eNOS, endothelial nitric oxide synthase; HCMEC-SV40, human cerebral microvascular endothelial cells- Simian virus 40; mRNA, messenger ribonucleic acid; RTqPCR, quantitative reverse transcription polymerase chain reaction.

3.2.4 CS suppresses eNOS protein expression

Given that the mRNA expression of eNOS was suppressed by 18 hours of CS at both 5% and 20%, it was next investigated whether the mRNA down-regulation was corroborated at the protein expression level. Since the mRNA was down-regulated at both 5% and 20% of CS, an additional intermediate stretching length of 10% was performed to observe if it was otherwise at that CS extension.

The total eNOS protein expression was measured after the cells were subjected to 18 hours of CS at 5%, 10% or 20%. Concordant with the mRNA expression results (Figure 10), protein expression after 18 hours of CS of HCMEC-SV40 at 5%, 10% and 20% was significantly suppressed compared to the static control (P<0.0001) as indicated by densitometric analysis of the protein bands and the representative western blot (Figure 11).

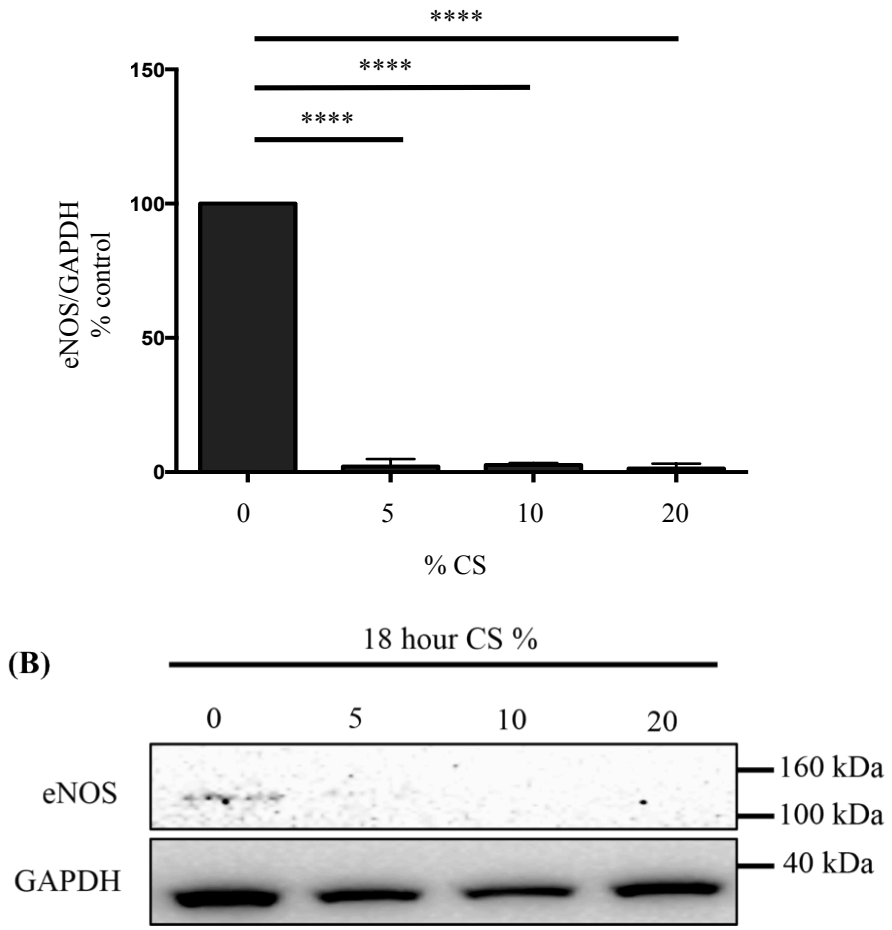

Figure 11. Effect of CS on eNOS protein expression in HCMEC-SV40. (A) Densitometric analysis of % control of the band intensity in HCMEC-SV40 after 18 h of 0%, 5%, 10% or 20% CS at 1 Hz. Data shown represents mean ± SD, (n=1 with 6 replicates for 10 %, n=3 with 2 replicates for 0%, 5% and 20%); ****P<0.0001 by one-way ANOVA with post-hoc Bonferroni-corrected multiple comparison tests. **(B)** Representative western blots demonstrating decreased eNOS protein expression (upper panels) in HCMEC-SV40 after 18 h of 0%, 5%, 10% or 20% CS at 1 Hz compared to the control (0% CS). The lower portion of the membrane was probed with GAPDH (lower panels) for normalization. Protein standards for 160, 100 and 40 kDa are shown. Abbreviations: CS, cyclic stretch; eNOS, endothelial nitric oxide synthase; GAPDH, Glyceraldehyde 3-phosphate dehydrogenase; HCMEC-SV40, human cerebral microvascular endothelial cells- Simian virus 40.

3.2.5 CS regulates the expression of ICAM-1

To explore the possible involvement of cellular inflammation, the protein expression of ICAM-1, a common endothelial inflammatory marker was investigated.

The ICAM-1 protein expression was analysed using densitometry after the cells were subjected to 18 hours of CS at 5%, 10% or 20%. ICAM-1 expression after 18 hours of CS of HCMEC-SV40 at 10% was significantly augmented compared to the static control, 5% or 20% CS conditions (P<0.01; Figure 12). ICAM-1 protein expression relatively, but not significantly increased at 5% and 20% CS compared to the static control (Figure 12). These changes in ICAM-1 expression were also consistent with the representative western

blot (Figure 12).

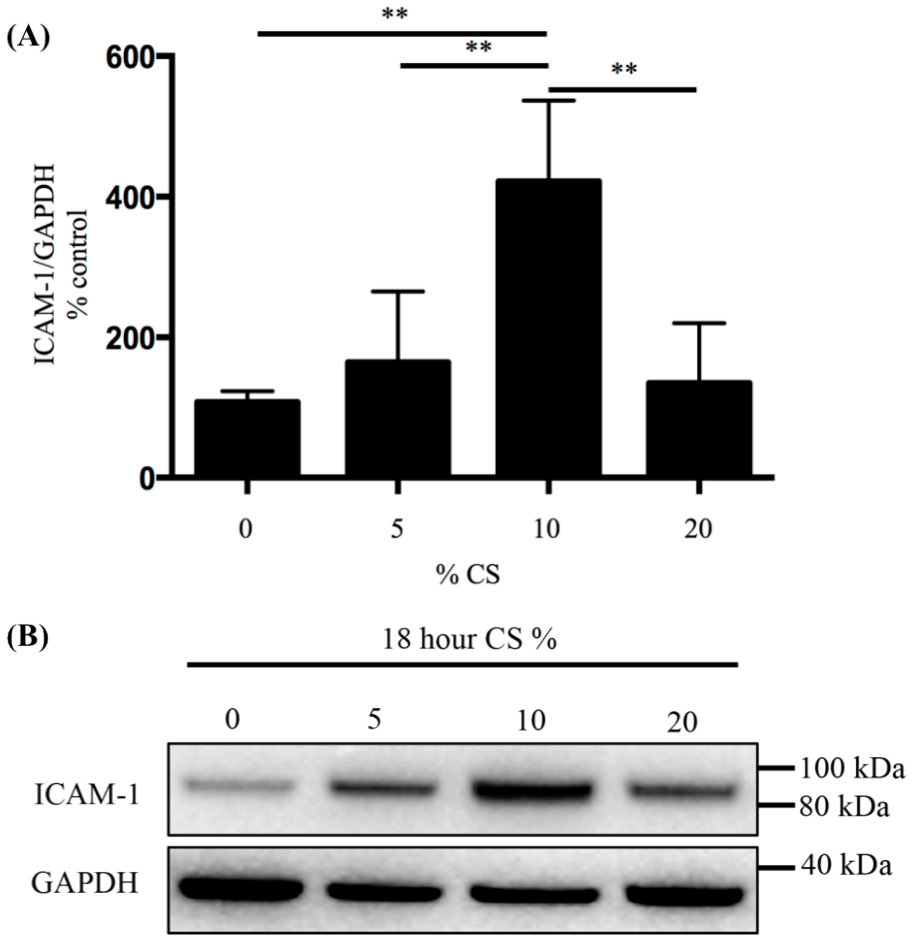

Figure 12. Effect of CS on ICAM-1 protein expression in HCMEC-SV40. (A) Densitometric analysis of % control of the band intensity in HCMEC-SV40 after 18 h of 0%, 5%, 10% or 20% CS at 1 Hz. Data shown represents mean ± SD, (n=1 with 6 replicates for 10 %, n=3 with 2 replicates for 0%, 5% and 20%); **P<0.01 by one-way ANOVA with post-hoc Bonferroni-corrected multiple comparison tests. **(B)** Representative Western blots demonstrating altered ICAM-1 expression levels (upper panels) in HCMEC-SV40 after 18 h of 0%, 5%, 10% or 20% CS at 1 Hz. The lower portion of the membrane was probed with GAPDH (lower panels) for normalization. Protein standards for 100, 80 and 40 kDa are shown. Abbreviations: CS, cyclic stretch; GAPDH, Glyceraldehyde 3-phosphate dehydrogenase; ICAM-1, intercellular cell adhesion molecule-1; HCMEC-SV40, human cerebral microvascular endothelial cells- Simian virus 40.

3.2.6 Effect of CS on cell viability and morphology

To confirm that the cells were still viable after the stretching conditions used in the experiments, the cell viability was measured using trypan-blue exclusion. HCMEC were subjected to 18 hours of CS at 5%, 10% or 20% prior to obtaining the live and dead cell counts. Additionally, photographs of the cells before and after stretching were obtained to examine the cell morphology using phase contrast microscopy (Figure 14).

The cell viability was not significantly affected by 18 hours of CS either at 5% or 20% in HCMEC-SV40 compared to the static control (Figure 13). The cell morphology was comparable to that of static control under each condition. However, increased cell detachment was observed under all stretching conditions (Figure 14).

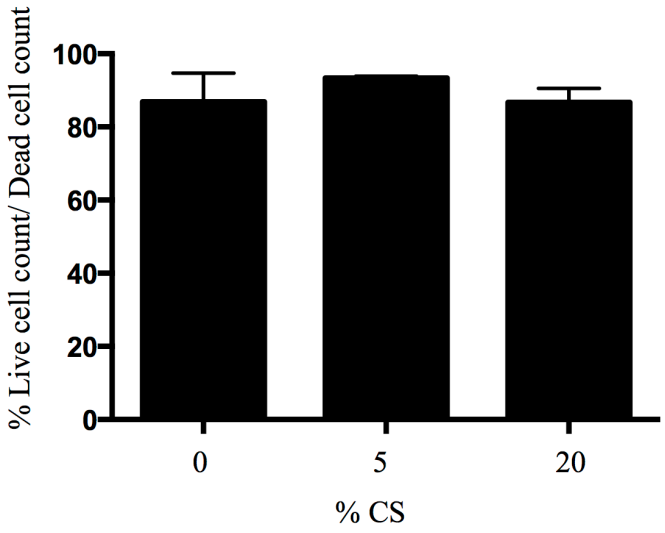

Figure 13. The effect of CS on cell viability of HCMEC-SV40. Cell viability of HCMEC-SV40 after 18 hours of CS at 5% or 20% by trypan blue exclusion as % live cell count/dead cell count. Abbreviations: CS, cyclic stretch; HCMEC-SV40, human cerebral microvascular endothelial cells- Simian virus 40.

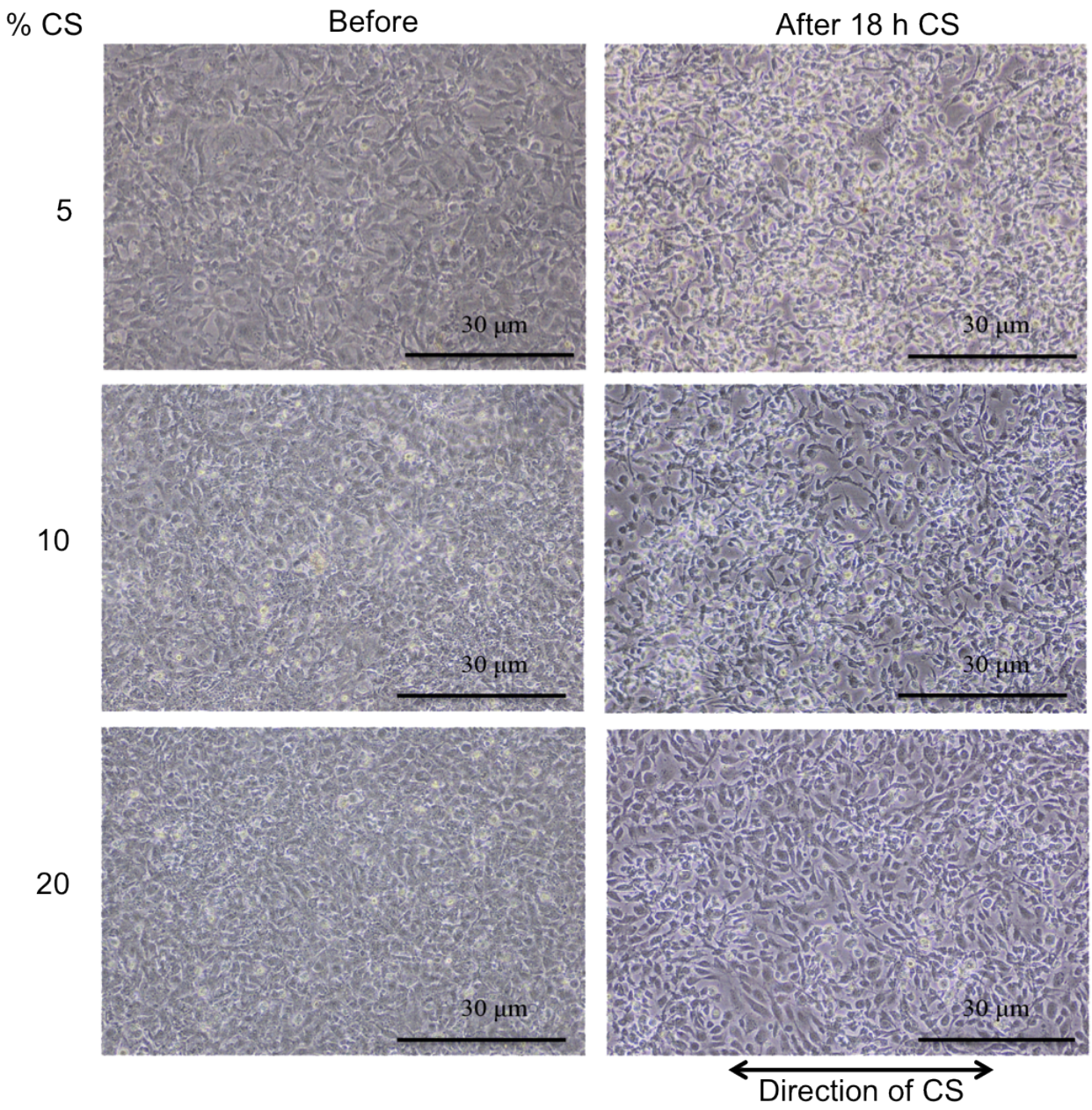

Figure 14. Effect of CS on the morphology of HCMEC-SV40. Phase contrast micrographs of the HCMEC-SV taken before and after 18 hours of 5%, 10% or 20% CS. The direction of CS was horizontally uni-axial as indicated. The corresponding stretch % is shown on the left. Abbreviations: CS, cyclic stretch; human cerebral microvascular endothelial cells- Simian virus 40.

4 Discussion

4.1 APP processing in a rodent model of hypertension

4.1.1 Amyloid deposition and Aβ oligomerisation in AD

One of the major findings of this study was that the amyloid burden in hypertensive rats was significantly higher than that in normotensive controls. Amyloid deposits have been observed in a number of postmortem tissue specimens including the brain, kidneys, spleen and liver as "lardaceous" or "waxy" substances in as early as the 1700's (Virchow, 1860; Glenner and Wong, 1984). Due to the starch-like appearance of these deposits, they were misidentified as starchy material and incorrectly named as 'amyloid' (literally meaning 'starch-like') (Toyama and Weissman, 2011; Virchow, 1860). However, it is now known that amyloids are self-propagating protein aggregates that are rich in β-sheets (Toyama and Weissman, 2011). They can form amyloid-like aggregates that are similar in structure, which are associated with diseases including AD (Toyama and Weissman, 2011). Amyloid deposits, which are a hallmark of AD, are mainly composed of Aβ fragments (Glenner and Wong, 1984).

Aβ peptides are proteolytic cleavage products of APP, which is a transmembrane protein expressed in a number of cell types including ECs (Selkoe, 2001; Masters and Selkoe, 2012). APP is cleaved and processed by a number of enzymes (Rajadas et al., 2013; Xia et al., 1997; Wan et al., 2012; Qia et al., 2014; Austin et al., 2013a). These include α-secretases such as, ADAM-family enzymes such as ADAM9, ADAM10 and ADAM17, β-secretases such as BACE1 and γ-secretases such as presenilin 1 or 2 (Rajadas et al., 2013; Xia et al., 1997; Wan et al., 2012; Qia et al., 2014; Austin et al., 2013a). Importantly, mutations of both *APP* and *presenilin* genes have been shown to be associated with familial AD, suggesting APP cleavage plays a critical role in the pathogenesis of AD, supporting the amyloid hypothesis (Scheuermann et al., 2001; Xia et al., 1997). APP cleavage by BACE1 via the amyloidogenic pathway (Figure 1) results in the formation of Aβ peptides such as Aβ40 and Aβ42, which could self-aggregate to form Aβ oligomers, fibrils, which could subsequently contribute to AD-plaque formation (Scheuermann et al., 2001; Gouras et al., 2010).

The present study demonstrated that in SHR HC and FC regions, the Aβ oligomerisation was higher as compared to normotensive WKY ($P<0.001$ for HC, ~ 5-fold; $P<0.0001$ for FC, ~ 6-fold; Figure 7). This was clearly reflected in the higher intensity of bands in western blot approximately resolved at 25 kDa, which were shown to be significantly higher by densitometric analysis ($P<0.001$ for HC, $P<0.0001$ for FC; Figure 7). Oligomerisation of Aβ leads to the formation of Aβ fibrils, and a number of different soluble oligomer species have been detected using SDS-PAGE and western blotting ranging from 4-25 kDa (Cleary et al., 2005; Ahmed et al., 2010; Masters and Selkoe, 2012; Pryor et al., 2012). This was consistent with the results of the present study showing an oligomer approximating to 25 kDa (Figure 7).

These results were obtained by SDS-PAGE coupled with western blotting. Amongst the many techniques in detecting Aβ, SDS-PAGE is reported to be the most commonly utilised (Pryor et al., 2012). The conditions of the assay may lead to aggregation of Aβ (Pryor et al., 2012). For example, the anionic micelles formed by SDS are known to separate the bands and induce non-native Aβ species (Sureshbabu et al., 2009). This was evident as

Aβ42 prepared in PBS exhibited monomer and trimer structures at ~13.5 kDa and ~18 kDa respectively, which were shown to be appearing at 20 and 50 kDa after the addition of 1.5 mM SDS to the samples (Sureshbabu et al., 2009). It was proposed that the addition of 1.5 mM SDS resulted in a partial helical structure in Aβ42, which was hydrophobic (Sureshbabu et al., 2009). The hydrophobicity induced by the addition of 1.5 mM SDS was attributed for the aggregate formation (Sureshbabu et al., 2009). Regardless of whether bands were representative of the size or the extent of hydrophobicity, the intense appearance of the bands provided qualitative evidence that the SHR had higher amyloid burden than the WKY rats. Native-PAGE analysis where native protein structures are relatively preserved will further help confirm the endogenous origin of these high molecular weight aggregates (Pryor et al., 2012).

The results indicated that Aβ is accumulated within the brain of the SHR rats (Figure 7) implying that hypertension is associated with abnormal APP processing, expression or clearance from the brain, thus leading to accumulation of Aβ, which is discussed in detail in section 4.1.2.

4.1.2 AD, hypertension and haemodynamics

Hypertension is a major factor amongst the many risk factors that are concomitant with AD (Arendash et al., 1999; Langbaum et al., 2012; Mitchell et al., 2011; Meng et al., 2014). In line with this, the results of the present study demonstrated a higher brain Aβ burden in the aged SHR hypertensive model compared to the normotensive WKY model (Figure 7). Similar effects were detailed in a number of recent studies (Kurata et al., 2014b, 2014a; Schreiber et al., 2014; Qia et al., 2014). The representative rat model of chronic hypertension, stroke, and progressive dementia, SHR-stroke resistant (SHR-SR) after transient middle cerebral artery occlusion (tMCAO) showed age-dependent positive intracellular and extracellular Aβ staining in ipsilateral and contralateral cerebral cortex and hippocampus at 6, 12, and 18 months of age (Kurata et al., 2014b). SHR-SR-tMCAO rats were treated with a low and high dose of telmisartan (Kurata et al., 2014b). Telmisartan, which a pleiotrophic metabo-sartan, with anti-neuroinflammatory, anti-neurotoxic and blood pressure (BP) lowering effects, dose dependently decreased the elevated intracellular and extracellular Aβ in SHR-SR-tMCAO (Kurata et al., 2014b). Additionally, the high-dose telmisartan induced the expected significant BP lowering effect (Kurata et al., 2014b). Further supporting these data, age dependent increases in cortical extracellular deposition of Aβ and APP expression were observed in non-transgenic spontaneously hypertensive stroke-prone rats (SHR-SP) compared to WKY rats (Schreiber et al., 2014). The deposition of Aβ was represented by lectin staining and plasma protein immunocytochemistry while the protein expression being evaluated using western blotting (Schreiber et al., 2014). In ocular hypertensive models of rat glaucoma, up-regulation of caspase-3-mediated APP cleavage in hypertensive retina relative to control retina has been reported (McKinnon et al., 2002). Consistently, another study showed significant increases in hippocampal Aβ42 coincident with elevated mRNA expression levels of RAGE and BACE-1 in SHR compared to WKY rats (Qia et al., 2014). The mRNA and protein expression of LRP-1 were down-regulated in contrast to APP, which were up-regulated (Qia et al., 2014). The mRNA was analysed using agarose gel electrophoresis while protein was analysed using western blotting (Qia et al., 2014). However, these differences did not reach a statistical significance (Qia et al., 2014). Nonetheless, these results, together with the other studies described, provided additional confirmatory evidence that altered APP processing and/or expression was associated with hypertension (Qia et al., 2014; Kurata et al., 2014b; McKinnon et al., 2002; Schreiber et

al., 2014).

The involvement of hypertension in AD could be attributed to haemodynamic factors as according to "peripheral sink theory" where blood flow is eventually involved in the clearance of APP-derived Aβ peptides (Wang et al., 2006b; Lee and Landreth, 2013). This was evidenced by the studies showing that haemodynamic factors such as pulsatility index and pulse pressure were positively correlated with AD (Stefani et al., 2009; Nation et al., 2013). These two factors are independent markers of vascular stiffness (Tan et al., 2012; Nation et al., 2013; Petersen et al., 1995; Mitchell et al., 2011). Vascular stiffness has been shown to be associated with hypertension and reported to play a role in initiating the cognitive deficits in AD (Mitchell et al., 2011; Ng et al., 2012; Laurent et al., 2001; Hanon et al., 2005; Avolio et al., 2014; Tan et al., 2014; Wu et al., 2014; Langbaum et al., 2012).Together these findings suggested a possible role of mechanical effects of hypertension such as EC stretch in hypertension and its links with AD supported by the assumption that positive correlation with increased pulsatility index, pulse pressure and/or stiffness would presumably coincide increased mechanical stretch.

Importantly, mechanical stretch was shown to proportionally induce vascular stiffness *in vivo* and *in vitro* (Wu et al., 2014; Avolio et al., 1998). This was indicated by augmented collagen deposition or expression in hypertension-induced rats by angiotensin II infusion and in cultured aortic fibroblasts after being subjected to mechanical stretch respectively (Wu et al., 2014). Therefore, mechanical stretch may proportionally induce changes in vascular stiffness (Wu et al., 2014). Similar effects imposed by elevated mechanical stress were shown by fractal analysis of pressure-fixed aortic sections stained for elastin (Avolio et al., 1998). Increased loss of medial elastin function, which is characteristic of wall stiffness, was concomitant with cumulative effect of pulsations (Avolio et al., 1998).

Concordantly, the relationship between intra-arterial BP and mechanical stretch and wall stiffness was reported as early as in the 1970s (Toda et al., 1978). It was stated that increases in intra-arterial pressure imposed greater wall stiffness by establishing a length-tension relationship in helically cut strips of canine cerebral, coronary, mesenteric, renal, and femoral arteries after being stretched (Toda et al., 1978). Apart from the role of elevated mechanical stretch in systemic high BP, it was also demonstrated to be involved in intracranial or intraocular BP-related pathologies such as normal pressure hydrocephalus, traumatic brain injury and glaucoma. Interestingly, these pathologies are also related to AD-characteristics (McKinnon et al., 2002; Wostyn et al., 2008; Golomb et al., 2000). Notably, normal pressure hydrocephalus itself is a subtype of dementia, whilst traumatic brain injury is a risk-factor for AD (Kizu et al., 2001; Fleminger, 2003). These studies further stressed that mechanical stretch could be involved in the pathogenesis of AD.

The biochemical analysis of brain tissue of the SHR and WKY rat in the present study showed higher cerebral amyloid burden in hypertensive rats (Figure 7). This, along with the previous studies linking AD, stiffness and hypertension, consistently highlighted a possible role of mechanical stretch that may affect APP processing pathways.

In the light of the associations described above, between AD, high BP, vascular stiffness and mechanical stretch, the second major aim of this study sought to investigate a possible role of pulsatile CS on APP expression, using cell culture techniques to construct a highly controlled experiment to isolate the stretch phenomenon. The mechanical stretch was explored in terms of pulsatile CS in HCMEC-SV40 cell line as a way of scrutinising

whether mechanical stretch plays a role in APP processing or expression at the cerebral EC level.

4.2 Effect of CS on endothelial function in HCMEC-SV40

4.2.1 CS differentially regulates APP mRNA and protein expression at different magnitude of stretch

The results of the study of the SHR and WKY rat models indicated that APP processing was altered significantly in hypertensive rats. Additionally, elevated pulsatility index and pulse pressures were observed in both hypertension and AD (Stefani et al., 2009). Together with these observations and as discussed in section 4.1.2, a role of mechanical stretch was implicated in the pathophysiology of AD. To explore the effect of CS on the expression of APP in the brain endothelium, a cell line representative of ECs of the BBB was used.

The results indicated that the expression of APP is altered at different magnitudes of CS (Figure 8 & Figure 9). To the best of our knowledge, the direct effect of CS on the expression of APP in ECs associated with the BBB has not been studied before. However, there is considerable evidence to support these results that CS modified the expression of APP as outlined by studies elucidating the involvement of mechanical stretch in Aβ deposition and or APP expression (Wostyn et al., 2008; Loane et al., 2009; Amissah et al., 1998; Graham et al., 1995). Neuronal expression of APP was found to be significantly higher followed by traumatic brain injury or hypoxic ischaemic injury in human neonatal and adult brains, and animal models as shown by immunostaining and/or western blotting (Loane et al., 2009; Amissah et al., 1998; Graham et al., 1995; Bramlett et al., 1997). Additionally, hypertension-induced rabbits showed *APP* up-regulation (Ong et al., 2013). Thus, these findings together with the novel finding in this study showing increased APP expression up to 18 hours of 10% CS in HCMEC collectively suggested that mechanical stretch alters the expression of APP (Figure 8 & Figure 9). The down-regulation of APP at 20% CS (Figure 8) however may have been the result of higher susceptibility of mRNA degradation or decline in mRNA synthesis at higher stretch exposures as discussed in section 4.2.4.

An inverse correlation between APP expression and eNOS activity has been reported (d'Uscio et al., 2012; Austin et al., 2010, 2013b, 2013a). Over-expression of APP in Tg2576 mice has been demonstrated to lead to ED, thereby mitigating the endothelial vasorelaxation mediated by eNOS and to decrease eNOS activity with a concomitant decrease in bioavailable NO (d'Uscio et al., 2012). These findings were further extended by Austin et al. (Austin et al., 2010, 2013b, 2013a) elaborating a significant role of NO in modulating the expression of APP. In human brain microvascular ECs treated with the NOS inhibitor, N (G)-Nitro-L-Arginine Methyl Ester (L-NAME) for 3 days and in eNOS−/− mice, it was revealed that the expression of APP and BACE1, and Aβ levels were up-regulated (Austin et al., 2010). These effects in eNOS−/− mice were reversed by supplementation with NO by treating the animals with nitroglycerine, which resulted in a marked increase in cyclic guanosine monophosphate (cGMP) levels (Austin et al., 2013a). Since, cGMP, in addition to its other biological effects, is a known mediator of NO, these findings illustrated that NO-cGMP pathway is an important signaling pathway that could regulate the expression and processing of APP (Austin et al., 2013a).

In addition, other studies have elaborated that ED was associated with Aβ (Thomas et al., 1996; Crawford et al., 1998; Suo et al., 1998; Torre et al., 2013; de la Torre and Aliev,

2005). ED is characterised by diminished NO bioavailability due to the uncoupling of the enzyme, eNOS, whereby eNOS leads to the formation of reactive oxygen species (ROS) such as hydrogen peroxide and peroxynitrite, consequently leading to impaired vasodilation of blood vessels (Cheng et al., 2008; Landmesser et al., 2003; Huang et al., 2012). In 1997, Thomas et al. (Thomas et al., 1997) demonstrated that treating intact bovine cerebral arteries with Aβ40 resulted in ED. This was characterised by enhanced vasoconstriction and diminished vasodilation shown by measuring the % contraction and relaxation of the vessels with and without the Aβ40 treatment (Thomas et al., 1997). Aβ40-mediated vasoactive effects were reversed by antioxidants such as superoxide dismutase (SOD) indicating the possible involvement of oxidative stress, which will be expanded upon in section 4.2.3 (Thomas et al., 1997). Endothelial damage was further demonstrated by electron micrographs (Thomas et al., 1997). These vasoactive effects were suggestively due to an imbalance between NO and superoxide radicals, which in turn resulted in ED (Thomas et al., 1997). Another study also demonstrated similar vasoconstrictive effects *in vivo* utilising intra-arterial infusion of solubilised Aβ40 in rats (Suo et al., 1998). This study showed a decreased cerebral blood flow and cerebrovascular resistance measured using fluorescent microspheres, which was also suggested to be mediated via the same mechanism described in the previous study (Suo et al., 1998). These two studies along with many other studies have elucidated that cerebrovascular dysfunction was associated with APP expression and/or processing (de la Torre and Aliev, 2005; Austin et al., 2013b).

An intriguing feedback mechanism between NO bioavailability and Aβ can be illustrated by these studies along with the study of Rajadas et al. (Rajadas et al., 2013). This study showed that in the immortalised human hepatic EC line, Hep-3, fibrillar Aβ1–42 treatments of 5 and 10 μM for 12 hours caused an up-regulation of eNOS expression (Rajadas et al., 2013). This is consistent with a compensatory mechanism dependent on NO bioavailability as increased Aβ may trigger eNOS expression to compensate for the reduced levels of bioavailable NO (Rajadas et al., 2013). Further supporting this idea of a feedback mechanism, diminished endothelium-dependent vasodilatory effects due to a reduction in eNOS phosphorylation at serine1177, as a result of 24-48 hour treatment with Aβ25–35 in rat basilar arteries was also reported (Chisari et al., 2010). Consistently, 1 μM Aβ40 treatments attenuated the vasoconstrictive responses to noradrenaline in rat aortic rings while 5 μM Aβ40 showed opposite effects (Smith et al., 2004).

Due to the associations between APP and eNOS activity and expression, and the involvement of eNOS in hypertension (Wu et al., 2014; Ziegler et al., 1998b; Wood et al., 2013) it was next explored whether eNOS expression was altered with CS in a similar fashion.

4.2.2 CS suppresses eNOS mRNA and protein expression

The results showed that eNOS expression was significantly decreased with increasing stretch at both the transcription and translational level (Figure 10 & Figure 11). This is consistent with the findings of previous studies described in section 4.2.1, such that an increase in APP correlated with a decrease in eNOS expression at 18 hours of 10% CS. The results suggested that eNOS activity may be pivotal in regulating the expression of APP. This is because the increase in APP, with a decrease in eNOS expression levels indicated a possible compensatory mechanism dependent upon NO bioavailability, consistent with the findings of Rajadas et al. (Rajadas et al., 2013) that up-regulation of eNOS expression was correlated with an up-regulation of APP expression at the translational level in a hepatic EC line. However, whether these effects of CS on eNOS and

APP in the present study were directly interdependent or not have to be further investigated, which will be discussed in section 4.4.2.

In the milieu of the endothelium, eNOS serves as a major source of NO, which is an important second messenger and a mediator of vasodilation (Cheng et al., 2008; Bauer et al., 2010; Northcott et al., 2012). Although the direct effects of CS on cerebral eNOS expression have not been extensively studied, mechanical stretch effects on eNOS activation have been well studied (Hu et al., 2013; Spescha et al., 2014; Thacher et al., 2010; Takeda et al., 2006; Awolesi et al., 1995; Dancu et al., 2004). One of the prominent associations is the relationship between eNOS and BP regulation, which is well established, such that eNOS activation being central to alleviating BP insults to preserve the endothelium (Facemire et al., 2009; Northcott et al., 2012; Bauer et al., 2010; Wood et al., 2013; Cheng et al., 2012). This suggests that eNOS activation provides a negative feedback loop, counteracting elevated mechanical stretch in high BP by producing NO to mediate vasorelaxation (Facemire et al., 2009; Northcott et al., 2012; Bauer et al., 2010; Wood et al., 2013; Cheng et al., 2012). In line with this, the majority of the studies elucidating effects of CS on the expression and/or the activation of eNOS have shown that eNOS activation, eNOS mediated NO production and/or expression were up-regulated as a result of CS (Awolesi et al., 1995; Takeda et al., 2006; Hu et al., 2013; Ziegler et al., 1998a; Spescha et al., 2014; Thacher et al., 2010).

Several studies have demonstrated the involvement of calcium signaling and NO production in ECs in response to mechanical stretch (Takeda et al., 2006; Berrout et al., 2012). In bEnd3 cells, a mouse brain EC line, grown on collagen-coated-BioFlex plates with silastic membranes, Berrout et al. (Berrout et al., 2012) showed a calcium influx mediated by transient receptor potential (TRP) channels 1 and 2 induced by 20-55% of biaxial stretch over 1 minute. Delivering 50 ms bursts of nitrogen gas that produced a downward deformation of the silastic membrane and adherent cells propagated the stretch pulses in this system (Berrout et al., 2012). Consequently, calcium influx mediated increased NO production by eNOS and cytoskeletal actin-stress-fiber formation (Berrout et al., 2012). This study also demonstrated a threshold of greater than 10% of stretch for bEnd3 cells to induce a change in calcium influx (Berrout et al., 2012). However, in the present study, 10% of CS over 18 hours appeared to be the peak threshold value for APP and ICAM-1 protein expression (Figure 9 & Figure 12), while eNOS expression was down-regulated at both mRNA and protein level at all magnitudes of CS (Figure 10 & Figure 11).

Concordant with Berrout et al. (Berrout et al., 2012), short-term NO production in response to CS-mediated-calcium influx was also demonstrated in bovine arterial ECs (Takeda et al., 2006). This study deployed the same apparatus that was used in the present study, where elastic silicon chambers coated with fibronectin were subjected to uni-axial CS (1 Hz, 20% in length for 5 or 20 minutes; Takeda et al., 2006). Moreover, a biphasic NO production, short and long term, was demonstrated via two different mechanisms, stretch activated channel-mediated-increase in calcium influx and phosphatidylinositol 3 OH-kinase/ serine/threonine-specific protein kinase Akt (PI3K/Akt) pathways respectively (Takeda et al., 2006). Similarly, the former was also demonstrated in human umbilical vein ECs (HUVEC) in a c-src dependent manner, which mediated EC morphological changes downstream of calcium signaling (Naruse et al., 1998a; Suzuki et al., 1997). A similar bi-phasic pattern of eNOS activation and NO production due to acute mechanical stretch was reported in another study (Hu et al., 2013). This study utilised a single-well device, which was uniformly stretched by vertical indentation (Hu et al., 2013). However, this study

reported the activation of protein kinase A (PKA) pathway along with the PI3K/Akt pathway at 15 and 30 minutes respectively, as HUVECs were subjected to 20–50% continuous bi-axial stretch (Hu et al., 2013). The involvement of PI3K/Akt pathway in stretch-mediated-NO production has also been demonstrated in pulmonary vascular ECs *in situ* (Kuebler et al., 2003). This study employed models of the intact lung and isolated-perfused rat lungs where the vascular pressure was elevated to induce stretch (Kuebler et al., 2003).

Taken together, mechanical stretch has been demonstrated to induce calcium influx mediated, PKA and/or PI3K/Akt dependent NO production (Takeda et al., 2006; Suzuki et al., 1997; Berrout et al., 2012; Awolesi et al., 1995; Hu et al., 2013). From initial considerations, these studies may appear to be different to results of the present study that showed down-regulation of eNOS at both transcriptional and translational levels after CS. However, one must be aware that there are factors that need to be taken into close consideration that make these studies and the present study directly somewhat incomparable. Firstly, these studies demonstrated eNOS activation in contrast to eNOS expression as was quantified in the present study. The activity of eNOS may not necessarily be proportional to the expression of eNOS due to various reasons. For example, post-transcriptional modifications such as DNA methylation and polyadenylation have been reported as regulatory mechanisms that decided the cell specific expression and mRNA stability of eNOS, which could in turn lead to variations in eNOS expression and/or activity (Chan et al., 2004; Weber et al., 2005). On the other hand, post-translational modifications, such as phosphorylation could regulate eNOS activity regardless of the expression levels (Takeda et al., 2006; Hu et al., 2013). Therefore activity of eNOS could be independent of the level of expression of mRNA or protein. Secondly, experimental conditions of these studies were not the same as the present study. For example, in the study of Berrout et al. (Berrout et al., 2012), the difference may be due to the different range of applied stress (0% to 20% in the present study, compared with 20% to 55% in the study of Berrout et al.) or the duration of stress (a longer term 18 hour protocol in the present study compared to 1 minute in the study by Berrout et al.), with the smaller cell stretch range and longer time period being more representative of the true physiological scenario related to the main focus of the present study which was hypertension, rather than post- traumatic brain injury in the case of the study of Berrout et al. Collectively, let alone the differences in different stretch magnitudes, all these studies have investigated relatively short-term (within 2 hours) stretch-induced-eNOS activation as opposed to eNOS expression after a prolonged 18 hours of stimulation, which the present study demonstrated. The present study did not assess eNOS activity or NO production. Future studies to reveal these may render clarification for whether eNOS activity would still be preserved or not, regardless of the suppression of eNOS mRNA and protein levels after prolonged CS in brain ECs as shown by other studies of short-term CS in brain and other ECs.

Nevertheless, there is evidence in the literature suggesting the possibility of eNOS mRNA and protein down-regulation in association with decreased NO release (Oemar et al., 1998; Dancu et al., 2004). Thus, although the present study did not assess eNOS activation, the down-regulation of mRNA and protein levels of eNOS at all levels of CS may coincide with a subsequent reduction in eNOS activation and thereby a reduction in bioavailable NO. This is suggested by the findings in atherosclerotic arteries and mechanical stretch studies in bovine aortic EC (BAEC; Oemar et al., 1998; Dancu et al., 2004). Both eNOS protein expression and NO release were markedly reduced in atherosclerotic human carotid arteries, as shown in immunohistochemistry and calcium ionophore stimulation (Oemar et

al., 1998). In addition, similar to the finding of eNOS mRNA expression by RT-PCR in the present study, it has been shown in BAEC where CS and asynchronous mechanical force patterns (SPA=−180°) down-regulated eNOS mRNA levels, with an increase in endothelin-1 (ET-1; a potent vasoconstriction mediator, thus has antagonistic effects to eNOS) mRNA expression and a reduction in NO (Dancu et al., 2004). This suggests that reduced eNOS protein expression may coincide with reduced NO release, thus the significant reduction of both mRNA and protein expression could indicate a reduction in bioavailable NO, thereby resulting in ED. However, this needs further investigation, as there is still the possibility that the activity of eNOS may not be altered regardless of the decreased protein and mRNA expression. This is because down-regulation of eNOS mRNA and protein could be the result of an intricate regulation of a feedback mechanism such that increased eNOS activity leading to subsequent down-regulation of transcripts and protein by degradation of mRNA and/or protein. Thus, post-translational modifications such as activation of eNOS via phosphorylation is a possible explanation for the results presented, which should be investigated in further studies as outlined in section 4.4.2.

Apart from studies showing the enhanced release of NO as a consequence of mechanical stretch, alterations of eNOS expression, which was found in the present study, has also been reported (Dancu et al., 2004; Gan, 2000; Oemar et al., 1998). In cultured BAEC, 24 hours of 6% and 10 % strain have resulted in an up-regulation of eNOS transcripts and protein levels as shown by northern blot analysis, nuclear run-off transcription assays and western blotting (Awolesi et al., 1995). The BAEC were grown on flexible membranes, which were subjected to deformation at 60 cycles/min with -5 or -20 kPa of vacuum in a vacuum manifold with recessed ports (Awolesi et al., 1995). Even though this study deployed similar CS conditions as the present study, the strain pattern in this system was reported to be uneven across the membrane as opposed to even CS used across the silicon chambers in the present study. Additionally, the cells that have been used in this study were primary aortic ECs of bovine origin, in contrast to the present study, which utilised a brain EC line of human origin. Moreover, the present study did not encompass pressure as such, only the factor related to circumferential CS was considered. These changes in experimental modalities may account for the changes in subsequent outcomes of the experiment. These contrasting results also imply that there may be species variability and/or the origin of the cell line, which has in fact been reported (Ziegler et al., 1998b, 1998a). Zieger et al. (Ziegler et al., 1998a) reported that EA hy926, a hybridoma cell line created by fusing primary HUVECs with a human carcinoma cell line, appeared more sensitive to shear stress (SS) changes compared to BAEC. Thus, brain ECs may be more sensitive to CS insults as compared to aortic ECs. It could also be that aortic ECs may be better adapted to mechanical stretch stimuli as opposed to brain ECs. This can be explained by the fact that the aorta would be under higher physiological mechanical stretch *in vivo* relative to BBB ECs. Therefore, degradation of protein and mRNA due to high mechanical stretch may more readily concur in the BBB ECs. Additionally, immortalised cell lines such as the one that has been utilised in the present study may respond differently to primary cells, which will be expanded upon in section 4.3.2.2.

Interestingly, several studies have elucidated that eNOS mRNA expression is differentially regulated based on the type of stretch that was involved (Ziegler et al., 1998b, 1998a; Shikata et al., 2005). One study deployed combinations of pressure, unidirectional SS, oscillatory SS and CS for 24 hours on BAEC and EA hy926 grown in perfused silicon tubes (Ziegler et al., 1998b). The stretching conditions included pulsatile SS with unidirectional flow comprising a component of 6 dyne/ cm^2 (amplitude = 6 dyne/ cm^2) and SS with an oscillatory flow with a mean of 0.3 dyne/ cm^2 (amplitude = 6 dyne/ cm^2)

combined with or without 4% CS (mean pulsatile pressure = 100 mm Hg) (Ziegler et al., 1998b). Notably, the % of CS was calculated as the ratio of the diameter amplitude to the mean diameter rather than % increase in length of the stretching chamber as in the present study, thus the % stretch are not directly comparable (Ziegler et al., 1998b). Northern blot analysis showed that unidirectional SS lead to a dose-dependent increase in eNOS mRNA expression in both BAEC and EA hy926 cell line compared to the no shear static control (Ziegler et al., 1998b). In contrast, with oscillatory SS, it was shown that the mRNA expression of eNOS was significantly down-regulated at 0.3 dyne/ cm^2 of SS (Ziegler et al., 1998b). This effect was not significantly increased with the added component of 4% CS in either of the conditions (Ziegler et al., 1998b). Additionally, eNOS promoter activity was measured by luciferase activity followed by transient transfection of the cells with a sequence coding for the functional human eNOS promoter coupled to a luciferase reporter (Ziegler et al., 1998b). The luciferase activity revealed that the eNOS promoter activation was magnitude-dependently incremental with unidirectional SS (Ziegler et al., 1998b). Although the EA hy926 cell line appeared more sensitive to SS changes, both cell lines demonstrated similar trends (Ziegler et al., 1998b). Remarkably, regardless of the eNOS de-regulation at the mRNA level, the eNOS promoter activation was 7- to 10-fold increased by oscillatory SS, which in contrast, was significantly suppressed by CS at all SS variations used (Ziegler et al., 1998b). In another study by Ziegler et al. (Ziegler et al., 1998a) using the same apparatus as described, mRNA expression of eNOS was shown to be completely abolished as SS was reduced from 0.3 to 0.08 dyne/cm^2. Furthermore, it was reported that CS did not have additional effects on eNOS mRNA expression in the presence of low, high or oscillatory SS (Ziegler et al., 1998a). The differential expression of eNOS due to unidirectional SS was attributed to occur via nuclear factor kappa B (NFκB) activation while oscillatory SS was suggested to occur subsequent to activation of an unidentified negative *cis*-acting element present in the *NOS III* gene (Silacci et al., 2000).

These results collectively indicated that the eNOS expression was regulated at both transcriptional and post-transcriptional levels depending on the type of mechanical stimuli involved. Moreover, it was stated that unidirectional SS regulated the eNOS expression at the transcriptional level while oscillatory SS and CS posing regulatory effect at the post-transcriptional level that suppressed eNOS promoter activity or mRNA eNOS expression at low SS (Ziegler et al., 1998a). Consistent with these findings, the present study may add on to these results as the results indicated that the regulatory effect of CS at low SS on eNOS expression was translational, since both mRNA and protein expression were down-regulated (Figure 10 & Figure 11). However, it is noteworthy that the present study incorporated minute SS without a pressure component and that further studies are required to confirm post-translational modifications and eNOS activity, which will be discussed in section 4.4.2.

As discussed earlier, there is a possibility that prolonged CS may lead to ED. This is further supported by the finding that ET-1 was upregulated due to mechanical stress (Ziegler et al., 1998a; Dancu et al., 2004; Juan et al., 2004; Liu et al., 2003a; Gan, 2000; Toda et al., 2008). This is because ET-1 possesses antagonistic effects to eNOS, resulting in diminished eNOS-mediated-NO production, hence mediating ED (Dancu et al., 2004; Toda et al., 2008). ED is known to be associated with cell adhesion molecule expression such as ICAM-1, and therefore it was decided to determine the effect of CS on the expression of ICAM-1 (Hlubocká et al., 2002).

4.2.3 CS regulates the expression of ICAM-1

ICAM-1, which is an inflammatory marker associated with EC membranes, is a glycosylated transmembrane protein that belongs to the ICAM family of proteins (Lee et al., 2000). ICAM-1 protein expression, was significantly increased at 10% CS compared to 0% CS (Figure 12). Previous studies have shown that ICAM-1 expression was up-regulated with CS (Cheng et al., 1996; Riser et al., 2001; Fu et al., 2013). A recent study, which deployed a similar system to the present study, showed that in human pulmonary artery ECs, both mRNA and protein expression of ICAM-1 were upregulated after 24 hours of 20% CS (Fu et al., 2013). However, this study used a frequency of 0.5 Hz, in contrast to 1 Hz in the present study (Fu et al., 2013). Cheng et al. (Cheng et al., 1996) showed similar effects in a different system. In a vacuum controlled strain unit, HUVECs were deformed by a sinusoidal negative pressure with a peak level of −10, -15 or -20 kPa to produce respective average strain % of ~9%, ~11% or ~12% at a frequency of 1 Hz, which were calculated by averaging radial strain over the total plate surface area (Cheng et al., 1996). The stretching over the membrane was stated to be heterogeneous (Cheng et al., 1996). Released levels of soluble ICAM-1 increased dose-dependently at 9%, 11% or 12% strain over 24, 36 and 48 hours of strain as shown by enzyme linked immunoassay (Cheng et al., 1996). The expression of ICAM-1 mRNA and protein levels were also shown to follow a similar pattern over 1, 3, 12 or 24 hours as shown by northern blot analysis and flow cytometry respectively (Cheng et al., 1996). Although the systems and/or the conditions that these studies had employed were not the same as the one that was used in the present study, the results of the protein expression after 18 hours of CS were comparable up to 10% CS, as similar overall trends were shown. However, there was a striking down-regulation of ICAM-1 at 20% stretch in the present study, in contrast to Fu et al. (Fu et al., 2013), which may be accounted for the differences in stretch frequency (1Hz in the present study as opposed to 0.5 Hz in the study of Fu et al.). Additionally, this could also be accounted for by possible cellular damage, as emphasised in section 4.2.4.

Up-regulation of ICAM-1 protein expression associated with mechanical stress could lead to a number of cellular and physiological consequences (Cheng et al., 1996; Riser et al., 2001; Hlubocká et al., 2002). Increases in ICAM-1 expression, subsequent to 20 hours of CS at 11% and 12% have been demonstrated in HUVECs (Cheng et al., 1996). This coincided with increased monocyte adhesion to ECs implicating a pathophysiological phenomenon involved in vascular diseases (Cheng et al., 1996). Similar effects were shown in an *in vitro* model of intraglomerular hypertension, where mesangial cells, a type of smooth muscle cells from the kidneys, were subjected to CS (Riser et al., 2001). The enhanced permeability of ECs due to elevated ICAM-1 expression could also serve as a marker of ED (Hlubocká et al., 2002). In serum samples from uncomplicated essential hypertension patients, the soluble ICAM-1 and ET-1 levels were markedly increased, both of which were indicative of ED (Hlubocká et al., 2002). This denoted the possibility that the marked up-regulation of ICAM-1 protein expression along with the dramatically reduced eNOS mRNA and protein expression in this study could indicate that CS eventuate monocyte adhesion to ECs and/or ED, thus highlighting a possible role of CS in the pathogenesis of early stage hypertension. This can be further investigated in future studies as outlined in section 4.4.2.

Increased ICAM-1 expression has been associated with AD-plaques (Apelt et al., 2002; Lee et al., 2000; Rozemuller et al., 1989). This was shown by immunofluorescence in cortical regions of Tg2576 mice (Apelt et al., 2002). Immunostained cortical sections showed dispersedly ICAM-1-positive regions in activated microglial and brain capillary

cells that were localised in close proximity to senile plaques (Apelt et al., 2002). Cluster-like accumulation of ICAM-1-immunoreactivity was also consistently shown by immunohistochemistry technique (Apelt et al., 2002). This study along with other studies has revealed the involvement of inflammatory responses in amyloid deposition or APP processing (Apelt et al., 2002; Rozemuller et al., 1989; Akiyama et al., 2000; Eikelenboom et al., 1994). Thus, the concomitant dose-dependent ICAM-1 and APP increase after 18-hour-CS up till 10% in the present study (Figure 9 & Figure 12), may indicate that increased APP was associated with increased ICAM-1 expression as observed in AD-plaques. However, it remains to be studied whether the association between the two is due to a causal relationship as outlined in section 4.4.2.

ICAM-1 expression was found to be proportionally mediated by NO release facilitated by the angiogenic growth factor, vascular endothelial growth factor (VEGF) (Radisavljevic et al., 2000). This was demonstrated in mouse brain microvascular EC, where the ECs were treated with VEGF, which facilitated an increase in NO production subsequently increasing ICAM-1 expression (Radisavljevic et al., 2000). The elevated NO production was found to be mediated via PI3K/Akt signaling pathway (Radisavljevic et al., 2000). Radisavljevic et al. (Radisavljevic et al., 2000) suggested that this NO release was through the activity of eNOS, which was consistent with those studies that elaborated PI3K/Akt-dependent CS-mediated-NO-release as discussed in section 4.2.2. This was further supported by the finding that eNOS expression was regulated via the VEGF receptor 2 (Facemire et al., 2009). Even though the present study did not demonstrate the effect of CS on eNOS activity, as discussed in section 4.2.2, CS could up-regulate the activity of eNOS (Takeda et al., 2006; Suzuki et al., 1997). Thus, it can be proposed that the increase in NO due to CS may have lead to the subsequent heightened protein expression of ICAM-1. Additionally, since the PI3K/Akt signaling pathway was implicated as a transduction pathway that mediated CS-induced-NO production, the involvement of the PI3K/Akt pathway can be further emphasised as a possible underlying mechanism for the results presented (Figure 19; Takeda et al., 2006; Kuebler et al., 2003). However, it remains to be determined in future studies whether the increase in ICAM-1 expression was NO-dependent as discussed in section 4.4.2.

Given that enhanced NO production coupled with amplified ICAM-1 expression could be concomitant with CS, the combined effect could lead to ED (Cheng et al., 2008; Hlubocká et al., 2002). In a dysfunctional endothelium, uncoupled eNOS together with enhanced NO production could potentiate deleterious effects on the cellular redox status, shifting it towards the production of ROS (Dick et al., 2013; Cheng et al., 2008). Uncoupling of eNOS has been demonstrated to accumulate ROS in mouse models of deoxycorticosterone acetate–salt-hypertension and diabetes (Huang et al., 2012; Landmesser et al., 2003). The latter study showed that SS-induced dilation of mesenteric arteries of diabetic mice was impaired due to ROS (Huang et al., 2012). These studies highlighted the pivotal role of eNOS in maintaining the vascular tone, which is critically regulated by the abundance of ROS, imbalance of which could result in ED (Huang et al., 2012; Landmesser et al., 2003). Since the former study involved hypertension, which is known to be associated with elevated mechanical stress, both these studies consistently accentuated the cumulative effects of elevated mechanical stress in the regulation of redox status of the endothelium (Huang et al., 2012; Landmesser et al., 2003). To further illustrate the associations between mechanical stress and ROS, free radical induced cell injury was demonstrated by permeability to propidium iodide (PrI) in rabbit and aortic ECs subjected to CS (McKinney et al., 1996). The cells grown on silastic membranes were deformed by a 50-millisecond pulse of gas to produce 54%, 89%, 130%, and 180% stretch (McKinney et al., 1996).

Following 24 hours of corresponding CS, the PrI permeability was significantly increased (McKinney et al., 1996). This increase was abolished by polyethylene glycol–conjugated SOD, which is an anti-oxidative enzyme, indicating that ECs were a source of free radicals post-injury by CS (McKinney et al., 1996). Moreover, in anesthetized cats equipped with cranial windows, the vasodilatory effect in response to topical acetylcholine treatment of cerebral arterioles was replaced by a vasoconstrictive effect followed by acute hypertension (Wei et al., 1985). This effect was restored by treating with SOD and catalase, emphasising the involvement ROS in the context of a pathological condition to which mechanical stretch may contribute (Wei et al., 1985). Activation of nicotinamide adenine dinucleotide phosphate oxidase via hypertension-related integrin α5β1 and c-Jun N-terminal kinase phosphorylation of p66 (Shc) at Serine 36 was implicated as a mechanism by which ECs produced ROS in response to CS (Spescha et al., 2014). Additionally, lipid peroxidation due to ROS was associated with AD (Bhatia et al., 2013). The elevated ICAM-1 expression along with increased APP at 10% CS and the reduced eNOS levels in the present study may therefore coincide ROS production, which remains to be determined in future studies (as described in section 4.4.2).

Elevated ROS could lead to the activation of the NFκB inflammatory pathway, which is a regulatory pathway involved in the expression of ICAM-1 (Schreck et al., 1991; Antonelli et al., 2001). Pulsatile stretch induced superoxide production leading to NFκB activation in human coronary smooth muscle cells (Hishikawa et al., 1997). The cells were deformed by applying −5 and −20 kPa of vacuum to maximal and average strains of 12.5%, 6%, 25%, and 10% at a frequency of 1 Hz for up to 24 hours (Hishikawa et al., 1997). Activation of NFκB was sustained for 24 hours and was abolished by the use of antioxidants (Hishikawa et al., 1997). This study illustrated that pulsatile stretch may lead to elevated ROS and thereby sustained activation of NFκB, which could possibly be involved in the present study as indicated by the marked increase in ICAM-1 expression at 10% CS (Hishikawa et al., 1997). Another study showed that high pulsatile flow with a pulsatility index (indicator of vascular stiffness) of 1.5 for 24 hours, was shown to activate NFκB leading to elevated ICAM-1 expression in pulmonary artery ECs (Tan et al., 2014). The cells were grown in stiffness-induced silicon tubes (Tan et al., 2014). The varied elastic moduli of the tubes were achieved by mixing the silicon elastomer base and curing agent at different ratios (Tan et al., 2014). Cells that were grown on stiffer tubes with high pulsatility index showed higher inflammatory marker release compared to the static or the low pulsatility index (Tan et al., 2014). Although the present study incorporated little SS, the possibility of NFκB activation leading to elevated ICAM-1 expression cannot be ruled out, due to the marked increase in ICAM-1 expression at 10% CS (Figure 12).

Additionally, ICAM-1 expression could induce the release of cytokines such as tumour necrosis factor (TNF)-α as reported in ICAM-1 ligation studies in astrocytes (Lee et al., 2000). TNF-α could in turn activate NFκB, thereby enhancing more ICAM-1 expression (Lin et al., 2005; Panes et al., 1996). This cytokine was also found to down-regulate eNOS mRNA expression by lowering its half-life from 48 hours under basal conditions to 3 hours (Yoshizumi et al., 1993). As little as 0.1 ng/mL of TNF-α reduced eNOS mRNA levels by 50% in HUVECs (Yoshizumi et al., 1993). Taken together, this could be suggestive of the involvement of TNF-α-mediated degradation of eNOS mRNA and ROS- and/or TNF-α-mediated ICAM-1 expression via NFκB pathway in the present study. This can be explored in future studies. Elevated inflammation and ROS levels could also indicate ED in addition to the factors that have already been discussed (Lin et al., 2005; Hlubocká et al., 2002).

4.2.4 Effect of CS on cell viability and morphology

The cell viability of HCMEC did not significantly differ from the static control after 18 hours of 5% or 20% stretch (Figure 13). However, prominent cell detachment was observed after all stretching conditions relative to the static control (Figure 14).

Although the cell viability at 20% CS was comparable to that of the static control (Figure 13), at this CS condition, the mRNA and/or protein expression of APP, eNOS and ICAM-1 were comparable to baseline levels, specially APP and ICAM-1, which have peaked at 10% CS followed by a dramatic decrease (Figure 8, Figure 9, Figure 10, Figure 11 & Figure 12). This suggested that at 18 hours of 20% CS there could be a threshold where the cells were beginning to go into an initial phase of apoptosis and/or cellular damage leading to increased degradation or decreased production of mRNA and/or protein.

Reportedly, mechanical stretch has been identified as a causative factor in cell injury and/or apoptosis (Abbott et al., 2012; Gao et al., 2014). Consistent with the suggested threshold at 20% CS for apoptosis, Liu et al. (Liu et al., 2003b) reported that in BAEC, physiological levels of 6%-10% CS at 1Hz inhibited TNF-α-induced-apoptosis, PI3K/Akt dependently, in contrast to 20% CS (1 Hz), which lead to apoptosis. Additionally, human degenerated annulus fibrosus (AF) cells, which are associated with the intervertebral fibrocartilage, stretch-induced apoptosis resulted as cellular reorientation was restricted (Abbott et al., 2012). Cells were grown and stretched in an earlier version of the system (STREX) that was used in the present study, and were subjected to 10%, 15% or 20% CS for 24 hours at 1 Hz in hypoxic conditions (Abbott et al., 2012). This study showed that at 20% CS in AF cells responded to CS by reorienting perpendicular to the axis of stretch while posing some caspase-3 activity with no statistical significance, which was significantly induced by restricting the reorientation response (Abbott et al., 2012). In human type II-like alveolar epithelial cells (A549 cells), apoptosis induction was present at as low as 6 hours of 20% CS with a frequency of 0.25 Hz in a vacuum-controlled stretching system designed to deliver uniform CS (Gao et al., 2014). In this study, 20% CS was claimed as pathophysiologically relevant while 5% was stated as physiologically relevant (Gao et al., 2014). Moreover, this study provided evidence that 5%-CS preconditioning, where by an initial 0-6 hour-20%-CS was followed by a sequential application of a 0-120 minute-5% CS and a 0-6 hour-20%-CS, could recover cellular damage while suppressing apoptosis (Gao et al., 2014). Together these studies evidenced that CS could lead to pre-apoptotic changes, which could also be involved in the present study as indicated by the marked reduction of protein and mRNA expression at 20% CS (Figure 8, Figure 9, Figure 10, Figure 11 & Figure 12). Future studies could investigate the relationship between apoptosis and reduced protein expression (outlined in section 4.4.2).

4.3 Methodological approaches in the present study

4.3.1 SHR model

4.3.1.1 SHR as a model of hypertension to study the effect of high BP on cerebral amyloid burden

The SHR model has been widely used as an animal model comprising the representative milieu of the hypertensive vasculature (Kurata et al., 2014b; Qia et al., 2014; Ng et al., 2012; Meneses and Hong, 1998; Schreiber et al., 2014). The SHR model was developed by an inbred model of the WKY, such that the systolic BP (SBP) and the heart rate in the SHR were significantly higher with respect to WKY (Meneses and Hong, 1998; Qia et al., 2014). In addition to hypertension, SHR exhibited characteristic features of a number of other pathological conditions (Meneses and Hong, 1998; Qia et al., 2014). Resemblance of cognitive deficits in learning and memory such as in AD has also been previously reported (Meneses and Hong, 1998). Learning and memory was evaluated in SHR and WKY rats by the autoshaping task (evaluation of classic and instrumental-operant conditioning) and reacquisition ability (an index of memory) (Meneses and Hong, 1998). The decreased conditioning scores of SHR by 1.4-fold at 3 months and 3.4-fold at 12 months indicated age-dependent decreased memory and learning relative to WKY (Meneses and Hong, 1998). This effect was shown partially reversed by the calcium channel blocker, nimodipine (0.4 mg/kg/day for 3 weeks; Meneses and Hong, 1998). The nimodipine-treated-SHR group displayed an initial SBP lowering effect, which gradually increased, eventually reaching the SBP comparable to non-treated-SHR group by the second week of post-treatment (Meneses and Hong, 1998). Persistent BP lowering effects were presented by the nimodipine-treated-WKY (Meneses and Hong, 1998). However, the learning deficits were shown improved in the nimodipine-treated-SHR group compared to the non-treated-SHR group as indicated by improved conditioned response scores regardless of the heightened SBP (Meneses and Hong, 1998). This study demonstrated the cumulative effects of hypertension and aging leading to cognitive impairments, which were partially reversed by the direct action of the nimodipine treatment on the central nervous system (Meneses and Hong, 1998). In contrast to this study in which the improved cognition was attributed as drug dependent, rather than a consequence of lowering BP, other studies have shown that decreasing the BP may disseminate lower cognitive deficits as shown by decreased cerebral amyloid load (Kurata et al., 2014b; Schreiber et al., 2014; Qia et al., 2014; Sontag et al., 2013). These studies are detailed in section 4.1.2.

Taken together, the SHR model is a well-established model of hypertension, which is reportedly the most studied animal model of hypertension (Kurtz and Morris, 1987). Since the present study first sought to reveal associations between Aβ and hypertension, this model was highly relevant to investigate the first aim of the present study.

4.3.1.2 Advantages and limitations of the SHR model

Two of the studies that showed elevated amyloid deposition in SHR have utilised slightly different strains of SHR, namely SHR-SP and SHR-SR-tMCAO (Kurata et al., 2014b; Schreiber et al., 2014). These variations may provide better-suited models for respective studies depending on the focus of the study, thus the SHR model can be modified to suit the purpose of the study.

As the SHR model confers specific and uniform genetic predisposition, it enables convenient modeling of the milieu of hypertension and other related pathologies such as AD, cerebral small vessel disease, ischaemic stroke and attention deficit hyperactivity

disorder to name a few (Sontag et al., 2013; Meneses and Hong, 1998; Schreiber et al., 2014; Qia et al., 2014; Kurata et al., 2014b). Therefore it allows speculation of mechanisms, causes and behavioural consequences with the additional advantage of its use in comparing efficacy of therapeutic interventions in an array of related vascular pathologies (Meneses and Hong, 1998).

The main trigger influence in SHR included central neurohormonal mechanisms in simulating hypertension. This allows one to study the combinatory effects of age, hypertension, cognition and physiology on different developmental stages (Meneses and Hong, 1998).

Nevertheless, it should be pointed out that SHR being a genetic model, the experimental outcomes could be consequent of the specific genetic make up of the model, not exclusively of the disease of interest in a study per se (Meneses and Hong, 1998).

4.3.2 Modeling the BBB in an *in vitro* setting

4.3.2.1 General overview of the development of BBB models

For better understanding of the underlying molecular mechanisms in regulating APP expression in the BBB and to facilitate improved drug delivery to the central nervous system in treating AD and other conditions, the BBB has been extensively studied using both *in vivo* and *in vitro* models (Naik and Cucullo, 2012). Although *in vivo* models provide insights into the pathophysiology of the BBB, *in vitro* studies are more feasible in terms of molecular and functional understanding (Patabendige et al., 2013; Sloan et al., 2012). *In vivo* models are relatively expensive, laborious to establish and maintain, and are limited in terms of translational significance (Naik and Cucullo, 2012). In contrast, *in vitro* studies, which can precede and compliment animal and human studies, are relatively inexpensive, convenient to use and can be manipulated in modeling the dynamic milieu of the BBB within sophisticated artificial systems minimising the use of animals (Naik and Cucullo, 2012; Patabendige et al., 2013). Owing to the advantages of *in vitro* studies, the present study employed a cell culture model of the BBB.

4.3.2.2 Primary culture and immortalised cell lines

In vitro BBB models have been established using primary and immortalised cell lines (Patabendige et al., 2013). They have been initiated from primary culture of brain EC (Naik and Cucullo, 2012; Paolinelli et al., 2013). Despite primary culture being the more preferred, the BBB phenotype of primary cultured EC is compromised as its cross talk with the 'neurovascular unit' comprising pericytes and astrocytes is disturbed (Paolinelli et al., 2013). This has led to the development of co-culture systems where astrocytes were co-cultured along with primary EC cultures to maintain the BBB phenotype (Gaillard et al., 2001). Nonetheless, complex primary isolation techniques, batch variation, poor yield, rapid senescence, the use of animals each time cultures are to be established and limited number of passages have been reported as limitations (Patabendige et al., 2013; Garberg et al., 2005; Kamiichi et al., 2012).

Consequently, immortalised cell lines, such as the one that has been used in the present study, have been developed (Patabendige et al., 2013; Naik and Cucullo, 2012; Garberg et al., 2005). These models have been promising in addressing most of the above-mentioned issues as it is less time consuming, less laborious, cost effective and retains the EC differentiating properties even after repetitive passages (Patabendige et al., 2013; Naik and Cucullo, 2012; Garberg et al., 2005).

However, the ability to retain the key characteristics of the BBB phenotype is important in evaluating the *in vitro* techniques (Naik and Cucullo, 2012). These key characteristics include high transendothelial electrical resistance due to the presence of complex intercellular tight junctions and localisation of receptors and transporters that are highly polarised (apical: basal; Patabendige et al., 2013). Thus, immortalised *in vitro* models of the BBB have been extensively studied with respect to *in vivo* BBB characteristics to develop standardised models in evaluating the reliability (Paolinelli et al., 2013; Lindner et al., 2012). Murugunandam et al. (Muruganandam et al., 1997) developed an immortalised line of human capillary and microvascular endothelial cells (HCEC) by transfecting the cells with the pSV3-neoplasmid, coding for the early region of SV 4O, which is comparable to the cell line used in the present study. This immortalised SV-HCEC line exhibited the desirable characteristics of high proliferation rate, preserved morphology at confluence and stable non-invasive nuclear expression of the SV40 (Muruganandam et al., 1997). Maintenance of the major phenotypic features of early passage control cells such as expression of factor VIII-related antigen, acetylated-low- density-lipoprotein uptake, lectin binding and high enzyme activity of BBB-specific enzymes such as alkaline phosphatase and γ-glutamyl transpeptidase was also observed (Muruganandam et al., 1997). Another study in line with several other studies, validated the bEnd3 cell line, showing its plausibility as an adequate BBB model demonstrating high transendothelial electrical resistance, tight junction protein expression and increased paracellular permeability against hypoxic stress, that were comparable to that of respective primary ECs (Brown et al., 2007; Song and Pachter, 2003; Omidi et al., 2003). The immortalised human brain EC line, hCMEC/D3 has also demonstrated P-glycoprotein and other adenosine triphosphate (ATP)-binding cassette (ABC) transporter expression, and paracellular permeability of inulin and sucrose that were parallel to that of corresponding primary brain ECs (Vu et al., 2009; Tai et al., 2009; Poller et al., 2008).

In contrast, in a stroke model of the immortalised hCMEC/D3 cell line, the *in vivo* regulation of ABC transporters associated with ischemic stroke could not be replicated, which was possibly due to lack of interactions with the neurovascular unit (Lindner et al., 2012). It was also suggested that the incorporation of human telomerase reverse transcriptase subunit and the SV40 large T antigen in the process of immortalisation of hCMEC/D3, could confer the ECs to be more resistant to stimuli such as oxidative stress, thus requiring increased exposure times to hypoxia than that of an *in vivo* or *ex vivo* representations (Lindner et al., 2012). This is because human telomerase reverse transcriptase subunit and SV40 large antigen, serve to deactivate tumour suppressor proteins such as p53 and pRb, thereby inhibiting apoptosis and enhancing cell proliferation, respectively (Lindner et al., 2012). Nevertheless, co-culture with astrocytes could improve the results, as this would more closely mimic the cellular interactions that are associated with the neurovascular unit *in vivo* (Lindner et al., 2012; Chaitanya et al., 2014).

In static models using immortalised cell lines that are associated with studies of BBB permeability and transporters that are outlined above, the limitations reported may at least in part arise due to immortalisation process itself (Lindner et al., 2012). The loss of BBB phenotypic features such as cell differentiation as the cells are grown in an artificial system is considered another limitation (Naik and Cucullo, 2012). Such limitations could be accounted for by the absence of hemodynamic forces as well (Naik and Cucullo, 2012; Cucullo et al., 2008).

Hemodynamic factors such as pulsatile and shear forces that the BBB is exposed to *in vivo*, affect the BBB properties and functions of ECs (Santaguida et al., 2006). Therefore it should be noted that hemodynamic forces are important features in retaining the BBB properties of ECs independent of whether a primary or an immortalised cell culture model is being employed (Neuhaus et al., 2006; Naik and Cucullo, 2012). For example, the effects of CS and/or SS have been elucidated in brain and other ECs (Figure 15; Neuhaus et al., 2006; Santaguida et al., 2006; Siddharthan et al., 2007). In BBB ECs in particular, SS facilitated the formation of tight junctions and the expression of multidrug resistance transporters (Naik and Cucullo, 2012; Neuhaus et al., 2006; Siddharthan et al., 2007).

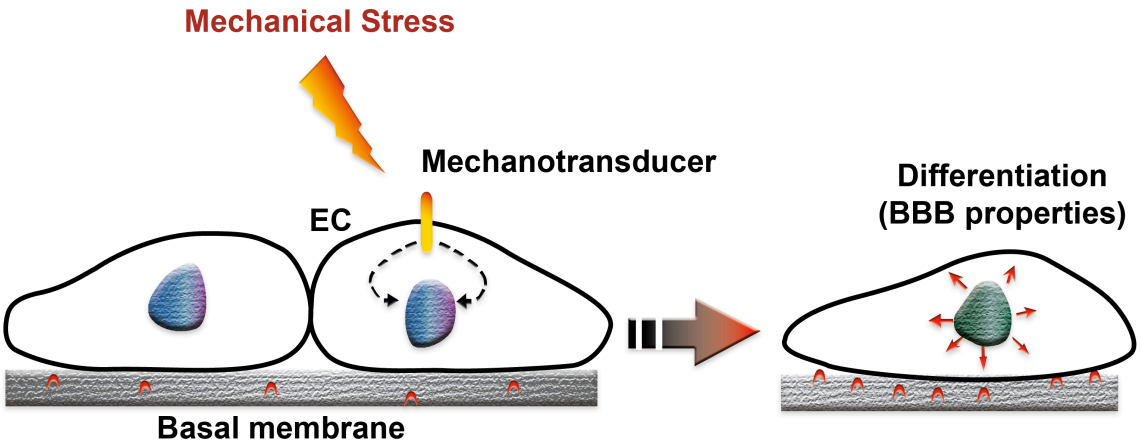

Figure 15. The responses of BBB ECs to mechanical stress. An array of physiological functions is mediated through EC mechanotransducer-signaling in response to mechanical stress in the BBB. These include changes in cell orientation, release of NO, mitotic and cell survival mechanisms, alterations in glucose metabolism, formation of tight junctions and differentiation of EC into a truly polarised phenotype (Adapted from Naik and Cucullo, 2012). Abbreviations: BBB, blood brain barrier; EC, endothelial cell; SS, shear stress.

4.3.2.3 Dynamic BBB models

Hemodynamic forces such as CS and SS are known to influence the BBB phenotypic characteristics and functions of ECs (Naik and Cucullo, 2012; Siddharthan et al., 2007; Garberg et al., 2005; Cucullo et al., 2008). In addressing issues arising due to the absence of hemodynamic forces in static cell culture models, dynamic *in vitro* BBB models have been developed introducing the dimensions of pulsatile and shear forces (Naik and Cucullo, 2012; Cucullo et al., 2002; Neuhaus et al., 2006; Siddharthan et al., 2007; Nagai et al., 2012; Cucullo et al., 2011). These include, but not limited to, the dynamic *in vitro* BBB model (DIV-BBB) and collagen 3D matrix supports 3D extracellular matrix protein (ECM)- based BBB models (Naik and Cucullo, 2012; Cucullo et al., 2013; Siddharthan et al., 2007; Nagai et al., 2012; Cucullo et al., 2011, 2002).

In the DIV-BBB model, ECs can be co-cultured with astrocytes in capillary-like hollow fibers in the presence of intraluminal flow while 3D ECM- based BBB models are grown on self-polymerizing ECM scaffolds providing an alternative to the use of artificial capillary-like structural supports as in the DIV-BBB model (Naik and Cucullo, 2012; Cucullo et al., 2013; Nagai et al., 2012; Cucullo et al., 2002). These models have demonstrated BBB properties comparable to that of *in situ*, such as high transendothelial

electrical resistance, expression of ion channels such as TRP channels and paracellular sucrose permeability showing adequate tightness of the BBB (Cucullo et al., 2011, 2002; Thodeti et al., 2009). For example, TRP-mediated-cytoskeletal remodeling and cell stress fiber reorientation was demonstrated in primary bovine capillary ECs (BCEC) cultured on fibronectin-coated flexible ECM substrates under 10-15% stretch and 1 Hz frequency for 1-2 hours (Thodeti et al., 2009). TRP-Vanilloid-4 (TRPV4) activation has lead to the activation and binding of actin receptors in a PI3K- dependent manner (Thodeti et al., 2009). Another study also reported calcium influx through TRPV4 channels in BCEC and human dermal microvascular ECs that was mediated by force-dependent integrin signaling (Matthews et al., 2010). However, this study used a different approach called 'magnetic pulling cytometry' (Matthews et al., 2010). This involved the cultured cells being exposed to brief (500 ms) pulses of increasing tensional force (100, 450, 850 and 2000 pN) through bound magnetic micro beads (4.5 μm diameter) using an electromagnetic needle (Matthews et al., 2010).

In the present study, immortalized HCMEC-SV40 was be used to model the endothelial layer of the BBB in a dynamic model, as described in section 2.2.1, 2.2.2 & 4.3.2.4.

4.3.2.4 The current BBB model

The BBB has previously been shown to be involved in the clearance of Aβ (Pflanzner et al., 2011; Deane et al., 2004; Owen et al., 2010; Mackic et al., 1998). Given that the Aβ oligomerisation was significantly higher in the SHR, amyloid processing was investigated in the HCMEC-SV40 cell line, representative of the BBB coupled with combinations of CS, simulating the mechanical stretch component that is involved in hypertension.

In the present study, the BBB EC model included culturing hCMEC-SV40 in fibronectin-coated-silicon chambers that were subjected to uni-axial CS using the ShellPa stretch System as detailed in section 2.2.2 (B-Bridge International; Figure 4). Fibronectin was used to enhance EC attachment to the chamber (Naruse et al., 1998a; Suzuki et al., 1997). The chambers were attached to a stretching apparatus of which, one end was fixed and the other connected to an air compressor unit (Figure 4 & Figure 5; Naruse et al., 1998a). The ratio of stretching could be adjusted on an incremented scale of 2, 4, 5, 6, 8, 10, 12, 15 and 20% while the stretch frequency: 1-120 cycle(s)/min could also be modified, that enabled simulating factors such as mechanotransduction, pulsatile circumferential distension of the vessel wall and heart rate (Figure 5 & Figure 6; Suzuki et al., 1997). Such flexibility in manipulating cell culture conditions allows convenient modeling of the effects of mechanical stretch on cell function, and thus provides a platform to characterize possible underlying molecular mechanisms involved in diseases such as AD (Naik and Cucullo, 2012). Thus, this model was considered plausible in achieving the second major aim of the present study, which was to investigate endothelial functions in response to different magnitudes of CS.

4.3.2.5 Advantages and limitations of the current BBB model

As exemplified by *in vitro* studies that have been discussed under sections 4.2, 4.3.2.1 and 4.3.2.2, *in vitro* models have been extensively used to elucidate molecular mechanisms underlying physiological consequences *in vivo* (Section 4.3.2.1 briefly outlines the advantages of *in vitro* models compared to *in vivo* models). As discussed in 4.3.2.3, dynamic BBB models provided more realistic conditions for experimentation, such as the model used in the present study. Thus the current BBB EC model was feasible in achieving the aims that were set in this study, as introducing CS into the model provided improved results as it mimicked the pulsatile microenvironment similar to that of *in vivo*. With the ease of being able to modify the magnitude of % CS, the effect of CS could be

conveniently detailed in a strictly controlled system that allowed investigating the direct effects of CS.

However, the mechanical stress within the vasculature is not limited to CS, but SS and pressure components as well. These factors may mediate different responses in the vasculature as discussed in section 4.2.2. For example, increased NO production, enhanced eNOS expression and phosphorylation were mediated by SS in bEnd3 EC line derived by transformation with polyoma middle T antigen were demonstrated (Mao et al., 2014). This implicates that SS was involved in altering EC function. Since *in vivo* mechanical stress is represented by the combinatory effects of CS, SS and pressure, the current model may only be a part representation of the physiological milieu. Therefore, the lack of incorporation of SS and pressure did not allow for a complete characterization of the effects of *in vivo* mechanical stress, which was a limitation of the current BBB model. Another limitation was that the current model only included ECs, however the BBB comprises other factors such as neuronal, glial and astrocytic components that work in concert to differentially coordinate endothelial function (Naik and Cucullo, 2012). Not incorporating SS, pressure and other BBB factors could narrow the associated physiological factors as suggested by some studies (Ziegler et al., 1998b; Dancu et al., 2004). This system could be improved by incorporating SS and other BBB factors to more closely mimic the *in vivo* microenvironment. Additionally, as per the issue raised by Lindner et al. (Lindner et al., 2012), using an immortalised cell line may impose modifications in gene or protein expression, regardless of the advantages discussed in section 4.3.2.2 and 4.3.2.3, thus the cell line may need validation comparing to a primary cell model.

Although the current model provided insights into CS-related endothelial modifications independent of other mechanical stressors present in the BBB *in vivo*, studies have shown that there were some effects on the endothelium exerted by different combinations of those mechanical factors independent of each other (explained in detail in section 4.2.2). Therefore, this model still sufficed to provide important evidence that was sought to achieve the aims of the study. Additionally, the second aim was to study the independent effects of CS rather than combinatory effects, justifying the use of this model in this study further as it provided a well-controlled setting.

4.3.3 Western blotting

4.3.3.1 Overview of the western blotting procedure

Western blotting is a widely used analytical tool to date and was used in the present study to study the protein expression levels (Anderson et al., 2011). Western blotting is a separation method based on affinity interactions (Anderson et al., 2011). It is applied in a broad spectrum of clinical and biological applications (Hughes and Herr, 2012). Clinically it is useful as a confirmatory test for clinical assays and regulatory tests while in biological research, it is employed in assaying proteins in complex mixtures (Anderson et al., 2011). It is a well-established technique that is used to analyse the presence, post-translational modifications and relative abundance and molecular mass of proteins (MacPhee, 2010). Moreover, combined with immunoprecipitation, western blotting can be used to study protein-protein interactions (MacPhee, 2010).

In western blotting, proteins are first separated using SDS-PAGE, based on their molecular weight (Figure 16; Anderson et al., 2011; Hughes and Herr, 2012). In this process, the proteins migrate through the porous SDS-PA gel, and the protein sizes are determined against a standardised protein ladder (Anderson et al., 2011; Hughes and Herr, 2012). Denatured proteins become negatively charged as SDS, a strong anionic detergent, binds to their hydrophobic regions, which facilitates the negatively charged SDS-protein complexes to run through the gel (MacPhee, 2010). Then the separated protein bands are transferred on to a membrane such as PVDF and nitrocellulose, by electro-blotting, followed by a blocking step in which the membrane is treated with a protein solution such as bovine serum albumin (Anderson et al., 2011; Hughes and Herr, 2012; MacPhee, 2010). Electro-blotting on to the membrane immobilises the proteins while protein coating ensures blocking of non-specific membrane interactions (MacPhee, 2010). Sequential probing with a primary antibody and a secondary antibody conjugated with a label then allows the target protein to be detected using chemiluminescence or chemifluorescence (Figure 16; Anderson et al., 2011; Hughes and Herr, 2012).

Followed by an appropriate stripping procedure, re-probing of the same membrane can be achieved, which could save time and reagent use. Moreover, cutting of the membranes according to the molecular weight of the protein of interest using the standard ladder as a guide could also serve to save effort, time, protein samples and antibodies (MacPhee, 2010). Even though the membranes were not stripped in the present study, cutting of the membranes allowed simultaneous detection of a number of proteins.

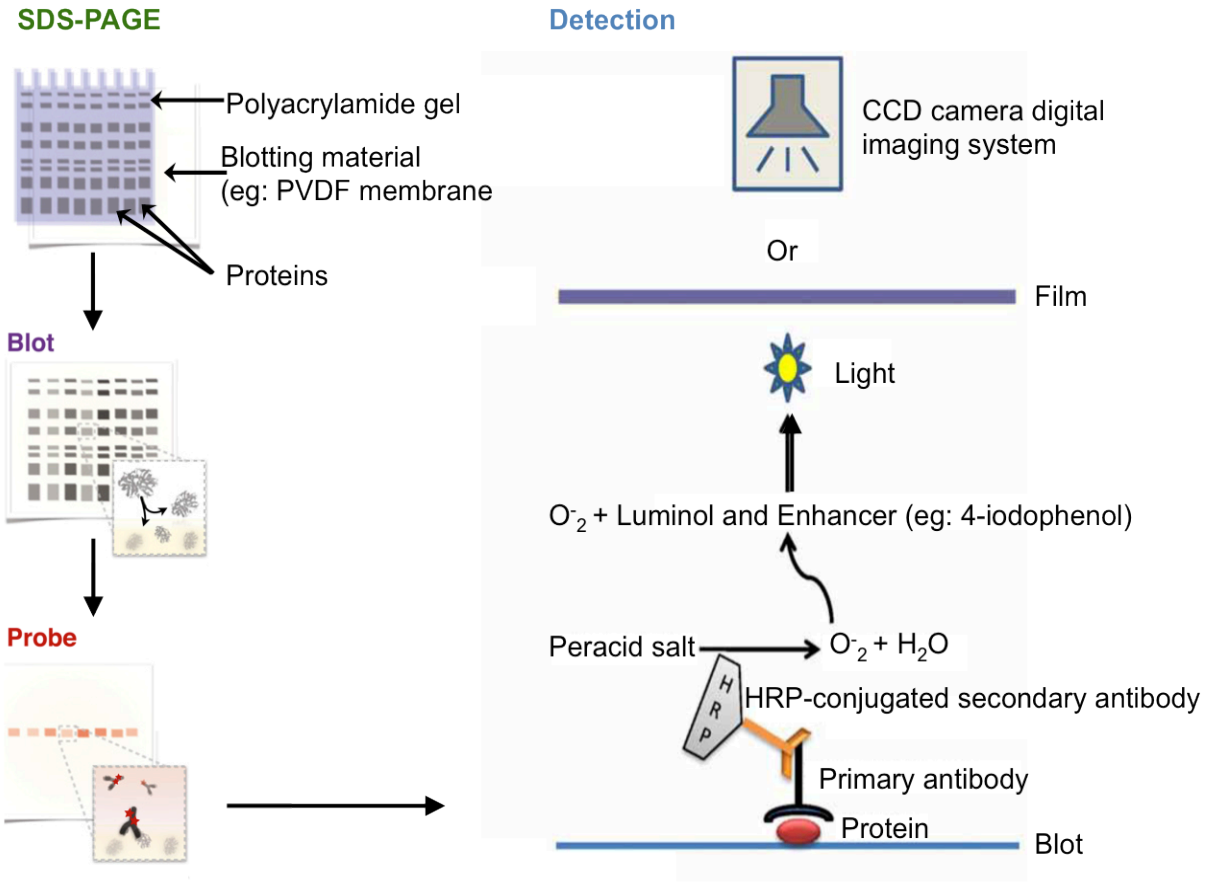

Figure 16. The process of SDS-PAGE. SDS-PAGE allows the proteins to be separated into bands according to their molecular weight, which then are transferred onto a blotting material (eg: PVDF membrane). The blotted replica of the protein bands is probed with primary and secondary antibodies. The secondary antibody is conjugated to HRP. The HRP catalyzes a reaction that results in oxidation of phenolic enhancers, which react with 5-amino-2, 3-dihydro-1, 4- phthalazinedione (luminol). Light is produced as an end result that can be captured on film or by a digital imaging system (Modified from MacPhee, 2010; Hughes and Herr, 2012). Abbreviations: CCD, charge coupled device; HRP, horseradish peroxidase; PVDF, Polyvinylidene difluoride; SDS-PAGE, Sodium dodecyl sulfate polyacrylamide gel electrophoresis.

The results of western blotting are affected by other factors, which have to be taken into account in improving the outcome. The quality of the protein lysate is an important factor in this aspect, which is largely dependent upon the choice of lysis buffer. The buffer should essentially be able to preserve the antigenic sites of the proteins enabling efficient antibody binding while allowing optimal extraction of the protein of interest. In terms of optimally yielding the protein of interest, the choice of buffer should be selected considering whether it is designed for the specific protein; for example, certain detergents would be more effective in extracting membrane receptor proteins. In preserving the protein integrity, enzymic activity of phosphatases and proteases, which could potentially degrade the proteins, should be avoided using phosphatase/protease inhibitor cocktails and carrying out the lysis procedure quickly while chilled. Moreover, rapid freezing for proper storage is required to avoid protein degradation by enzymes (MacPhee, 2010). The present study involved detecting proteins that are mainly localised in the membrane. The choice of buffer was determined accordingly such that a strong version of the RIPA lysis buffer, a

commonly utilised buffer for protein solubilisation, was utilised, which allowed a sufficient protein yield for western blotting.

Another aspect in improving the western blotting outcomes is the composition of the PA gels and quality of reagents that ensure optimal porosity and separation. The percentage of acrylamide is chosen based on the molecular weight of the protein of interest. For separation of proteins, the standard bisacrylamide–acrylamide ratio is reported to be 1:29, however commercially available precast gels and pre-mixes are considered to be more convenient and consistent. The pH and ionic strength of the running buffer and the buffer used in casting the gel should be adequate to ensure good resolution of the SDS-PAGE. Tris base is recommended to avoid formation of diffused protein bands. Amount of protein transfer and proper adsorption onto the membrane are also important parameters that could improve results. For adequate protein transfer the membrane quality and design (eg: pore size) must be considered while for effective analysis, the heterogeneity of protein transfer should be confirmed using staining-destaining methods. Membrane fixation may reduce protein loss during washing. Lastly, the choice of blocking solution, blocking and antibody incubation times, the choice of antibody, optimisation of antibody concentrations (monoclonal or polyclonal), adequate washing, method of detection, exposure time and the quality of the detection reagents would provide optimal resolution with minimised background (MacPhee, 2010). Considering all these factors, commercial pre-cast Bis-Tris gels were utilised in the present study. 4-12% precast gels allowed detection of the protein size range in the present study. The incubation time, antibody concentrations and the recipe for washing buffer were standardised for optimal detection.

Western blotting was suggested to be a popular method in conjunction with SDS-PAGE, which was shown to be more sensitive in protein detection as it utilises confirmation or sequence specific antibody in the process of detection (Pryor et al., 2012). The present study utilised a primary mouse monoclonal antibody 6E10 mouse monoclonal antibody (Covance). This antibody was claimed to be reactive to the amino acid residues 1-16 of Aβ, of which the epitope lies within amino acids 3-8 of Aβ (EFRHDS) in the human Aβ sequence. Importantly, the samples of the study were of rat origin. Multiple sequence analysis (Multalin) was performed of corresponding Aβ sequences of rat, mouse and human (Figure 17). This was to confirm whether the sequence along the epitope region was conserved enough amongst different species for the antibody to potentially cross-react with the Aβ of rat origin. The sequences were obtained from uniprot database (www.uniprot.org) and the multiple sequence analysis was performed using multalin multiple sequence alignment tool (http://multalin.toulouse.inra.fr/multalin/). Only one amino acid difference was shown by the sequence analysis, thus the antibody was chosen for the present study (Figure 17). This is because the sequence of the epitope for 6E10, which is the specific region where 6E10 binds at, was not substantially different from the human or mouse sequences.

Figure 17. Multiple sequence alignments of Aβ42 sequence of human, rat and mouse origin. A single amino acid difference was detected by multiple sequence analysis using multalin multiple sequence alignment tool (http://multalin.toulouse.inra.fr/multalin/) within the epitope where the 6E10 antibody binds. The sequences were obtained from uniprot database (www.uniprot.org). The epitope lies within amino acids 3-8 of Aβ as indicated.

4.3.3.2 Advantages and limitations

There are advantages of western blotting that make it one of the most commonly used analytical tools. Detection specificity is a major advantage as it is based on the respective protein size and specific antibody binding (Anderson et al., 2011; Hughes and Herr, 2012). Reliability and simplicity of the technique are also reported (Anderson et al., 2011).

However, there are well-known limitations of western blotting as well. It is a time consuming technique, which is manually intensive, as it requires multiple steps to be performed with long incubation times (Anderson et al., 2011; Hughes and Herr, 2012). Reduced sensitivity restricts it from being used in sample-limited analysis (Anderson et al., 2011). Difficulty of transferring large proteins from slab gels, extensive use of reagents such as buffers and antibodies and the possibility of reduced reproducibility due to many manual steps being involved are also considered limitations (Hughes and Herr, 2012; Zhu et al., 2012; Anderson et al., 2011).

In addressing these issues, modified or novel western blotting approaches such as western blotting using capillary electrophoresis and microfluidic western blotting have emerged, which have shown advantages such as automation, shorter separation times and efficient separation with less reagent use (Hughes and Herr, 2012; Zhu et al., 2012; Anderson et al., 2011). However, for the purpose of the present study, the SDS-PAGE technique allowed adequate and relatively inexpensive detection of the proteins studied while providing the advantage of specificity, which was sought as more important than sensitivity as the protein yield and expression levels were sufficient for analysis of the respective proteins. Furthermore, since western blotting is a validated and well-established technique, it offered reliable results. Although there are other techniques such as enzyme-linked immunosorbent assay and mass spectrometry to detect protein levels, SDS-PAGE most suited the purpose, availability of resources and technical demands required to perform the technique, thus was chosen over those others for this study.

4.3.4 RT-qPCR

4.3.4.1 Overview of the real-time RT-qPCR technique

RT-qPCR, which was utilised in the present study to study, has emerged as the method of choice for mRNA expression analysis over the past years (Forlenza et al., 2012). Its use is not limited to the analysis of mRNA, thus is used in an array of applications such as DNA copy number measurements and confirmation of microarray data (Ginzinger, 2002). RT-

qPCR is based on the principals of PCR amplification, where copies of a DNA template are exponentially amplified (Ginzinger, 2002; Forlenza et al., 2012). Specific probes or DNA-intercalating dyes that binds to double-stranded DNA at the end of each PCR cycle are used for detection (Figure 18; Forlenza et al., 2012). The relationship between the initial amount of DNA in a given sample and the amount of amplified PCR product during the exponential phase is used for the quantitative analysis of mRNA or DNA present in the sample (Forlenza et al., 2012). Notably, the starting amount of template can only be extrapolated during the exponential phase of a PCR reaction (Ginzinger, 2002).

In real-time PCR quantification, a plot of signal fluorescence and cycle number is generated in real-time as the PCR products are amplified. The cycle number at which the fluorescent signal is greater than the baseline due to background fluorescence is denoted as the 'cycle threshold' or 'Ct'. The Ct values of each sample can be used to calculate the mRNA expression levels or DNA copy number, as the Ct values are directly comparative to the amount of starting template. There are two fundamental ways of analysing PCR data, one of which uses a standard curve of known samples to calculate the unknowns while the second being the comparative Ct method. The latter uses the comparison of Ct values with a control gene, which is known to not vary in copy number or expression level amongst the samples of study (Ginzinger, 2002). The present study utilised the comparative Ct method, which was more appropriate for the purpose of the study, using two control genes, GAPDH and β2m, to improve the reliability of the results.

The integrity of the starting material (RNA or DNA) is crucial in obtaining reliable RT-qPCR data (Forlenza et al., 2012). The present study used the TaqMan® gene expression assay probes, which provided more specificity and reliability. This is because the dual-labeled probes (consisting of a reporter dye and a quencher dye) in these assays are specific to the exon-exon junctions and a fluorescent signal is only given out as the reporter dye is cleaved off by Taq DNA polymerase in the primer extension step (Figure 18), in contrast to the conventional SYBR dye method, in which a fluorescent signal is given out whenever the dye binds to double-stranded DNA including non-specific DNA that may be present (Ginzinger, 2002). Nonetheless, the present study used RT- samples, which were processed without the addition of the reverse transcriptase to ensure there was no genomic DNA contamination was present. A two-step PCR process of RT and real-time qPCR was utilised in the present study. This produced cDNA that can be used in multiple experiments with different genes while minimising the handling of RNA, which is prone to degradation. Validated pre-designed primer probes were utilised to improve the reliability and reproducibility.

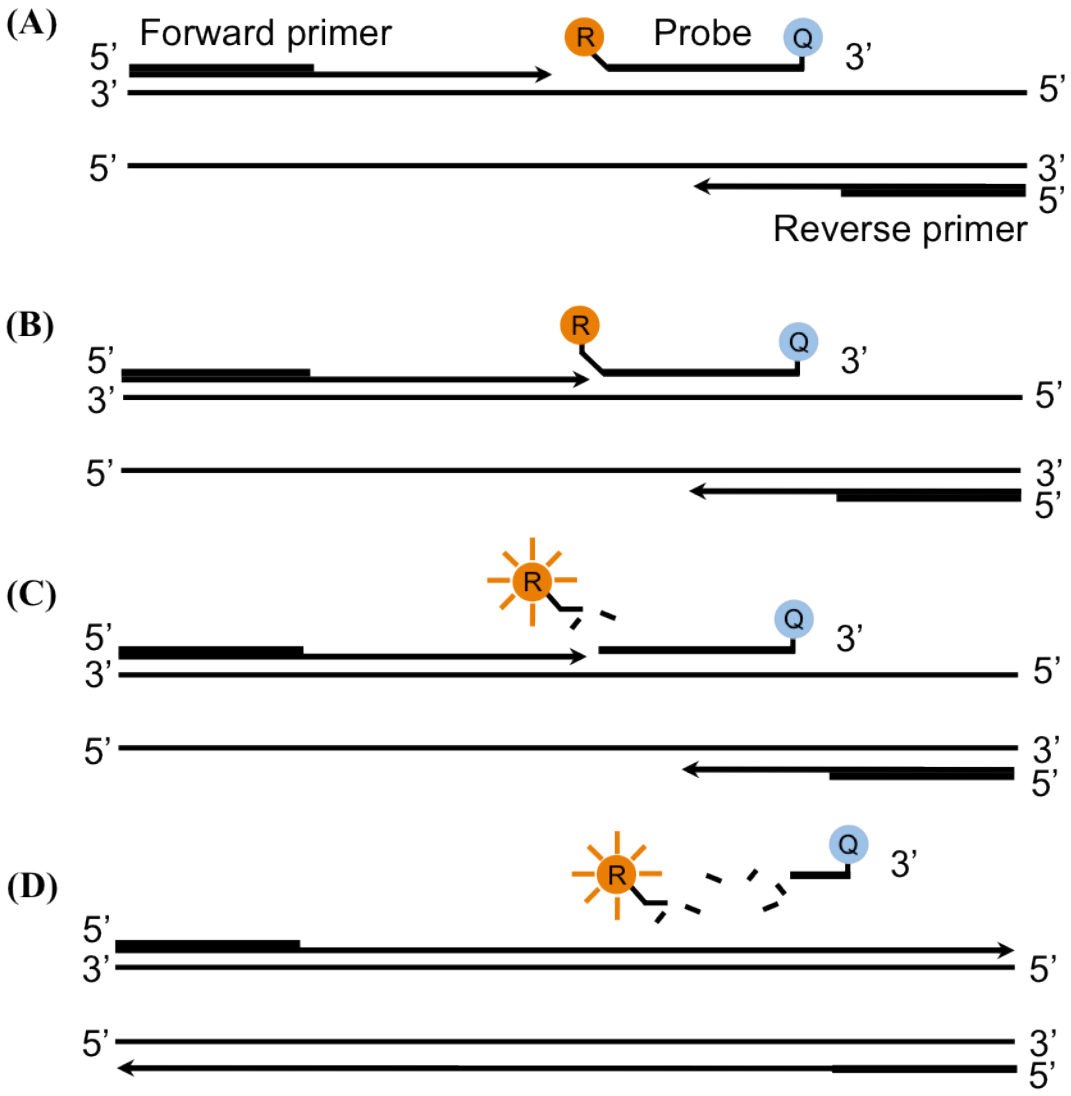

Figure 18. Diagrammatical representation of the TaqMan® assay chemistry. (A) Polymerisation: The TaqMan® probe comprise a fluorescent reporter dye (R) and a quencher (Q) at the 5' and 3' end respectively. **(B)** Strand displacement: The quencher dye quenches any fluorescence emitted by the reporter dye in intact probes. **(C)** Cleavage: During the primer extension step, the reporter dye is cleaved off by Taq DNA polymerase. **(D)** Polymerisation completed: The reporter dye emits its characteristic fluorescence, which is quantified once it is separated from the quencher dye. Abbreviations: DNA, deoxyribonucleic acid, R, reporter; Q, quencher (Modified from http://www.lifetechnologies.com).

4.3.4.2 Advantages and limitations

Real-time PCR improves the reliability of the data relative to end-point PCR. The unreliability of end-point PCR could arise due to the possibilities that some samples may have reached the plateau phase of the PCR reaction and that there would be inconsistencies in the rate of PCR product generation, such that different samples yielding different amounts of PCR end-products. Since real-time PCR measures the PCR products in the exponential phase as they are accumulated in real-time, it provides reliability over end-point PCR (Ginzinger, 2002). Moreover, real-time RT-qPCR provides quantitative

accuracy and sensitive detection, thus can be used in situations where the sample size is limited (Forlenza et al., 2012).

The TaqMan® pre-designed probes provides improved specificity at it eliminated the possibility of non-specific signals due to mis-priming, as might occur when not using a hybridization probe and simplified the RNA purification process by avoiding the need for a DNase I treatment step (Ginzinger, 2002). Thus this method was chosen over the SYBR dye method, so that the need for melt curves due to the possibility of primer-dimer formation was avoided.

A disadvantage of the TaqMan® would be the requirement of different probes for different sequences, which would make it relatively expensive than the SYBR dye primers.

However, overall, the real-time PCR using TaqMan® probes provided greater reliability, specificity and sensitivity compared to other mRNA quantification techniques while providing rapid and convenient quantification without the need for running gels, which is relatively more technically demanding and time consuming as in northern blotting. Therefore, this method was chosen over other methods of mRNA quantification.

4.4 Future directions

4.4.1 Future directions for animal studies

Elevated amyloid deposition in the brain of different SHR models such as the SHR-SR have been demonstrated to be lowered using the BP-lowering drug, telmisartan, a pleiotrophic metabo-sartan belonging to the class of angiotensin receptor blockers (Kurata et al., 2014b, 2014a). The present study can be extended to investigate any effects of BP-lowering drugs. Different classes of BP-lowering drugs may be tested. Moreover, this could verify whether the effect of cerebral amyloid load observed in this study was merely due to a genetic variation of the SHR itself or whether it was due to the elevated BP, thereby establishing a causal relationship between BP and amyloid burden.

It has been reported that treating the SHR briefly with the angiotensin converting enzyme inhibitor, perindopril at an early stage, attenuated high BP compared to late-treated or non-medicated SHR (Ng et al., 2012; Harrap et al., 1990). This effect was reported to be persistent after cessation of the early treatment (Ng et al., 2012; Harrap et al., 1990). The present study could be extended to investigate similar effects in terms of cerebral amyloid load, which would further evaluate whether there is a causal relationship between BP and amyloid burden.

Age is a related risk factor for both AD, hypertension and vascular stiffness (Avolio et al., 2014; Schreiber et al., 2014; Langbaum et al., 2012; Mitchell et al., 2011; Hanon et al., 2005; Park et al., 2014). Thus, exploring age-dependent variations in amyloid deposition in SHR would be meaningful (Kurata et al., 2014b).

Although it is well established that SHRs have higher blood pressures compared to WKY, the present study did not measure the blood pressure of the animals, which should be addressed as a limitation of the study. The BP of the conscious animals can be measured by the tail cuff method, which could improve the conclusions of the study by clarifying whether there is an association between BP and amyloid burden. Additionally, other vascular parameters such as arterial stiffness in the rats and quantification of APP, eNOS and ICAM-1 in the rat brains could be used to further support the *in vivo* and *in vitro* findings of the study allowing comparison between the two study models. Endothelial function could also be assessed in isolated SHR and WKY arteries in an organ bath. This would allow testing for any associations between BP, stiffness and amyloid burden.

This study was a pilot study to establish sample sizes required for future studies and therefore obtaining power calculations was not possible at this stage. Sample sizes for future work should now be calculated based on the standard deviations of the present study.

4.4.2 Future directions for *in vitro* studies

The present study showed that the APP and ICAM-1expression at 10% CS was significantly up-regulated, with a concomitant down-regulation of eNOS under the same conditions. Present study only investigated the individual expression levels of these proteins. However, as discussed under section 4.2, previous studies have elucidated associations between these proteins in the context of AD or AD-related factors (Radisavljevic et al., 2000; Austin et al., 2010, 2013b, 2013a; Tan et al., 2014; Panes et al., 1996; Apelt et al., 2002). Since the present study showed that CS did alter EC expression of ICAM-1, APP and eNOS, it may be of importance now to elucidate whether these

proteins affect each other in altering their individual expression levels. Thus, relationships between these proteins should be determined as part of investigating possible underlying mechanisms. Associations between these findings can be identified in many ways, of which some are briefly outlined below.

Direct associations between proteins could be determined using different techniques. To name a few amongst the many, techniques such as co-immunoprecipitation, mass spectroscopy and yeast two hydrid can be utilised. As discussed in section 4.2, eNOS facilitated NO release in ECs in response to CS while NO could modify APP expression and ICAM-1 expression (Radisavljevic et al., 2000; Austin et al., 2010, 2013b, 2013a). Thus, it remains to be verified whether the APP and ICAM-1 expression were altered in an eNOS-mediated-NO-dependent fashion. One way to verify this is to inhibit eNOS-mediated-NO production and observe if the APP and ICAM-1 expression levels are altered as a consequence. For example, eNOS-mediated-NO production can be inhibited pharmacologically using L-NAME. Alternatively, eNOS knockdown can reveal any direct relationships between eNOS-mediated-NO and APP or ICAM-1 expression.

In addition to looking at correlations between the proteins studied in the present study, there are many other avenues for future studies to expand the present study. The possibility of activation of eNOS via post-translational modification to release NO after CS was discussed in section 4.2.2. Phosphorylation of eNOS can be investigated using western blotting and mass spectroscopic approaches.

ICAM-1 expression can be modulated by TNF-α as discussed in section 4.2.3. To investigate whether the ICAM-1 expression was TNF-α-mediated, the cells can be stimulated using TNF-α prior to CS and observe any effects imposed. Including a TNF-α control would verify whether the changes would be mediated by TNF-α alone or combinatory with CS. Alternatively, the effects of TNF-α knockdown will illustrate the role of this protein on ICAM-1 expression.

The involvement of ROS in modifying APP, ICAM-1 and eNOS expression has been reported as discussed in section 4.2.3 (Mao et al., 2014; Lin et al., 2005; Graham et al., 1995; Cheng et al., 2008). This can be verified by treating the ECs with an antioxidant prior to CS. For example, SOD can be introduced into the system to investigate possible outcomes on the expression of APP, eNOS and ICAM-1.

Monocyte adhesion to ECs due to elevated ICAM-1 followed by CS was reported (Cheng et al., 1996). This can be investigated using a monocyte adhesion assay. In the context of AD, monocyte adhesion was reportedly involved in dispersing Aβ deposits through phagocytosis and proteolytic degradation (Zhang et al., 2012).

Cell apoptosis can be induced by CS, which can be quantified in a number of ways. Cell apoptosis or cellular damage can be investigated using immunofluorescence or caspase activity.

Study of mechanotransduction pathways could be another major future direction. Mechanotransduction may activate different cell signaling pathways depending on factors such as time-course and magnitude of the stimulus as discussed under section 4.2. Possible mechanisms that may be elucidated in this setting include, but not limited to, PI3K/Akt pathway, NFκB activation, and PKA pathway as discussed in the preceding sections (Figure 19; Hu et al., 2013; Wung et al., 1997). Furthermore, ET-1 was reported to

transiently up-regulate at the mRNA level followed by CS (Ziegler et al., 1998a). ET-1 is known to be up-regulated by CS via extracellular signal-regulated kinase, which could be a possible mechanism by which CS mediated the down-regulation of eNOS (Juan et al., 2004; Liu et al., 2003a).

The present study provided evidence that CS altered endothelial gene and protein expression. This *in vitro* model needs to be validated using a corresponding *in vivo* model such as SHR (Naik and Cucullo, 2012).

Additionally, it should be addressed that the present study did not assess the degree of CS across the cell stretching chambers. Although this system has been used and validated by other studies (Naruse et al., 1998a, 1998b; Takeda et al., 2006) and the manufaturer claimed that the machine exerts uniform stretch across the stretch chamber, it would still be important to assess that all the cells are being uniformly stretched. One way to address this would be to calculate the % stretch of cells that are attached on the stretch chamber at different locations (for example, the middle and the edges of the chambers) using cell micrographs or high resolution video imaging.

5 Summary and conclusions

In summary, the cerebral deposition of Aβ in SHR was shown to be higher than that of WKY normotensive rats. In the BBB EC model, 18 hours of CS dose-dependently increased the expression of APP and ICAM-1 up to 10% of CS, both of which were significant at 10% of CS, whereas the eNOS expression was significantly decreased at all CS levels. Both APP and ICAM-1 were back to basal levels at 20% CS suggestive of possible cellular damage. Together, these results provided evidence that hypertension may be related to AD as a consequence of altered cerebral processing of APP resulting in Aβ aggregation. In addition, the findings within the *in vitro* EC work provide a causal relationship between the extent of CS (greater with high pulse pressures and hypertension) and altered mRNA and/or protein expression, which could in turn modulate EC function. Thus, alleviating mechanical stress in the vasculature through existing anti-hypertensive therapies may contribute to lower amyloid burden and thereby reduce neurodegeneration.

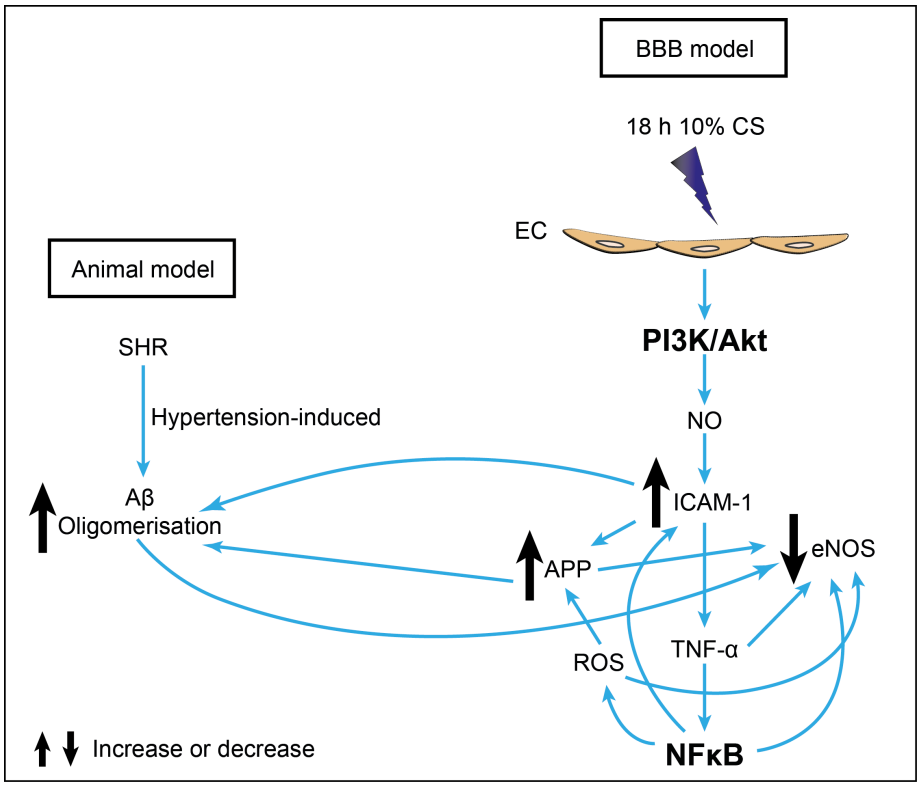

Figure 19. Diagrammatical representation elucidating relationship between CS, hypertension and associated biochemical pathways. The figure summarises both *in vitro* (right) and *in vivo* (left) findings of the present study. 18 hours of CS at 10% has increased APP and ICAM-1 with a concomitant decrease in eNOS at protein level. PI3K pathway is well known to mediate CS-induced-long-term-NO production (Takeda et al., 2006; Hu et al., 2013). NO release and/or CS could induce ICAM-1 expression, which is known to mediate TNF-α secretion, which could in turn activate NFκB (Lee et al., 2000; Radisavljevic et al., 2000; Antonelli et al., 2001; Lin et al., 2005; Riser et al., 2001). NFκB is pivotal in regulating eNOS expression, inflammatory responses through a negative feedback mechanism, such that sustained NFκB activation due to decreased bioavailable NO levels leading to inflammation (thus, up-regulating ICAM-1) and decreased eNOS expression (Grumbach et al., 2005; Silacci et al., 2000). In addition, CS could lead to increased ROS levels (not shown on the figure), thus it can be assumed that CS-induced NO would readily react with ROS manifesting oxidative stress as redox status is shifted towards the formation of ROS (Schreck et al., 1991; Wung et al., 1997). Additionally, this could lead to eNOS uncoupling, whereby eNOS would produce ROS rather than NO (Landmesser et al., 2003; Cheng et al., 2008). Collectively, these factors could lead to ED thereby continuously exacerbating deleterious effects on the endothelium. Moreover, increased ROS could lead to increased APP expression, which could also mitigate eNOS expression causing further damage to EC (Revett et al., 2013; Paris et al., 2000; d'Uscio et al., 2012). On the other hand, increased APP and ICAM-1, and deceased eNOS expression is simultaneously linked with enhanced Aβ oligomerisation, thereby providing a possible link between the *in vivo* and *in vitro* findings of the present study (Revett et al., 2013; Paris et al., 2000; d'Uscio et al., 2012; Apelt et al., 2002; Austin et al., 2013b, 2013a, 2010). Abbreviations: Aβ, amyloid beta; APP, amyloid precursor protein; BBB; blood brain barrier, CS, cyclic stretch; EC, endothelial cell; eNOS, endothelial nitric oxide synthase; ICAM-1, intercellular cell adhesion molecule-1; NFκB, nuclear factor kappa B; NO, nitric oxide; PI3K/Akt, phosphatidylinositol 3 OH-kinase/ serine/threonine-specific protein kinase Akt; ROS, reactive oxygen species; SHR, spontaneously hypertensive rat; TNF-α, tumour necrosis factor alpha.

6 References

Abbott, R. D., Howe, A. K., Langevin, H. M., and Iatridis, J. C. (2012). Live free or die: stretch-induced apoptosis occurs when adaptive reorientation of annulus fibrosus cells is restricted. *Biochem. Biophys. Res. Commun.* 421, 361–6.

Ahmed, M., Davis, J., Aucoin, D., Sato, T., Ahuja, S., Aimoto, S., Elliott, J. I., Van Nostrand, W. E., and Smith, S. O. (2010). Structural conversion of neurotoxic amyloid-β(1–42) oligomers to fibrils. *Nat. Struct. Mol. Biol.* 17, 561–7.

Akiyama, H., Barger, S., Barnum, S., Bradt, B., Bauer, J., Cole, G. M., Cooper, N. R., Eikelenboom, P., Emmerling, M., and Fiebich, B. L. (2000). Inflammation and Alzheimer's disease. *Neurobiol. Aging* 21, 383–421.

Amissah, B., Joashi, Blumberg, Mehmet, Edwards, and Cox (1998). Expression of amyloid precursor protein (β-APP) in the neonatal brain following hypoxic ischaemic injury. *Neuropathol. Appl. Neurobiol.* 24, 346–352.

Anderson, G. J., M. Cipolla, C., and Kennedy, R. T. (2011). Western blotting using capillary electrophoresis. *Anal. Chem.* 83, 1350–1355.

Antonelli, A., Bianchi, M., Crinelli, R., Gentilini, L., and Magnani, M. (2001). Modulation of ICAM-1 expression in ECV304 cells by macrophage-released cytokines. *Blood Cells. Mol. Dis.* 27, 978–91.

Apelt, J., Leßig, J., and Schliebs, R. (2002). β-amyloid-associated expression of intercellular adhesion molecule-1 in brain cortical tissue of transgenic Tg2576 mice. *Neurosci. Lett.* 329, 111–115.

Arendash, G. W., Su, G. C., Crawford, F. C., Bjugstad, K. B., and Mullan, M. (1999). Intravascular β-amyloid infusion increases blood pressure: implications for a vasoactive role of β-amyloid in the pathogenesis of Alzheimer's disease. *Neurosci. Lett.* 268, 17–20.

Austin, S. A., D'Uscio, L. V., and Katusic, Z. S. (2013a). Supplementation of nitric oxide attenuates AβPP and BACE1 protein in cerebral microcirculation of eNOS-deficient mice. *J. Alzheimers Dis.* 33, 29–33.

Austin, S. A., Santhanam, A. V, Hinton, D. J., Choi, D.-S., and Katusic, Z. S. (2013b). Endothelial nitric oxide deficiency promotes Alzheimer's disease pathology. *J. Neurochem.* 127, 691–700.

Austin, S. A., Santhanam, A. V, and Katusic, Z. S. (2010). Endothelial nitric oxide modulates expression and processing of amyloid precursor protein. *Circ. Res.* 107, 1498–1502.

Avolio, A., Butlin, M., and Protogerou, A. (2014). "Pulse pressure amplification and arterial stiffness in middle age," in *Blood Pressure and Arterial Wall Mechanics in Cardiovascular Diseases*, eds. M. E. Safar, M. F. O'Rourke, and E. D. Frohlich (Springer London), 281–295.

Avolio, A., Jones, D., and Tafazzoli-Shadpour, M. (1998). Quantification of Alterations in Structure and Function of Elastin in the Arterial Media. *Hypertension* 32, 170–175.

Awolesi, M. A., Sessa, W. C., and Sumpio, B. E. (1995). Cyclic strain upregulates nitric oxide synthase in cultured bovine aortic endothelial cells. *J. Clin. Invest.* 96, 1449–54.

Barnes, D. E., and Yaffe, K. (2011). The projected effect of risk factor reduction on Alzheimer's disease prevalence. *Lancet Neurol.* 10, 819–828.

Bauer, E. M., Qin, Y., Miller, T. W., Bandle, R. W., Csanyi, G., Pagano, P. J., Bauer, P. M., Schnermann, J., Roberts, D. D., and Isenberg, J. S. (2010). Thrombospondin-1 supports blood pressure by limiting eNOS activation and endothelial-dependent vasorelaxation. *Cardiovasc. Res.* 88, 471–81.

Berrout, J., Jin, M., and O'Neil, R. G. (2012). Critical role of TRPP2 and TRPC1 channels in stretch-induced injury of blood–brain barrier endothelial cells. *Brain Res.* **1436**, 1–12. doi:10.1016/j.brainres.2011.11.044.

Bhatia, S., Jenner, A. M., Li, H., Ruberu, K., Spiro, A. S., Shepherd, C. E., Kril, J. J., Kain, N., Don, A., and Garner, B. (2013). Increased apolipoprotein D dimer formation in Alzheimer's disease hippocampus is associated with lipid conjugated diene levels. *J. Alzheimer's Dis.* 35, 475–486.

Bramlett, H. M., Kraydieh, S., Green, E. J., and Dietrich, W. D. (1997). Temporal and regional patterns of axonal damage following traumatic brain injury: a β-amyloid precursor protein immunocytochemical study in rats. *J. Neuropathol. Exp. Neurol.* 56, 1132–1141.

Brown, R. C., Morris, A. P., and O'Neil, R. G. (2007). Tight junction protein expression and barrier properties of immortalized mouse brain microvessel endothelial cells. *Brain Res.* 1130, 17–30.

Castellano, J. M., Kim, J., Stewart, F. R., Jiang, H., DeMattos, R. B., Patterson, B. W., Fagan, A. M., Morris, J. C., Mawuenyega, K. G., and Cruchaga, C. (2011). Human apoE isoforms differentially regulate brain amyloid-β peptide clearance. *Sci. Transl. Med.* **3**, 89ra57. doi:10.1126/scitranslmed.3002156.

Chaitanya, G. V., Minagar, A., and Alexander, J. S. (2014). Neuronal and astrocytic interactions modulate brain endothelial properties during metabolic stresses of *in vitro* cerebral ischemia. *Cell Commun. Signal.* **12**, 7–21. doi:10.1186/1478-811X-12-7.

Chan, Y., Fish, J. E., D'Abreo, C., Lin, S., Robb, G. B., Teichert, A.-M., Karantzoulis-Fegaras, F., Keightley, A., Steer, B. M., and Marsden, P. A. (2004). The cell-specific expression of endothelial nitric-oxide synthase: a role for DNA methylation. *J. Biol. Chem.* 279, 35087–100.

Cheng, J., Ou, J.-S., Singh, H., Falck, J. R., Narsimhaswamy, D., Pritchard Jr, K. A., and Schwartzman, M. L. (2008). 20-hydroxyeicosatetraenoic acid causes endothelial dysfunction via eNOS uncoupling. *Am. J. Physiol. Circ. Physiol.* 294, H1018–H1026.

Cheng, J., Wung, B.-S., Chao, Y.-J., and Wang, D. L. (1996). Cyclic strain enhances adhesion of monocytes to endothelial cells by increasing intercellular adhesion molecule-1 expression. *Hypertension* 28, 386–391.

Cheng, W.-H., Lu, P.-J., Hsiao, M., Hsiao, C.-H., Ho, W.-Y., Cheng, P.-W., Lin, C.-T., Hong, L.-Z., and Tseng, C.-J. (2012). Renin activates PI3K-Akt-eNOS signalling through the angiotensin AT_1 and Mas receptors to modulate central blood pressure control in the nucleus tractus solitarii. *Br. J. Pharmacol.* 166, 2024–35.

Chisari, M., Merlo, S., Sortino, M. A., and Salomone, S. (2010). Long-term incubation with β-amyloid peptides impairs endothelium-dependent vasodilatation in isolated rat basilar artery. *Pharmacol. Res.* 61, 157–61.

Cleary, J. P., Walsh, D. M., Hofmeister, J. J., Shankar, G. M., Kuskowski, M. A., Selkoe, D. J., and Ashe, K. H. (2005). Natural oligomers of the amyloid-β protein specifically disrupt cognitive function. *Nat Neurosci* 8, 79–84.

Crawford, F., Suo, Z., Fang, C., and Mullan, M. (1998). Characteristics of the *in vitro* vasoactivity of β-amyloid peptides. *Exp. Neurol.* 150, 159–68.

Csiszar, A., Tucsek, Z., Toth, P., Sosnowska, D., Gautam, T., Koller, A., Deak, F., Sonntag, W. E., and Ungvari, Z. (2013). Synergistic effects of hypertension and aging on cognitive function and hippocampal expression of genes involved in β-amyloid generation and Alzheimer's disease. *Am. J. Physiol. Circ. Physiol.* 305, H1120–H1130.

Cucullo, L., Couraud, P.-O., Weksler, B., Romero, I.-A., Hossain, M., Rapp, E., and Janigro, D. (2008). Immortalized human brain endothelial cells and flow-based

vascular modeling: a marriage of convenience for rational neurovascular studies. *J. Cereb. Blood Flow Metab.* 28, 312–328.

Cucullo, L., Hossain, M., Tierney, W., and Janigro, D. (2013). A new dynamic *in vitro* modular capillaries-venules modular system: Cerebrovascular physiology in a box. *BMC Neurosci.* **14**, 18. doi:10.1186/1471-2202-14-18.

Cucullo, L., Marchi, N., Hossain, M., and Janigro, D. (2011). A dynamic *in vitro* BBB model for the study of immune cell trafficking into the central nervous system. *J. Cereb. Blood Flow Metab.* 31, 767–777.

Cucullo, L., McAllister, M. S., Kight, K., Krizanac-Bengez, L., Marroni, M., Mayberg, M. R., Stanness, K. A., and Janigro, D. (2002). A new dynamic *in vitro* model for the multidimensional study of astrocyte–endothelial cell interactions at the blood–brain barrier. *Brain Res.* 951, 243–254.

d'Uscio, L. V, Das, P., Santhanam, A. V. R., He, T., Younkin, S. G., and Katusic, Z. S. (2012). Activation of PPARδ prevents endothelial dysfunction induced by overexpression of amyloid-β precursor protein. *Cardiovasc. Res.* 96, 504–12.

Dancu, M. B., Berardi, D. E., Vanden Heuvel, J. P., and Tarbell, J. M. (2004). Asynchronous shear stress and circumferential strain reduces endothelial NO synthase and cyclooxygenase-2 but induces endothelin-1 gene expression in endothelial cells. *Arterioscler. Thromb. Vasc. Biol.* 24, 2088–94.

Deane, R., Wu, Z., Sagare, A., Davis, J., Du Yan, S., Hamm, K., Xu, F., Parisi, M., LaRue, B., Hu, H. W., et al. (2004). LRP/amyloid-β peptide interaction mediates differential brain efflux of Aβ isoforms. *Neuron* 43, 333–44.

Dias, A., Ferri, C., Graham, N., Ineichen, B., Prince, M., and Uwakwe, R. (2006). *Neurological Disorders: public health challenges*. World Health Organization.

Dick, A. S., Ivanovska, J., Kantores, C., Belcastro, R., Keith Tanswell, A., and Jankov, R. P. (2013). Cyclic stretch stimulates nitric oxide synthase-1-dependent peroxynitrite formation by neonatal rat pulmonary artery smooth muscle. *Free Radic. Biol. Med.* 61, 310–319.

Eikelenboom, P., Zhan, S. S., Kamphorst, W., van der Valk, P., and Rozemuller, J. M. (1994). Cellular and substrate adhesion molecules (integrins) and their ligands in cerebral amyloid plaques in Alzheimer's disease. *Virchows Arch.* 424, 421–427.

Facemire, C. S., Nixon, A. B., Griffiths, R., Hurwitz, H., and Coffman, T. M. (2009). Vascular endothelial growth factor receptor 2 controls blood pressure by regulating nitric oxide synthase expression. *Hypertension* 54, 652–8.

Faxén-Irving, G., Freund-Levi, Y., Eriksdotter-Jönhagen, M., Basun, H., Hjorth, E., Palmblad, J., Vedin, I., Cederholm, T., and Wahlund, L.-O. (2013). Effects on Transthyretin in Plasma and Cerebrospinal Fluid by DHA-Rich n–3 Fatty Acid Supplementation in Patients with Alzheimer's Disease: The OmegAD Study. *J. Alzheimer's Dis.* **36**, 1–6. doi:10.3233/JAD-121828.

Ferri, C. P., Prince, M., Brayne, C., Brodaty, H., Fratiglioni, L., Ganguli, M., Hall, K., Hasegawa, K., Hendrie, H., Huang, Y., et al. (2005). Global prevalence of dementia: a Delphi consensus study. *Lancet* 366, 2112–7.

Fleminger, S. (2003). Head injury as a risk factor for Alzheimer's disease: the evidence 10 years on; a partial replication. *J. Neurol. Neurosurg. Psychiatry* 74, 857–862.

Forlenza, M., Kaiser, T., Savelkoul, H. F. J., and Wiegertjes, G. F. (2012). The use of real-time quantitative PCR for the analysis of cytokine mRNA levels. *Methods Mol. Biol.* 820, 7–23.

Fu, W., Mao, P., Zhang, R., Pang, X. Q., Mo, H. Y., He, W. Q., Liu, X. Q., and Li, Y. M. (2013). Effects of cyclic stretch on expression of cytokines and intercelluar adhesion molecule-1 in human pulmonary artery endothelial cell. *Zhonghua Wei Zhong Bing Ji Jiu Yi Xue* 25, 484–488.

Gaillard, P. J., Voorwinden, L. H., Nielsen, J. L., Ivanov, A., Atsumi, R., Engman, H., Ringbom, C., de Boer, A. G., and Breimer, D. D. (2001). Establishment and functional characterization of an *in vitro* model of the blood–brain barrier, comprising a co-culture of brain capillary endothelial cells and astrocytes. *Eur. J. Pharm. Sci.* 12, 215–222.

Gan, L. (2000). Temporal regulation of endothelial ET-1 and eNOS expression in intact human conduit vessels exposed to different intraluminal pressure levels at physiological shear stress. *Cardiovasc. Res.* 48, 168–177.

Gao, J., Huang, T., Zhou, L.-J., Ge, Y.-L., Lin, S.-Y., and Dai, Y. (2014). Preconditioning effects of physiological cyclic stretch on pathologically mechanical stretch-induced alveolar epithelial cell apoptosis and barrier dysfunction. *Biochem. Biophys. Res. Commun.* 448, 342–348.

Garberg, P., Ball, M., Borg, N., Cecchelli, R., Fenart, L., Hurst, R. D., Lindmark, T., Mabondzo, A., Nilsson, J. E., and Raub, T. J. (2005). *In vitro* models for the blood–brain barrier. *Toxicol. Vitr.* 19, 299–334.

Ghiso, J., Fossati, S., and Rostagno, A. (2014). Amyloidosis associated with cerebral amyloid angiopathy: cell signaling pathways elicited in cerebral endothelial cells. *J Alzheimers Dis.* 42, S167–76.

Ginzinger, D. G. (2002). Gene quantification using real-time quantitative PCR. *Exp. Hematol.* 30, 503–512.

Glenner, G. G., and Wong, C. W. (1984). Alzheimer's disease: initial report of the purification and characterization of a novel cerebrovascular amyloid protein. *Biochem. Biophys. Res. Commun.* 120, 885–90.

Golomb, J., Wisoff, J., Miller, D. C., Boksay, I., Kluger, A., Weiner, H., Salton, J., and Graves, W. (2000). Alzheimer's disease comorbidity in normal pressure hydrocephalus: prevalence and shunt response. *J. Neurol. Neurosurg. Psychiatry* 68, 778–81.

Gouras, G. K., Tampellini, D., Takahashi, R. H., and Capetillo-Zarate, E. (2010). Intraneuronal Aβ accumulation and synapse pathology in Alzheimer's disease. *Acta Neuropathol.* 119, 523–41.

Graham, D. I., Gentleman, S. M., Lynch, A., and Roberts, G. W. (1995). Distribution of β-amyloid protein in the brain following severe head injury. *Neuropathol. Appl. Neurobiol.* 21, 27–34.

Grumbach, I. M., Chen, W., Mertens, S. A., and Harrison, D. G. (2005). A negative feedback mechanism involving nitric oxide and nuclear factor κ-B modulates endothelial nitric oxide synthase transcription. *J. Mol. Cell. Cardiol.* 39, 595–603.

Grundke-Iqbal, I., Iqbal, K., George, L., Tung, Y. C., Kim, K. S., and Wisniewski, H. M. (1989). Amyloid protein and neurofibrillary tangles coexist in the same neuron in Alzheimer disease. *Proc. Natl. Acad. Sci.* 86, 2853–2857.

Gupta, V. B., Laws, S. M., Villemagne, V. L., Ames, D., Bush, A. I., Ellis, K. A., Lui, J. K., Masters, C., Rowe, C. C., Szoeke, C., et al. (2011). Plasma apolipoprotein E and Alzheimer disease risk: the AIBL study of aging. *Neurology* 76, 1091–8.

Gupta, V. K., You, Y., Klistorner, A., and Graham, S. L. (2012). Shp-2 regulates the TrkB receptor activity in the retinal ganglion cells under glaucomatous stress. *Biochim. Biophys. Acta* 1822, 1643–9.

Hanon, O., Haulon, S., Lenoir, H., Seux, M.-L., Rigaud, A.-S., Safar, M., Girerd, X., and Forette, F. (2005). Relationship between arterial stiffness and cognitive function in elderly subjects with complaints of memory loss. *Stroke.* 36, 2193–7.

Harrap, S. B., Van der Merwe, W. M., Griffin, S. A., Macpherson, F., and Lever, A. F. (1990). Brief angiotensin converting enzyme inhibitor treatment in young

spontaneously hypertensive rats reduces blood pressure long-term. *Hypertension* 16, 603–614.

Hishikawa, K., Oemar, B. S., Yang, Z., and Luscher, T. F. (1997). Pulsatile stretch stimulates superoxide production and activates nuclear factor κ-B in human coronary smooth muscle. *Circ. Res.* 81, 797–803.

Hlubocká, Z., Umnerová, V., Heller, S., Peleska, J., Jindra, A., Jáchymová, M., Kvasnicka, J., Horký, K., and Aschermann, M. (2002). Circulating intercellular cell adhesion molecule-1, endothelin-1 and von Willebrand factor-markers of endothelial dysfunction in uncomplicated essential hypertension: the effect of treatment with ACE inhibitors. *J. Hum. Hypertens.* 16, 557–62.

Hu, Z., Xiong, Y., Han, X., Geng, C., Jiang, B., Huo, Y., and Luo, J. (2013). Acute mechanical stretch promotes eNOS activation in venous endothelial cells mainly via PKA and Akt pathways. *PLoS One* **8**, e71359. doi:10.1371/journal.pone.0071359.

Huang, A., Yang, Y.-M., Feher, A., Bagi, Z., Kaley, G., and Sun, D. (2012). Exacerbation of endothelial dysfunction during the progression of diabetes: role of oxidative stress. *Am. J. Physiol. Regul. Integr. Comp. Physiol.* 302, R674–81.

Huang, Z., Huang, P. L., Panahian, N., Dalkara, T., Fishman, M. C., and Moskowitz, M. A. (1994). Effects of cerebral ischemia in mice deficient in neuronal nitric oxide synthase. *Science (80-.).* 265, 1883–1885.

Hughes, A. J., and Herr, A. E. (2012). Microfluidic western blotting. *Proc. Natl. Acad. Sci.* 109, 21450–21455.

Juan, S.-H., Chen, J.-J., Chen, C.-H., Lin, H., Cheng, C.-F., Liu, J.-C., Hsieh, M.-H., Chen, Y.-L., Chao, H.-H., Chen, T.-H., et al. (2004). 17β-Estradiol inhibits cyclic strain-induced endothelin-1 gene expression within vascular endothelial cells. *Am. J. Physiol. Heart Circ. Physiol.* 287, H1254–61.

Kamiichi, A., Furihata, T., Kishida, S., Ohta, Y., Saito, K., Kawamatsu, S., and Chiba, K. (2012). Establishment of a new conditionally immortalized cell line from human brain microvascular endothelial cells: a promising tool for human blood–brain barrier studies. *Brain Res.* 1488, 113–122.

Kizu, O., Yamada, K., and Nishimura, T. (2001). Proton chemical shift imaging in normal pressure hydrocephalus. *Am. J. Neuroradiol.* 22, 1659–1664.

Kuebler, W. M., Uhlig, U., Goldmann, T., Schael, G., Kerem, A., Exner, K., Martin, C., Vollmer, E., and Uhlig, S. (2003). Stretch activates nitric oxide production in pulmonary vascular endothelial cells in situ. *Am. J. Respir. Crit. Care Med.* 168, 1391–1398.

Kurata, T., Lukic, V., Kozuki, M., Wada, D., Miyazaki, K., Morimoto, N., Ohta, Y., Deguchi, K., Ikeda, Y., Kamiya, T., et al. (2014a). Telmisartan reduces progressive accumulation of cellular amyloid-β and phosphorylated Tau with inflammatory responses in aged spontaneously hypertensive stroke resistant rat. *J. Stroke Cerebrovasc. Dis.*, In press. doi:10.1016/j.jstrokecerebrovasdis.2014.05.023.

Kurata, T., Lukic, V., Kozuki, M., Wada, D., Miyazaki, K., Morimoto, N., Ohta, Y., Deguchi, K., Yamashita, T., Hishikawa, N., et al. (2014b). Long-term effect of Telmisartan on Alzheimer's amyloid genesis in SHR-SR after tMCAO. *Transl. Stroke Res.*, 1–9. doi:10.1007/s12975-013-0321-y.

Kurtz, T. W., and Morris, R. C. (1987). Biological variability in Wistar-Kyoto rats. Implications for research with the spontaneously hypertensive rat. *Hypertension* 10, 127–31.

De la Torre, J. C., and Aliev, G. (2005). Inhibition of vascular nitric oxide after rat chronic brain hypoperfusion: spatial memory and immunocytochemical changes. *J. Cereb. Blood Flow Metab.* 25, 663–72.

LaFerla, F. M., Green, K. N., and Oddo, S. (2007). Intracellular amyloid-β in Alzheimer's disease. *Nat. Rev. Neurosci.* 8, 499–509.

Landmesser, U., Dikalov, S., Price, S. R., McCann, L., Fukai, T., Holland, S. M., Mitch, W. E., and Harrison, D. G. (2003). Oxidation of tetrahydrobiopterin leads to uncoupling of endothelial cell nitric oxide synthase in hypertension. *J. Clin. Invest.* 111, 1201–9.

Langbaum, J. B. S., Chen, K., Launer, L. J., Fleisher, A. S., Lee, W., Liu, X., Protas, H. D., Reeder, S. A., Bandy, D., Yu, M., et al. (2012). Blood pressure is associated with higher brain amyloid burden and lower glucose metabolism in healthy late middle-age persons. *Neurobiol. Aging* **33**, 827.e11–9. doi:10.1016/j.neurobiolaging.2011.06.020.

Laurent, S., Boutouyrie, P., Asmar, R., Gautier, I., Laloux, B., Guize, L., Ducimetiere, P., and Benetos, A. (2001). Aortic stiffness is an independent predictor of all-cause and cardiovascular mortality in hypertensive Patients. *Hypertension* 37, 1236–1241.

Lee, C. Y. D., and Landreth, G. E. (2013). The role of microglia in amyloid clearance from the AD brain. 117, 949–960.

Lee, S. J., Drabik, K., Van Wagoner, N. J., Lee, S., Choi, C., Dong, Y., and Benveniste, E. N. (2000). ICAM-1-induced expression of proinflammatory cytokines in astrocytes: involvement of extracellular signal-regulated kinase and p38 mitogen-activated protein kinase pathways. *J. Immunol.* 165, 4658–4666.

Lin, S.-J., Shyne, S.-K., Hung, Y.-Y., Chen, Y.-H., Ku, H.-H., Chen, J.-W., Tam, K.-B., and Chen, Y.-L. (2005). S2-04 Superoxide dismutase inhibits the expression of VCAM-1 and ICAM-1 induced by TNF-α in human endothelial cells via the JNK/P38 pathways. *Arterioscler. Thromb. Vasc. Biol.* 25, 334–340.

Lindner, C., Sigrüner, A., Walther, F., Bogdahn, U., Couraud, P. O., Schmitz, G., and Schlachetzki, F. (2012). ATP-binding cassette transporters in immortalised human brain microvascular endothelial cells in normal and hypoxic conditions. *Exp. Transl. Stroke Med.* **4**, 1–10. doi:10.1186/2040-7378-4-9.

Liu, J.-C., Chen, J.-J., Chan, P., Cheng, C.-F., and Cheng, T.-H. (2003a). Inhibition of cyclic strain-induced endothelin-1 gene expression by resveratrol. *Hypertension* 42, 1198–205.

Liu, X., Ensenat, D., Wang, H., Schafer, A. I., and Durante, W. (2003b). Physiologic cyclic stretch inhibits apoptosis in vascular endothelium. *FEBS Lett.* 541, 52–56.

Loane, D. J., Pocivavsek, A., Moussa, C. E.-H., Thompson, R., Matsuoka, Y., Faden, A. I., Rebeck, G. W., and Burns, M. P. (2009). Amyloid precursor protein secretases as therapeutic targets for traumatic brain injury. *Nat. Med.* 15, 377–9.

Mackic, J. B., Stins, M., McComb, J. G., Calero, M., Ghiso, J., Kim, K. S., Yan, S. D., Stern, D., Schmidt, A. M., Frangione, B., et al. (1998). Human blood-brain barrier receptors for Alzheimer's amyloid-β 1- 40. Asymmetrical binding, endocytosis, and transcytosis at the apical side of brain microvascular endothelial cell monolayer. *J. Clin. Invest.* 102, 734–43.

MacPhee, D. J. (2010). Methodological considerations for improving Western blot analysis. *J. Pharmacol. Toxicol. Methods* 61, 171–177.

Maltese, W. A., Wilson, S., Tan, Y., Suomensaari, S., Sinha, S., Barbour, R., and McConlogue, L. (2001). Retention of the Alzheimer's amyloid precursor fragment C99 in the endoplasmic reticulum prevents formation of amyloid β-peptide. *J. Biol. Chem.* 276, 20267–79.

Mao, X., Xie, L., Greenberg, R. B., Greenberg, J. B., Peng, B., Mieling, I., Jin, K., and Greenberg, D. A. (2014). Flow-induced regulation of brain endothelial cells *in vitro*. *Vascul. Pharmacol.* 62, 82–7.

Masters, C. L., and Selkoe, D. J. (2012). Biochemistry of amyloid β-protein and amyloid deposits in Alzheimer disease. *Cold Spring Harb. Perspect. Med.* 2, a006262.

Matthews, B. D., Thodeti, C. K., Tytell, J. D., Mammoto, A., Overby, D. R., and Ingber, D. E. (2010). Ultra-rapid activation of TRPV4 ion channels by mechanical forces applied to cell surface β1 integrins. *Integr. Biol.* 2, 435–442.

McKinney, J. S., Willoughby, K. A., Liang, S., and Ellis, E. F. (1996). Stretch-induced injury of cultured neuronal, glial, and endothelial cells : effect of polyethylene glycol conjugated superoxide dismutase. *Stroke* 27, 934–940.

McKinnon, S. J., Lehman, D. M., Kerrigan-Baumrind, L. A., Merges, C. A., Pease, M. E., Kerrigan, D. F., Ransom, N. L., Tahzib, N. G., Reitsamer, H. A., and Levkovitch-Verbin, H. (2002). Caspase activation and amyloid precursor protein cleavage in rat ocular hypertension. *Invest. Ophthalmol. Vis. Sci.* 43, 1077–1087.

Meneses, A., and Hong, E. (1998). Spontaneously hypertensive rats : a potential model to identify drugs for treatment of learning disorders. *Hypertension* 31, 968–972.

Meng, X.-F., Yu, J.-T., Wang, H.-F., Tan, M.-S., Wang, C., Tan, C.-C., and Tan, L. (2014). Midlife vascular risk factors and the risk of Alzheimer's Disease: a systematic review and meta-analysis. *J. Alzheimers. Dis.*, In press. doi:10.3233/JAD-140954.

Mitchell, G. F., van Buchem, M. A., Sigurdsson, S., Gotal, J. D., Jonsdottir, M. K., Kjartansson, Ó., Garcia, M., Aspelund, T., Harris, T. B., Gudnason, V., et al. (2011). Arterial stiffness, pressure and flow pulsatility and brain structure and function: the Age, Gene/Environment Susceptibility--Reykjavik study. *Brain* 134, 3398–407.

Muruganandam, A., Herx, L. M., Monette, R., Durkin, J. P., and Stanimirovic, D. B. (1997). Development of immortalized human cerebromicrovascular endothelial cell line as an *in vitro* model of the human blood-brain barrier. *FASEB J.* 11, 1187–1197.

Nagai, Y., Yokoi, H., Kaihara, K., and Naruse, K. (2012). The mechanical stimulation of cells in 3D culture within a self-assembling peptide hydrogel. *Biomaterials* 33, 1044–1051.

Naik, P., and Cucullo, L. (2012). *In vitro* blood–brain barrier models: current and perspective technologies. *J. Pharm. Sci.* 101, 1337–1354.

Naruse, K., Sai, X., Yokoyama, N., and Sokabe, M. (1998a). Uni-axial cyclic stretch induces c-src activation and translocation in human endothelial cells via SA channel activation. *FEBS Lett.* 441, 111–115.

Naruse, K., Yamada, T., and Sokabe, M. (1998b). Involvement of SA channels in orienting response of cultured endothelial cells to cyclic stretch. *Am. J. Physiol.* 274, H1532–8.

Nation, D. A., Edland, S. D., Bondi, M. W., Salmon, D. P., Delano-Wood, L., Peskind, E. R., Quinn, J. F., and Galasko, D. R. (2013). Pulse pressure is associated with Alzheimer biomarkers in cognitively normal older adults. *Neurology* 81, 2024–7.

Neuhaus, W., Lauer, R., Oelzant, S., Fringeli, U. P., Ecker, G. F., and Noe, C. R. (2006). A novel flow based hollow-fiber blood–brain barrier *in vitro* model with immortalised cell line PBMEC/C1–2. *J. Biotechnol.* 125, 127–141.

Ng, K., Butlin, M., and Avolio, A. P. (2012). Persistent effect of early, brief angiotensin-converting enzyme inhibition on segmental pressure dependency of aortic stiffness in spontaneously hypertensive rats. *J. Hypertens.* 30, 1782–90.

Northcott, C. A., Billecke, S., Craig, T., Hinojosa-Laborde, C., Patel, K. P., Chen, A. F., D'Alecy, L. G., and Haywood, J. R. (2012). Nitric oxide synthase, ADMA, SDMA, and nitric oxide activity in the paraventricular nucleus throughout the etiology of renal wrap hypertension. *Am. J. Physiol. Heart Circ. Physiol.* 302, H2276–84.

Oemar, B. S., Tschudi, M. R., Godoy, N., Brovkovich, V., Malinski, T., and Luscher, T. F. (1998). Reduced endothelial nitric oxide synthase expression and production in human atherosclerosis. *Circulation* 97, 2494–2498.

Omidi, Y., Campbell, L., Barar, J., Connell, D., Akhtar, S., and Gumbleton, M. (2003). Evaluation of the immortalised mouse brain capillary endothelial cell line, b. End3, as

an *in vitro* blood–brain barrier model for drug uptake and transport studies. *Brain Res.* 990, 95–112.

Ong, W.-Y., Ng, M. P.-E., Loke, S.-Y., Jin, S., Wu, Y.-J., Tanaka, K., and Wong, P. T.-H. (2013). Comprehensive gene expression profiling reveals synergistic functional networks in cerebral vessels after hypertension or hypercholesterolemia. *PLoS One* **8**, e68335. doi:10.1371/journal.pone.0068335.

Owen, J. B., Sultana, R., Aluise, C. D., Erickson, M. A., Price, T. O., Bu, G., Banks, W. A., and Butterfield, D. A. (2010). Oxidative modification to LDL receptor-related protein 1 in hippocampus from subjects with Alzheimer disease: implications for Aβ accumulation in AD brain. *Free Radic. Biol. Med.* 49, 1798–803.

Panes, J., Perry, M., Anderson, D., Muzykantov, V., Carden, D., Miyasaka, M., and Granger, D. (1996). Portal hypertension enhances endotoxin-induced intercellular adhesion molecule 1 up-regulation in the rat. *Gastroenterology* 110, 866–874.

Paolinelli, R., Corada, M., Ferrarini, L., Devraj, K., Artus, C., Czupalla, C. J., Rudini, N., Maddaluno, L., Papa, E., and Engelhardt, B. (2013). Wnt activation of immortalized brain endothelial cells as a tool for generating a standardized model of the blood brain barrier *in vitro*. *PLoS One* **8**, e70233. doi:10.1371/journal.pone.0070233.

Paris, D., Town, T., Mori, T., Parker, T. A., Humphrey, J., and Mullan, M. (2000). Soluble β-amyloid peptides mediate vasoactivity via activation of a pro-inflammatory pathway. *Neurobiol. Aging* 21, 183–197.

Park, L., Koizumi, K., El Jamal, S., Zhou, P., Previti, M. Lou, Van Nostrand, W. E., Carlson, G., and Iadecola, C. (2014). Age-dependent neurovascular dysfunction and damage in a mouse model of cerebral amyloid angiopathy. *Stroke.* 45, 1815–1821.

Patabendige, A., Skinner, R. A., Morgan, L., and Joan Abbott, N. (2013). A detailed method for preparation of a functional and flexible blood–brain barrier model using porcine brain endothelial cells. *Brain Res.* 1521, 16–30.

Paxinos, G., and Watson, C. (2007). *The Rat Brain in Stereotaxic Coordinates*. London: Elsevier Inc. Academic Press.

Petersen, L. J., Petersen, J. R., Ladefoged, S. D., Mehlsen, J., and Jensen, H. A. (1995). The pulsatility index and the resistive index in renal arteries in patients with hypertension and chronic renal failure. *Nephrol. Dial. Transplant.* 10, 2060–2064.

Pflanzner, T., Janko, M. C., André-Dohmen, B., Reuss, S., Weggen, S., Roebroek, A. J. M., Kuhlmann, C. R. W., and Pietrzik, C. U. (2011). LRP1 mediates bidirectional transcytosis of amyloid-β across the blood-brain barrier. *Neurobiol. Aging* **32**, 2323.e1–11. doi:10.1016/j.neurobiolaging.2010.05.025.

Poller, B., Gutmann, H., Krähenbühl, S., Weksler, B., Romero, I., Couraud, P., Tuffin, G., Drewe, J., and Huwyler, J. (2008). The human brain endothelial cell line hCMEC/D3 as a human blood-brain barrier model for drug transport studies. *J. Neurochem.* 107, 1358–1368.

Pryor, N. E., Moss, M. A., and Hestekin, C. N. (2012). Unraveling the early events of amyloid-β protein (Aβ) aggregation: techniques for the determination of Aβ aggregate size. *Int. J. Mol. Sci.* 13, 3038–72.

Qia, O, J., Wang, X., Wenhui, L., Xinyang, W., and Ma, A. (2014). Abnormal expression level of BACE1 and RAGE of hippocampus related to cognitive impairment in SHR. *Ann Clin Exp Hypertens.* 2, 1010.

Radisavljevic, Z., Avraham, H., and Avraham, S. (2000). Vascular endothelial growth factor up-regulates ICAM-1 expression via the phosphatidylinositol 3 OH-kinase/AKT/Nitric oxide pathway and modulates migration of brain microvascular endothelial cells. *J. Biol. Chem.* 275, 20770–4.

Rajadas, J., Sun, W., Li, H., Inayathullah, M., Cereghetti, D., Tan, A., de Mello Coelho, V., Chrest, F. J., Kusiak, J. W., and Smith, W. W. (2013). Enhanced Aβ1–40

production in endothelial cells stimulated with fibrillar Aβ1–42. *PLoS One* **8**, e58194. doi:10.1371/journal.pone.0058194.

Revett, T. J., Baker, G. B., Jhamandas, J., and Kar, S. (2013). Glutamate system, amyloid ß peptides and tau protein: functional interrelationships and relevance to Alzheimer disease pathology. *J. Psychiatry Neurosci.* 38, 6–23.

Riser, B. L., Varani, J., Cortes, P., Yee, J., Dame, M., and Sharba, A. K. (2001). Cyclic stretching of mesangial cells up-regulates intercellular adhesion molecule-1 and leukocyte adherence: a possible new mechanism for glomerulosclerosis. *Am. J. Pathol.* **158**, 11–7. doi:10.1016/S0002-9440(10)63938-7.

Rozemuller, J. M., Eikelenboom, P., Pals, S. T., and Stam, F. C. (1989). Microglial cells around amyloid plaques in Alzheimer's disease express leucocyte adhesion molecules of the LFA-1 family. *Neurosci. Lett.* 101, 288–292.

Sabayan, B., Jansen, S., Oleksik, A. M., van Osch, M. J. P., van Buchem, M. A., van Vliet, P., de Craen, A. J. M., and Westendorp, R. G. J. (2012). Cerebrovascular hemodynamics in Alzheimer's disease and vascular dementia: a meta-analysis of transcranial Doppler studies. *Ageing Res. Rev.* 11, 271–277.

Santaguida, S., Janigro, D., Hossain, M., Oby, E., Rapp, E., and Cucullo, L. (2006). Side by side comparison between dynamic versus static models of blood–brain barrier *in vitro*: A permeability study. *Brain Res.* **1109**, 1–13. doi:10.1016/j.brainres.2006.06.027.

Scheuermann, S., Hambsch, B., Hesse, L., Stumm, J., Schmidt, C., Beher, D., Bayer, T. A., Beyreuther, K., and Multhaup, G. (2001). Homodimerization of amyloid precursor protein and its implication in the amyloidogenic pathway of Alzheimer's disease. *J. Biol. Chem.* 276, 33923–33929.

Schmittgen, T. D., and Livak, K. J. (2008). Analyzing real-time PCR data by the comparative CT method. *Nat. Protoc.* 3, 1101–1108.

Schreck, R., Rieber, P., and Baeuerle, P. A. (1991). Reactive oxygen intermediates as apparently widely used messengers in the activation of the NF-kappa B transcription factor and HIV-1. *EMBO J.* 10, 2247–58.

Schreiber, S., Drukarch, B., Garz, C., Niklass, S., Stanaszek, L., Kropf, S., Bueche, C., Held, F., Vielhaber, S., Attems, J., et al. (2014). Interplay between age, cerebral small vessel disease, parenchymal amyloid-β, and Tau pathology: longitudinal studies in hypertensive stroke-prone rats. *J. Alzheimers. Dis.* 42, S205–15.

Selkoe, D. J. (2001). Alzheimer's disease: genes, proteins, and therapy. *Physiol Rev* 81, 741–766.

Shikata, Y., Rios, A., Kawkitinarong, K., DePaola, N., Garcia, J. G. N., and Birukov, K. G. (2005). Differential effects of shear stress and cyclic stretch on focal adhesion remodeling, site-specific FAK phosphorylation, and small GTPases in human lung endothelial cells. *Exp. Cell Res.* 304, 40–49.

Siddharthan, V., Kim, Y. V, Liu, S., and Kim, K. S. (2007). Human astrocytes/astrocyte-conditioned medium and shear stress enhance the barrier properties of human brain microvascular endothelial cells. *Brain Res.* 1147, 39–50.

Silacci, P., Formentin, K., Bouzourène, K., Daniel, F., Brunner, H. R., and Hayoz, D. (2000). Unidirectional and oscillatory shear stress differentially modulate NOS III gene expression. *Nitric Oxide* 4, 47–56.

Sloan, C. D. K., Nandi, P., Linz, T. H., Aldrich, J. V, Audus, K. L., and Lunte, S. M. (2012). Analytical and biological methods for probing the blood-brain barrier. *Annu. Rev. Anal. Chem. (Palo Alto. Calif).* 5, 505–531.

Smith, C. C. T., Stanyer, L., and Betteridge, D. J. (2004). Soluble β-amyloid (Aβ) 40 causes attenuation or potentiation of noradrenaline-induced vasoconstriction in rats depending upon the concentration employed. *Neurosci. Lett.* 367, 129–32.

Song, F., Poljak, A., Crawford, J., Kochan, N. A., Wen, W., Cameron, B., Lux, O., Brodaty, H., Mather, K., and Smythe, G. A. (2012). Plasma apolipoprotein levels are associated with cognitive status and decline in a community cohort of older individuals. *PLoS One* **7**, e34078. doi:10.1371/journal.pone.0034078.

Song, L., and Pachter, J. S. (2003). Culture of murine brain microvascular endothelial cells that maintain expression and cytoskeletal association of tight junction-associated proteins. *Vitr. Cell. Dev. Biol.* 39, 313–320.

Sontag, T.-A., Fuermaier, A. B. M., Hauser, J., Kaunzinger, I., Tucha, O., and Lange, K. W. (2013). Spatial memory in spontaneously hypertensive rats (SHR). *PLoS One* **8**, e74660. doi:10.1371/journal.pone.0074660.

Spescha, R. D., Glanzmann, M., Simic, B., Witassek, F., Keller, S., Akhmedov, A., Tanner, F. C., Lüscher, T. F., and Camici, G. G. (2014). Adaptor protein p66Shc mediates hypertension-associated, cyclic stretch-dependent, endothelial damage. *Hypertension* 64, 347–53.

Stanyon, H. F., and Viles, J. H. (2012). Human serum albumin can regulate amyloid-β peptide fiber growth in the brain interstitium; implications for Alzheimer disease. *J. Biol. Chem.* 287, 28163–28168.

Stefani, A., Sancesario, G., Pierantozzi, M., Leone, G., Galati, S., Hainsworth, A. H., and Diomedi, M. (2009). CSF biomarkers, impairment of cerebral hemodynamics and degree of cognitive decline in Alzheimer's and mixed dementia. *J. Neurol. Sci.* 283, 109–15.

Suo, Z., Humphrey, J., Kundtz, A., Sethi, F., Placzek, A., Crawford, F., and Mullan, M. (1998). Soluble Alzheimers β-amyloid constricts the cerebral vasculature *in vivo*. *Neurosci. Lett.* 257, 77–80.

Sureshbabu, N., Kirubagaran, R., and Jayakumar, R. (2009). Surfactant-induced conformational transition of amyloid-β peptide. *Eur. Biophys. J.* 38, 355–67.

Suzuki, M., Naruse, K., Asano, Y., Okamoto, T., Nishikimi, N., Sakurai, T., Nimura, Y., and Sokabe, M. (1997). Up-regulation of integrin β3 expression by cyclic stretch in human umbilical endothelial cells. *Biochem. Biophys. Res. Commun.* 239, 372–376.

Tai, L. M., Reddy, P. S., Lopez-Ramirez, M. A., Davies, H. A., Male, A. D. K., Loughlin, A. J., and Romero, I. A. (2009). Polarized P-glycoprotein expression by the immortalised human brain endothelial cell line, hCMEC/D3, restricts apical-to-basolateral permeability to rhodamine 123. *Brain Res.* 1292, 14–24.

Takeda, H., Komori, K., Nishikimi, N., Nimura, Y., Sokabe, M., and Naruse, K. (2006). Bi-phasic activation of eNOS in response to uni-axial cyclic stretch is mediated by differential mechanisms in BAECs. *Life Sci.* 79, 233–9.

Tan, I., Butlin, M., Liu, Y. Y., Ng, K., and Avolio, A. P. (2012). Heart rate dependence of aortic pulse wave velocity at different arterial pressures in rats. *Hypertension* 60, 528–33.

Tan, Y., Tseng, P.-O., Wang, D., Zhang, H., Hunter, K., Hertzberg, J., Stenmark, K. R., and Tan, W. (2014). Stiffening-induced high pulsatility flow activates endothelial inflammation via a TLR2/NF-κB pathway. *PLoS One* **9**, e102195. doi:10.1371/journal.pone.0102195.

Thacher, T., Gambillara, V., da Silva, R. F., Silacci, P., and Stergiopulos, N. (2010). Reduced cyclic stretch, endothelial dysfunction, and oxidative stress: an ex vivo model. *Cardiovasc. Pathol.* **19**, e91–e98. doi:10.1016/j.carpath.2009.06.007.

Thodeti, C. K., Matthews, B., Ravi, A., Mammoto, A., Ghosh, K., Bracha, A. L., and Ingber, D. E. (2009). TRPV4 channels mediate cyclic strain–induced endothelial cell reorientation through integrin-to-integrin signaling. *Circ. Res.* 104, 1123–1130.

Thomas, T., McLendon, C., Sutton, E. T., and Thomas, G. (1997). Cerebrovascular endothelial dysfunction mediated by β-amyloid. *Neuroreport* 8, 1387–1391.

Thomas, T., Thomas, G., McLendon, C., Sutton, T., and Mullan, M. (1996). β-amyloid-mediated vasoactivity and vascular endothelial damage. *Nature* 380, 168–171.

Toda, M., Yamamoto, K., Shimizu, N., Obi, S., Kumagaya, S., Igarashi, T., Kamiya, A., and Ando, J. (2008). Differential gene responses in endothelial cells exposed to a combination of shear stress and cyclic stretch. *J. Biotechnol.* 133, 239–44.

Toda, N., Hatano, Y., and Hayashi, S. (1978). Modifications by stretches of the mechanical response of isolated cerebral and extracerebral arteries to vasoactive agents. *Pflügers Arch. Eur. J. Physiol.* 374, 73–77.

Toda, N., and Okamura, T. (2012). Cerebral blood flow regulation by nitric oxide in Alzheimer's disease. *J. Alzheimer's Dis.* 32, 569–578.

Torre, J. C. de la, Pappas, B. A., Prevot, V., Emmerling, M. R., Mantione, K., Fortin, T., Watson, M. D., and Stefano, G. B. (2013). Hippocampal nitric oxide upregulation precedes memory loss and Aβ 1-40 accumulation after chronic brain hypoperfusion in rats. *Neurol. Res.* 25, 635–41.

Toyama, B. H., and Weissman, J. S. (2011). Amyloid structure: conformational diversity and consequences. *Annu. Rev. Biochem.* 80, 557–85.

Trochu, J.-N., Bouhour, J.-B., Kaley, G., and Hintze, T. H. (2000). Role of endothelium-derived nitric oxide in the regulation of cardiac oxygen metabolism implications in health and disease. *Circ. Res.* 87, 1108–1117.

Verbeek, M. M., Otte-Höller, I., Wesseling, P., Ruiter, D. J., and de Waal, R. M. W. (1996). Differential expression of intercellular adhesion molecule-1 (ICAM-1) in the Aβ containing lesions in brains of patients with dementia of the Alzheimer type. *Acta Neuropathol.* 91, 608–615.

Virchow, R. (1860). "Lecture XVI. A more precise account of fatty metamorphosis.," in *Cellular pathology as based upon physiological and pathological histology* (RM De Witt), 409–410.

Vu, K., Weksler, B., Romero, I., Couraud, P.-O., and Gelli, A. (2009). Immortalized human brain endothelial cell line HCMEC/D3 as a model of the blood-brain barrier facilitates *in vitro* studies of central nervous system infection by Cryptococcus neoformans. *Eukaryot. Cell* 8, 1803–1807.

Wallace, S. M. L., McEniery, C. M., Mäki-Petäjä, K. M., Booth, A. D., Cockcroft, J. R., and Wilkinson, I. B. (2007). Isolated systolic hypertension is characterized by increased aortic stiffness and endothelial dysfunction. *Hypertension* 50, 228–233.

Wan, X.-Z., Li, B., Li, Y.-C., Yang, X.-L., Zhang, W., Zhong, L., and Tang, S.-J. (2012). Activation of NMDA receptors upregulates a disintegrin and metalloproteinase 10 via a Wnt/MAPK signaling pathway. *J. Neurosci.* 32, 3910–6.

Wang, Y.-J., Zhou, H.-D., and Zhou, X.-F. (2006a). Clearance of amyloid-β in Alzheimer's disease: progress, problems and perspectives. *Drug Discov. Today* 11, 931–8.

Wang, Y.-J., Zhou, H.-D., and Zhou, X.-F. (2006b). Clearance of amyloid-β in Alzheimer's disease: progress, problems and perspectives. *Drug Discov. Today* 11, 931–8.

Weber, M., Hagedorn, C. H., Harrison, D. G., and Searles, C. D. (2005). Laminar shear stress and 3' polyadenylation of eNOS mRNA. *Circ. Res.* 96, 1161–8.

Wei, E. P., Kontos, H. A., Christman, C. W., DeWitt, D. S., and Povlishock, J. T. (1985). Superoxide generation and reversal of acetylcholine-induced cerebral arteriolar dilation after acute hypertension. *Circ. Res.* 57, 781–787.

Wood, K. C., Cortese-Krott, M. M., Kovacic, J. C., Noguchi, A., Liu, V. B., Wang, X., Raghavachari, N., Boehm, M., Kato, G. J., Kelm, M., et al. (2013). Circulating blood endothelial nitric oxide synthase contributes to the regulation of systemic blood pressure and nitrite homeostasis. *Arterioscler. Thromb. Vasc. Biol.* 33, 1861–71.

Wostyn, P., Audenaert, K., and De Deyn, P. P. (2008). Alzheimer's disease-related changes in diseases characterized by elevation of intracranial or intraocular pressure. *Clin. Neurol. Neurosurg.* 110, 101–9.

Wu, J., Thabet, S. R., Kirabo, A., Trott, D. W., Saleh, M. A., Xiao, L., Madhur, M. S., Chen, W., and Harrison, D. G. (2014). Inflammation and mechanical stretch promote aortic stiffening in hypertension through activation of p38 mitogen-activated protein kinase. *Circ. Res.* 114, 616–25.

Wung, B. S., Cheng, J. J., Hsieh, H. J., Shyy, Y. J., and Wang, D. L. (1997). Cyclic strain induced monocyte chemotactic protein-1 gene expression in endothelial cells involves reactive oxygen species activation of activator protein 1. *Circ. Res.* **81**, 1–7. doi:10.1161/01.RES.81.1.1.

Xia, W., Zhang, J., Perez, R., Koo, E. H., and Selkoe, D. J. (1997). Interaction between amyloid precursor protein and presenilins in mammalian cells: Implications for the pathogenesis of Alzheimer disease. *Proc. Natl. Acad. Sci.* 94, 8208–8213.

Yoshizumi, M., Perrella, M. A., Burnett, J. C., and Lee, M. E. (1993). Tumor necrosis factor downregulates an endothelial nitric oxide synthase mRNA by shortening its half-life. *Circ. Res.* 73, 205–9.

Zhang, X., Wang, B., O'Callaghan, P., Hjertström, E., Jia, J., Gong, F., Zcharia, E., Nilsson, L. N. G., Lannfelt, L., and Vlodavsky, I. (2012). Heparanase overexpression impairs inflammatory response and macrophage-mediated clearance of amyloid-β in murine brain. *Acta Neuropathol.* 124, 465–478.

Zhu, Z., Lu, J. J., and Liu, S. (2012). Protein separation by capillary gel electrophoresis: A review. *Anal. Chim. Acta* 709, 21–31.

Ziegler, T., Bouzourène, K., Harrison, V. J., Brunner, H. R., and Hayoz, D. (1998a). Influence of oscillatory and unidirectional flow environments on the expression of endothelin and nitric oxide synthase in cultured endothelial cells. *Arterioscler. Thromb. Vasc. Biol.* 18, 686–92.

Ziegler, T., Silacci, P., Harrison, V. J., and Hayoz, D. (1998b). Nitric oxide synthase expression in endothelial cells exposed to mechanical forces. *Hypertension* 32, 351–355.